SU-SEL-70-037

Irregularities in the Quiet Ionosphere and Their Effect on Propagation

by

Philip A. Fialer

August 1970

Technical Report N° 156

Prepared under

Office of Naval Research Contract Nonr-225(64), NR 088-019, and Advanced Research Projects Agency ARPA Order N° 196

RADIOSCIENCE LABORATORY

STANFORD ELECTRONICS LABORATORIES

STANFORD UNIVERSITY · STANFORD, CALIFORNIA

DISCLAIMER NOTICE

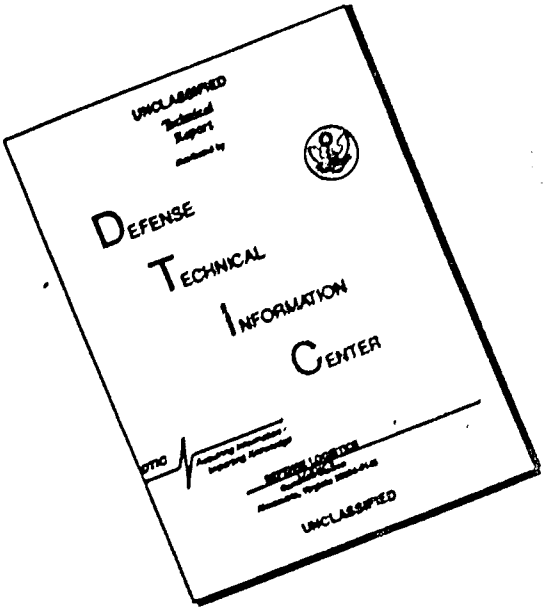

THIS DOCUMENT IS BEST QUALITY AVAILABLE. THE COPY FURNISHED TO DTIC CONTAINED A SIGNIFICANT NUMBER OF PAGES WHICH DO NOT REPRODUCE LEGIBLY.

SEL-70-037

IRREGULARITIES IN THE QUIET IONOSPHERE AND THEIR EFFECT ON PROPAGATION

by

Philip A. Fialer

August 1970

Technical Report No. 156

Prepared under

Office of Naval Research Contract
Nonr-225(64), NR 088-019, and
Advanced Research Projects Agency
ARPA Order No. 196

Radioscience Laboratory
Stanford Electronics Laboratories
Stanford University Stanford, California

ABSTRACT

The primary purpose of this investigation was to determine the nature and characteristics of a class of large, weak ionospheric irregularities which in certain circumstances significantly affects long-distance HF radio-wave propagation. A further purpose was to determine the relative practical importance of the diffraction produced by these inhomogeneities, in relation to the influence of other mechanisms such as Faraday rotation and scattering by small irregularities.

Measurements of quasi-periodic variations in phase-path length have been made on a 2600 km one-hop lower-ray F-region path. Variations of 8 to 75 wavelengths are regularly observed during winter daylight hours. They have a quasi period of about 20 minutes. Correlations of measurements made at spaced receiver locations indicate that these variations in phase-path length are produced by irregularities having a horizontal scale size of about 35 km. Multiple frequency measurements show a vertical scale size of about 15 km, with a maximum in the lower F region. A lower limit of 65 m/sec is determined for the horizontal velocity of the irregularities. A downward vertical velocity of 30 to 40 m/sec is observed. The irregularities limit achievable bandwidth and spatial resolution for one-hop HF ionospherically propagated waves under quiet ionospheric conditions.

A model of the irregularities has been devised and has been used to predict the signal-strength fluctuations which would result from propagation through a medium described by the model. Two classes of signal-strength behavior are predicted and observed experimentally, depending on the relative magnitude of the phase-path variations within the limits mentioned above. Signal-strength variations of a few dB, having a 20 min period, are observed when the changes in phase-path length are small, and are attributed to focusing caused by the irregularities. Larger, more rapid signal-strength fluctuations are also observed. These are attributed to multipath interference between several rays propagating through the same irregularity. Taken together, these rays make up what would be identified as the one-hop lower-ray F-layer mode, which is seen to be less homogeneous than had previously been supposed, for propagation over 2000-4000 km distances.

CONTENTS

CONTENTS (Cont)

TABLES

ILLUSTRATIONS

ILLUSTRATIONS (Cont)

ILLUSTRATIONS (Cont)

ACKNOWLEDGMENT

I wish to express special thanks to Professor O. G. Villard, Jr., for his guidance and encouragement throughout this work. I am also grateful to Professor L. A. Manning and Professor Thomas M. Cover for their suggestions in improving the technical quality of the manuscript. I gratefully acknowledge the assistance of Doctor Thomas A. Croft who developed most of the computer raytracing techniques which were used in this work. My thanks also go to Mrs. Mabel Rockwell and to Miss Jane King for their help in preparing the finished report.

This research was supported by the Advanced Research Projects Agency through the Office of Naval Research, Contract Nonr-225(64).

I. INTRODUCTION

A. PURPOSE

The purpose of the work described in this report was to determine the large-scale spatial properties of high-frequency (HF) radio waves which had propagated over an undisturbed (quiet) one-hop F-layer ionospheric path. These large-scale properties limit the maximum antenna size which may be efficiently employed in HF systems. A further purpose of the work was to determine the importance of ionospheric irregularities relative to other mechanisms in producing spatial distortions in HF waves.

B. BACKGROUND

Ionospheric communication is made possible by the refracting region of free electrons which exists at altitudes of about 70 to 300 km above the earth. Figure 1 is an example of a profile of electron density vs height which might be observed over a fixed point on the earth. This electron-density profile is typical of the midlatitude winter daytime ionosphere. Radio waves in the range of about one to thirty MHz are bent sufficiently that they will return to the earth at a considerable distance from the point of transmission. Figure 2 shows the paths of rays at a fixed radio frequency for an ionosphere which is described everywhere by the electron-density profile of Fig. 1.

At the point of return, the waves may be received, or they may be reflected from the surface to make additional "hops", often reaching distances two, three or four times those for a single hop. While traversing the ionospheric portion of their path, these waves are affected by any variations in electron concentration (and hence in refractive index) which they may encounter.

Variations (with time of day, season of the year, and location on the earth) in the angle at which the sun's energy is incident upon the ionosphere cause spatial variations on a global scale in observed profiles of electron density versus height. These spatial variations can contribute to small frequency shifts in the received signals and to small effective "tilts" in the refracting layer. Such frequency shifts

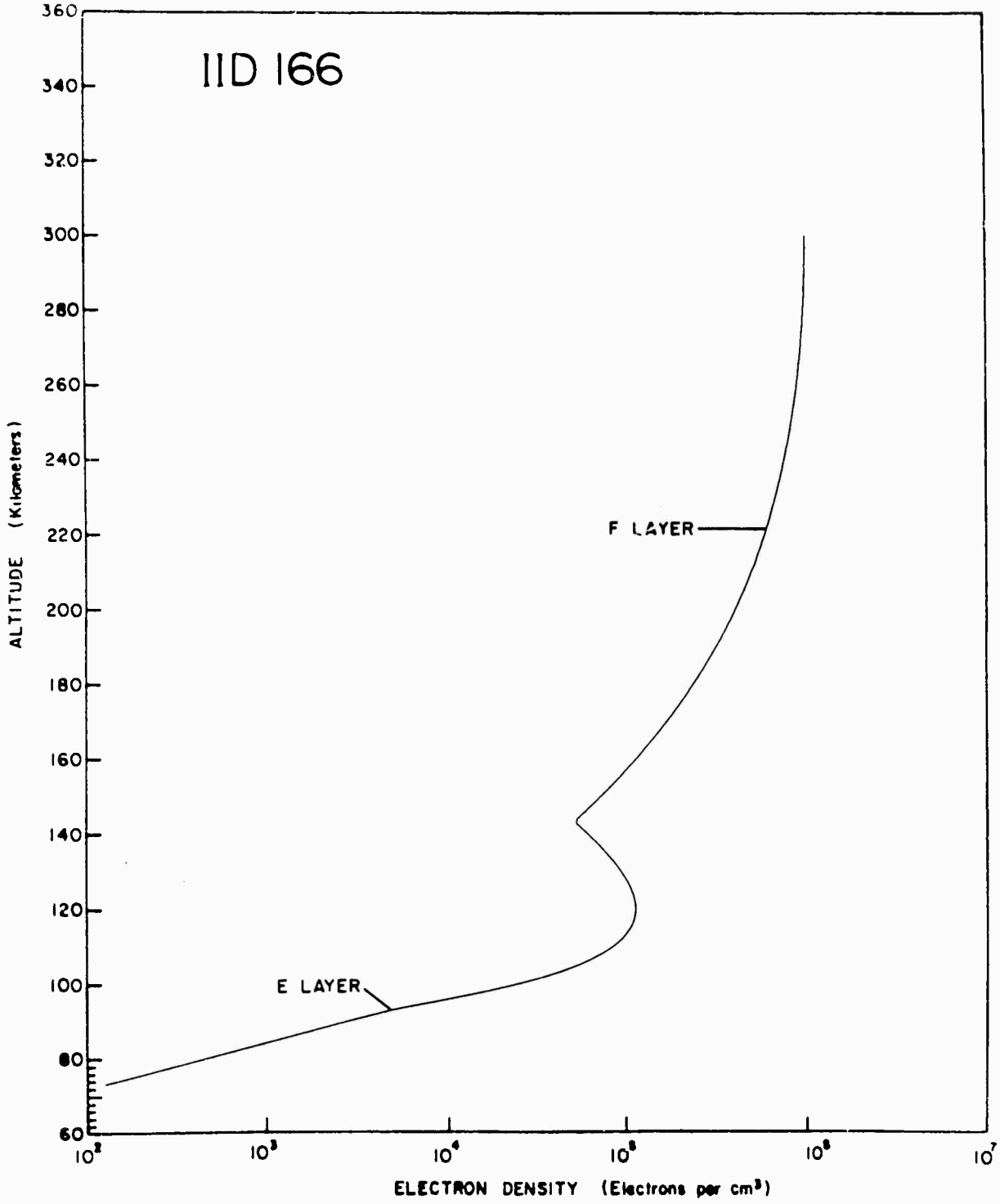

Figure 1. Ionospheric electron density profile. [From TR-112, SU-SEL-69-007, Stanford Electronics Laboratories, Stanford University, Stanford, California.]

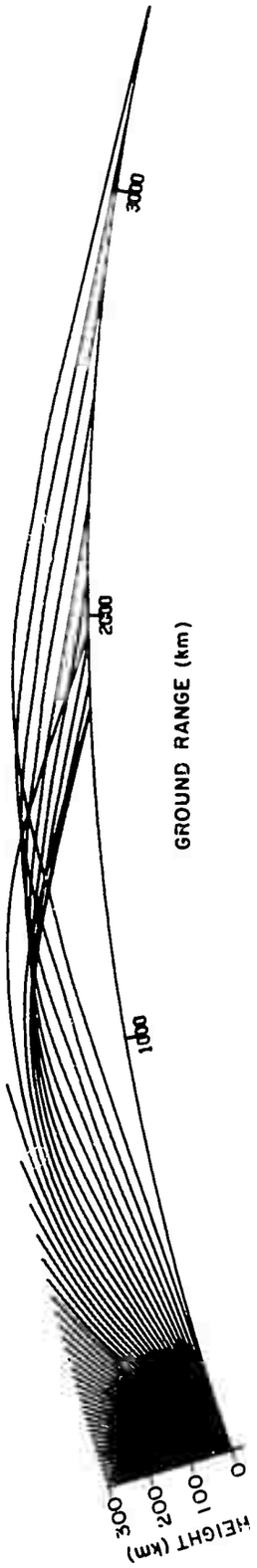

Figure 2. High-frequency radio ray paths in the ionosphere.

and tilts do not generally cause difficulty in the operation of high-frequency communication circuits.

More important degradations in the smoothness of received wave fronts (surfaces of constant phase) can be produced by localized variations in the electron-density profile of the ionosphere. These localized variations (ionospheric irregularities) scatter or refract the incident waves. If the irregularities are moving, they cause the amplitude and phase of the received signals to vary with time. Variations of this sort limit the useful bandwidths and antenna apertures that may be employed in HF communication systems.

1. Features of the Quiet Ionosphere

The gross characteristics of the ionosphere, through which ray paths joining any two points on the earth travel, may be determined from a sweep-frequency sounding over the path (an "oblique ionogram", Fig. 3). In such a record the time required for a group of waves to travel from transmitter to receiver is measured over a wide interval of radio frequencies (Barry and Fenwick '65). Figure 3a shows such an ionogram for a mid-latitude path on a typical winter day. Some important features are indicated in the figure. In the frequency interval labeled "single mode", only one major ionospheric path exists between the transmitter and the receiver. The ionogram of Fig. 3a was made during a period of undisturbed or "quiet" ionospheric conditions. Figure 3b shows the effect that an ionospheric disturbance produces in an oblique ionogram.

All of the experimental work in this paper was performed under the following conditions:

1. One-hop, lower-ray, F-layer propagation only.
2. East-west, midlatitude path.
3. Quiet ionospheric conditions.

2. Sources of Wavefront Distortion in the Quiet Ionosphere

Information on the spatial characteristics of HF ionospherically propagated waves is available in a variety of forms and representing

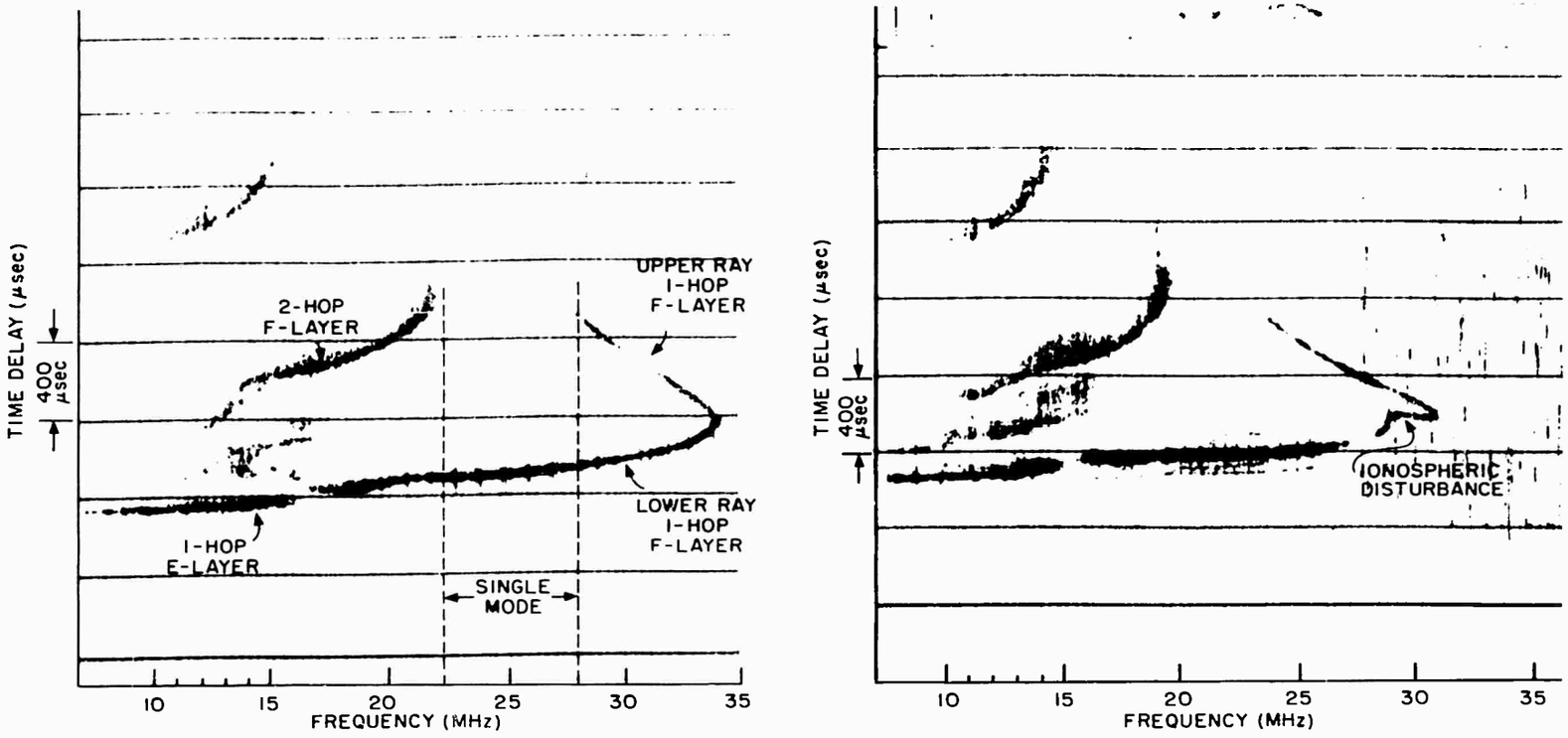

(a) Quiet ionosphere.

(b) Disturbed ionosphere.

Figure 3 Sweep-frequency soundings--Bearden, Ark. to Los Banos, Calif.

a wide range of ionospheric conditions. In this section some of the pre-existing relevant information and its relation to the present work are discussed.

a. Traveling Ionospheric Disturbances

Traveling ionospheric disturbances produce large ionospheric irregularities having horizontal spatial periods ranging from 50 km to over 1000 km. The disturbances occur at rates of a few per day for smaller disturbances to a few per month for larger ones. Munro ('50, '58), Georges ('67), Chan and Villard ('62) and others have studied such disturbances. The wavefront distortions which result are reasonably well understood. The low rate of occurrence of traveling disturbances decrease their influence on the performance of HF systems. The observations described in the present work were made under conditions when no large traveling disturbances were influencing propagation over the path (as determined by the absence of "kinks" in ionograms over the path--see Fig. 3).

b. Multi-mode Observations

The spatial characteristics and motion of the fading pattern produced by the interference of rays propagating over different ionospheric paths, that is, by different modes, has been studied by Ames ('64). The observed fading rates and motions of the fading patterns are adequately explained in terms of large-scale tilts and motions of the ionospheric layers. The observations of the present study are limited to the frequency range where only a single mode is propagating.

c. Single-mode Oblique-incidence Measurements

Measurements during periods of quiet ionospheric conditions, using frequencies for which only a single mode is propagating (or where modes are resolved using pulse methods), have been made by a number of investigators. Such measurements permit the most direct interpretation in terms of causative mechanisms in the ionosphere.

One category of single-mode oblique-incidence studies considers the scattering produced by large numbers of small (less than 5 km

horizontal extent) weak irregularities. The statistical properties of the resulting field are measured to determine the statistics of the scatterers. It is assumed that the received wave is composed of a single specular component plus a large number of weak scattered waves. The scattered energy introduces amplitude and phase fluctuations in the received signal which are statistically distributed in a characteristic manner that defines the ratio of the unscattered (specular) energy to the scattered energy. This ratio (β) is often referred to as the coherence ratio of the received signal. Al'pert ('63) summarizes a number of amplitude-distribution measurements of ionospherically propagated waves. Whale and Gardiner ('66) derive relations between the statistics of the phase difference measured on two spaced antennas, and the coherence of the received wave field. Coherence measurements have not produced a clear description of the influence of small irregularities on ionospheric communication. Phase measurements usually indicate much larger values for the coherence ratio than are found using amplitude measurements.

A second category of studies considers the effect that a smaller number of larger irregularities has on waves propagating through the ionosphere. The effects of each individual irregularity are measured, frequently at widely separated locations. These studies have mainly been concerned with irregularities in motion, primarily because the observation of temporal variations is experimentally easier than the observation of spatial variations. The velocity and size of large irregularities have been determined by measuring the time separation of the effects of a given irregularity at spatially separated points. The measurements of traveling ionospheric disturbances described above fall into this category. Also, Bramley ('53, '55) has studied variations in the angle of arrival of obliquely propagated waves at sites separated by 27 km to 213 km. He measures angular deviations in azimuth of about a degree, having a pseudo-period of about 20 minutes. These deviations are highly correlated at 27 km, but are nearly uncorrelated at the 213 km spacing. Although it is difficult to determine the shape and strength of irregularities from angle-of-arrival data only, Bramley attributes the observed variations in angle of arrival to weak traveling irregularities having spatial periods of 50 to 200 km.

A third category of measurements of the spatial properties of ionospherically propagated waves involves measuring the amplitude and phase of the waves at a large number of spatially separated points. (The multi-mode work of Ames, described above, used this technique.) The major work of this type for single-mode propagation under quiet ionospheric conditions is that of Sweeney ('70). He employed eight receiving elements equally spaced along a line 2.5 km long. He observed relatively linear wavefronts having mean angle-of-arrival variations similar to those observed by Bramley. In addition, Sweeney observed amplitude differences of about 10 dB and phase fluctuations of about $\pm 20^\circ$ on the individual elements. These fluctuations are more rapid (having periods of less than 1 min) than the variations in the mean angle of arrival. The mechanism that produces the more rapid fluctuations is not determined.

C. APPROACH IN PRESENT STUDY

This report describes a series of experiments performed to determine the large-scale (large compared with the 2.5 km aperture used by Sweeney) spatial properties of ionospherically propagated waves. A new phase-measuring technique is used to study the shape of the observed wavefronts. Phase measurements are made using a fixed receiver site plus an airborne receiving system. The use of an airborne receiving system allows phase changes to be measured simultaneously at two points whose separation may be changed rapidly. The moving airborne receiver is sensitive both to moving disturbances and to wavefront distortions which are fixed in space, that is, not varying significantly with time.

Data gathered by use of this technique reveal the presence of a new class of ionospheric irregularities, which appear to be a continuation to smaller sizes (approximately 35 km) and weaker strengths (approximately 1 per cent change in electron density), of the irregularities observed by Bramley and others. Simultaneous measurements with several radio frequencies are used to determine the vertical size (about 15 km) of these new irregularities. A computer model is then used to predict the influence of the irregularities on propagation. Amplitude fluctuations which result from propagation through such irregularities are predicted from the

model, and are compared with the fluctuations observed experimentally. The occurrence of these weak, medium-sized irregularities is shown to coincide with signal-strength fluctuations. The statistical distribution of amplitude fluctuations at the receiver is measured and compared with amplitude-fluctuation distributions predicted from the model. The predicted and measured amplitude-fluctuation distributions are in turn compared to distributions predicted by other models of fading mechanisms such as O-X interference and scattering by numerous small, weak irregularities. This analysis can explain some ambiguities in previous studies which attempted to explain amplitude fluctuations using a model based on the assumption of many weak irregularities.

Determinations of the apparent vertical velocity and a lower limit for the horizontal velocity are also drawn from the measurements. Finally, the performance of wide-aperture antennas in the presence of large irregularities is discussed. Appendix A provides a detailed description of the experimental method, together with the accuracy requirements of this method.

II. PHASE-PATH MEASUREMENTS

The experiments described in this report were performed in two series of measurements. The objective of the first was to establish a general understanding of the wave field of energy which has propagated over a one-hop lower-ray F-layer path through the ionosphere. The results of this first series of measurements showed that the major distortion of the received wave fronts appears to be caused by ionospheric irregularities having a temporal variation with a period of about 20 min, a horizontal scale size of approximately 35 km, and a maximum deviation of electron density in the range of 0.6 per cent to 6.0 per cent.

The second series of experiments, performed about one year after the first series, was concerned with determining the vertical scale size (determined to be about 15 km), and the range of magnitudes of the variations observed. In addition, data from the second series of experiments were used to study the signal-strength fluctuations produced by the irregularities, and to determine any observable motion of the irregularities.

A. CONDITIONS OF THE MEASUREMENTS

In order to minimize the possibility of ambiguities in the experimental side of this work and in the interpretation of the data, the measurements were performed under conditions which were expected to produce relatively smooth wave fronts. The path employed joins transmitters at Bearden, Arkansas and receivers at (or near) Los Banos, California (see map, Fig. 46 in Appendix A). The use of this midlatitude path avoids equatorial and polar anomalies. The great-circle distance from Bearden to Los Banos is 2600 km.

Measurements were made during winter daytime periods. At these times, ionospheric disturbances are infrequent, and a wide range of frequencies could be used which propagated by the one-hop lower-ray F-layer mode only. For unambiguous results, the measuring technique that was used requires single-mode propagation. Frequencies as low as 18 MHz (limited by the appearance of the two-hop F-layer mode or

the one-hop E-layer mode) and as high as 28 MHz (limited by the appearance of the one-hop F-layer upper-ray mode) were used. On most days a range of between 3 and 10 MHz was available, for which propagation was by the one-hop lower-ray F-layer mode only. During winter nights and during the summer, there are usually no frequencies which propagate by only a single mode over the Bearden-Los Banos path.

A high-resolution FMCW ("chirp") sounder was used to monitor conditions over the path. This sounder provides oblique ionograms having 8 μsec resolution in group time delay. Ionograms were made routinely, at intervals of a half hour to an hour and a half, to determine the "single-mode" frequency range and to check for the presence of large ionospheric disturbances. Additional ionograms were made if the phase-path measurements (described below) indicated that any ionospheric disturbances might be present on the path. Any traveling disturbances (as studied by Munro and others) produce noticeable "kinks" in the high-resolution ionogram. No data from the phase-path measurements were used for periods when ionospheric disturbances could be detected from the ionograms.

B. PHASE-PATH MEASUREMENT METHOD

The selection of a measuring technique to be used for this work was made on the basis of the known characteristics of wave fronts propagated over long, single-mode, one-hop F-layer paths--plus a desire to determine the nature of the mechanism producing wave-front distortions. The use of pulse measurement techniques was rejected because it was felt that the resolution possible with ionospherically propagated pulses (approximately 2 μsec at best) was not sufficient to provide any new information about small variations in wave-front shape. Angle-of-arrival measurements were considered impractical in view of the desire to make measurements at a wide variety of receiver spacings. (Accurate angle-of-arrival measurements require very carefully selected receiver sites.)

The use of continuous-wave (CW) measurements was selected for the following reasons:

1. Measured phase changes may be more simply interpreted in terms of refractive-index variations in the ionosphere, than is the case for group-path measurements.

2. The sensitivity of the measuring system to small phase changes is limited only by the stability of the frequency standards employed.

3. Dispersion--i.e., the propagation of different frequency components of a pulse over different paths--need not be considered.

4. The narrow bandwidth required allows the use of low peak power and reduces the system's sensitivity to interference.

The major disadvantage of CW measurements is that frequencies must be chosen at which only a single mode is propagating. The path used in the present study allowed the use of single-mode frequencies during winter daylight hours. The methods of acquiring and analyzing the data are described below.

Changes in the phase-path length (P) of rays propagated obliquely over a 2600 km ionospheric path were used to study irregularities in the received wave fronts and to infer some of the characteristics of the source mechanism in the ionosphere. The measured rays propagated over a "single-mode", one-hop, lower-ray F-layer path. In the absence of irregularities in the ionosphere, the resulting field at the receiver, produced by such "single-mode" propagation, consists of an ordinary and an extraordinary magnetoionic ray. As a result of the irregular bending of rays by ionospheric irregularities, more than one such pair of rays may arrive at the receiver.

The phase-path length of a ray propagating from transmitter to receiver through a medium of varying refractive index is defined by the relation

$$P = \int_{\text{RAY PATH}} \mu ds \quad , \tag{1}$$

where μ is the refractive index of the medium and ds is an incremental distance along the ray path. P is directly related to the phase φ of the received wave by

$$\varphi = \frac{2\pi P}{\lambda} \quad ,$$

where λ is the wavelength in the medium and equals λ_o/μ, in which λ_o is the free-space wavelength. If changes in phase-path length (ΔP) are measured in free space ($\mu = 1$), λ_o may be used in relating $\Delta\varphi$ to ΔP. In this context, φ is not periodic in 2π radians. The measurement of changes in P as a function of time is made by observing the changes in φ as a function of time--i.e., by counting the number of cycles (an integral number plus a fraction) of the received signal which occur during some sample interval (usually one second), and comparing this with the transmitted frequency. Such a measurement is unambiguous (unlike a simple phase measurement). That is, the resulting phase measurement is not limited to the range 0 to 2π radians.

The received signal is converted to an audio frequency by a phase-coherent receiver, and it is this audio signal which is measured. The use of an audio frequency much higher than any possible frequency shift in the received signal avoids any potential plus/minus ambiguity. The equipment and processing used in these measurements, and the accuracy of the measurements, are discussed in the appendix.

If only a single ray path joins the transmitter and the receiver, the meaning of such a measurement is clear. Let the received signal, E_r, be described in the form

$$E_r = E(t) \sin \left[2\pi f_o t + \varphi(t)\right] \quad , \qquad (2)$$

where t is time, f_o is the transmitted frequency (carrier), $E(t)$ is a slowly varying (compared to the carrier frequency) "envelope" amplitude, and $\varphi(t)$ is a slowly varying phase angle measured with respect to the carrier. The quantity φ will be referred to as the measured phase of the received signal. Again, note that the range of φ is not restricted to 2π radians. $E(t)$ is also measured at the sampling interval. A one-second sampling interval has been found to be satisfactory for the relatively stable signals observed under the measurement conditions.

The received signal E_r can be represented as a vector of length E at an angle φ relative to a coordinate system rotating at $2\pi f_o$ rad/sec (Fig. 4a). If truly only one signal is present, this picture, together with the meaning of the measurement, is clear. If the received signal is shifted in frequency from the carrier frequency, e.g., if a doppler shift is caused by motions in the ionosphere, then

$$\varphi(t) = 2\pi f_d t \quad , \tag{3}$$

where f_d (commonly called "doppler") is the difference between the transmitted and received frequencies.

If the received signal is produced by a summation of several rays, the interpretation of the measurement may or may not be clear. The phase measured is that of the vector sum of all components present. Some possible types of sums are shown in Figs. 4b and 4c and are described below.

Consider a received vector composed of a large signal vector (E_S) plus a small randomly phased vector (E_n). As has been pointed out, the measurements made in connection with this work were carried out under undisturbed ionospheric conditions, using frequencies for which only a single mode was propagating. Measurements by Sweeney ('70) and others show that under such conditions, phase changes are generally smooth for periods of several minutes, but that small, more rapid (5-20 sec period) phase fluctuations of about 10 deg are observed. Such fluctuations might arise from noise, interference, or scattering by small irregularities in the ionosphere. This type of fluctuation may be represented by a small random vector E_n added to the main signal vector (Fig. 4b). The measurement of phase is still unambiguous; however, a phase error is introduced. As long as the actual phase error introduced into the vector sum is not significant to the data derived from the measurement, the effect of such perturbations is not important, and does not modify the concept of the measurement. Actually, if one received signal vector is larger than the sum of the magnitudes of all other vectors, the unambiguous measurement is a meaningful representation of the larger (dominant) vector as long as an error in measured change in P of $\pm\lambda/4$ (equivalent to a change in φ of $\pm\pi/2$ radians) is acceptable. While an error of $\pi/2$

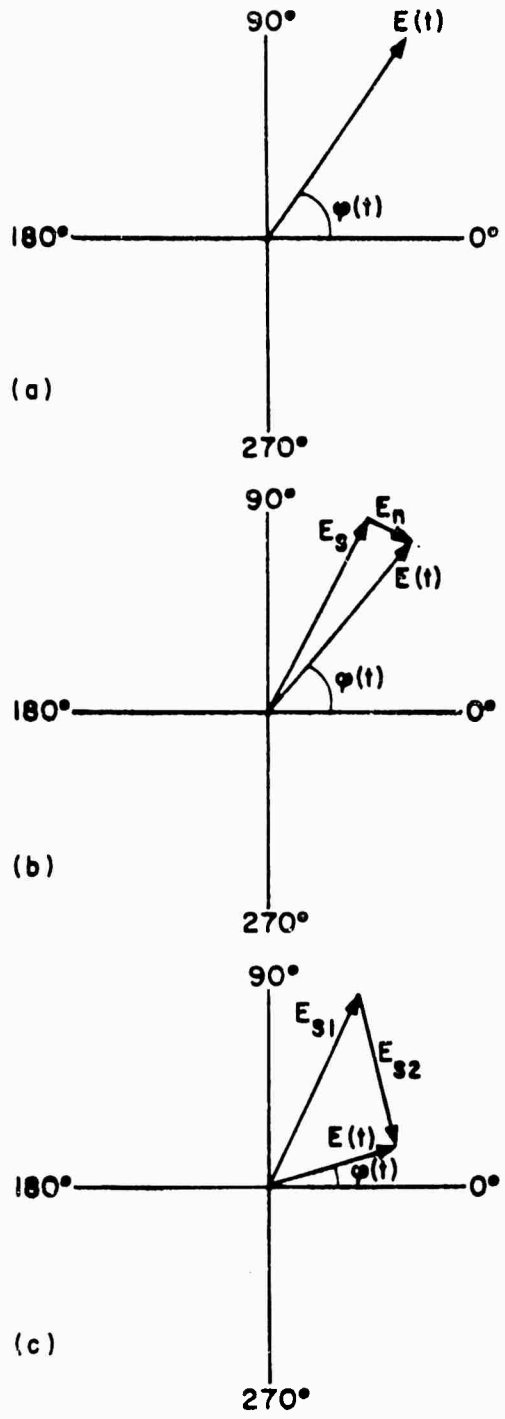

Figure 4. Vector representation of received signals.

(a) Single ray.
(b) Small perturbing component.
(c) Two rays of comparable amplitude.

radians might invalidate a simple phase measurement, errors of this magnitude will be negligible in the unambiguous phase-path-length measurements.

Now consider a measured resultant vector made up of two vectors of similar magnitude, E_{S1} and E_{S2}, whose lengths vary with time (Fig. 4c). Such a situation might represent two magnetoionic components (see Chapter III); or propagation by more than one mode; or "internal multipath"* effects produced by ionospheric irregularities. In the case of the ordinary and extraordinary magnetoionic components, the relative position and strength of the two component vectors will vary only slowly with time. With the exception of a complete cancellation, the measured phase and frequency shift of the resultant vector will be a reasonable estimate of the performance of either of the two rays. For rays of comparable amplitude which do not behave similarly to each other, we will observe the variations in length of phase path P for the stronger ray, within an accuracy of $\pm\lambda/4$. Since the relative amplitudes of the rays may vary with time, one ray and then the other may successively dominate the measurement. If such relative changes in amplitude occur slowly enough (i.e., if many samples are taken between changes), and if the frequency shifts f_o along the ray paths are different enough for the two rays, we will be able to observe an abrupt change in the slope of the phase-path record as the change occurs. Figure 5 shows the type of changes we would expect under these conditions.

For larger numbers of components, a simple intuitive understanding cannot be continued unless one of the above conditions can be approximated; i.e., unless one ray or several rays with very similar frequency shifts dominate the resultant vector for reasonably long intervals of time. Ultimately, the analysis of the amplitude and phase measurements will be limited by sampling theory and measurement noise; however, in this work the technique is applied only under conditions when the simple intuitive approach is applicable.

---

*The term "internal multipath" is used to describe multiple rays which propagate from a transmitter to a receiver via a single ionospheric mode. Internal multipath is present if ionospheric irregularities produce sufficient differential ray bending that rays cross before reaching the receiver location.

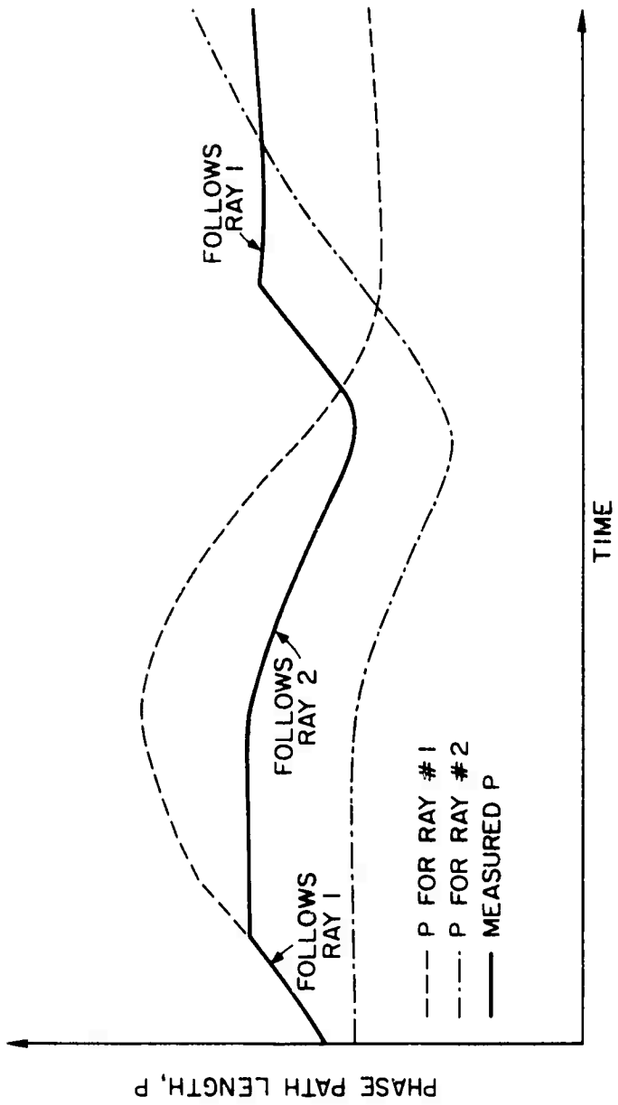

Figure 5. Alternate capture of phase-path measurement by two rays.

Using the measurement described above, it is possible, under certain conditions, to determine changes in P for the ray path joining a transmitter and a receiver, and conversely, it is frequently possible to determine from the measurement record whether the necessary conditions exist at the time of the measurement. Several implications of such measurements will now be discussed.

Variations in the phase-path length of an ionospherically propagated ray can occur in two ways. From Eq. (1) it is seen that variations in P may be caused both by variations in μ along a fixed path, and by changes in the position or length of the physical path. The frequency shift (doppler) which is produced by varying the phase-path length of a ray is

$$f_d = - \frac{f_o}{c} \frac{dP}{dt} \quad , \tag{4}$$

where c is the speed of light and f_o is the transmitted radio frequency. By measuring the slope of a phase-path record, we may determine the doppler shift of the ray that dominates the measurement.

An additional and perhaps unexpected relation for rays propagating between two fixed endpoints, through a medium in which the refractive index varies with time, is derived by Bennett ('67)

$$f_d = - \frac{f_o}{c} \int_{\text{RAY PATH}} \frac{\partial \mu}{\partial t} \, ds \quad . \tag{5}$$

This relation states that the instantaneous frequency shift is a function only of the instantaneous rate of change of refractive index along the present ray path, and does not include a contribution due to the simultaneous change in the position or length of the ray path which may be occurring. This fact will provide a more direct interpretation of our measurements in terms of the irregularities which cause them.*

---

* More precise statements of Eqs. (1) and (5), which account for the anisotropy of the ionosphere, include an additional term, $\cos \alpha$, within the integral, where α is the angle between the ray direction and the wave normal (see Budden, 1961). When considering small changes in long-range oblique ray paths, the error introduced by neglecting this term is negligible.

It is also useful to consider the technological constraints which will influence the usefulness of the measuring technique. The measured changes in phase-path length are not expected to occur at a rapid rate, since frequency shifts greater than one or two tenths Hz are rare under the stated experimental conditions. An error in integrated phase arising from the frequency sources used for transmitting and receiving will be reflected in a like error in the measured phase-path length. The more rapidly phase-path changes introduced by the ionosphere occur, the less rigid will be the requirements on the frequency sources used. Frequency errors (linear changes of phase) can be tolerated if a linear trend may be removed from the resulting data without loss of information. Instability in frequency, however, will degrade any data that make use of measurements of changes in P. Crystal frequency standards having a stability of about 10^{-9} will introduce errors in the measurement of P at a rate of about 1000 m/hr. Portable cesium-beam frequency standards having a stability of 10^{-11} will allow measurements with an error of about 10 m/hr. For the observed variations of the present experiments, this gain in accuracy is crucial.

C. MULTIPLE-LOCATION MEASUREMENTS

The effect of refractive-index irregularities on waves propagating through them is principally determined by the strength (per cent alteration of the refractive index) and the spatial extent of the irregularities.

The first series of measurements performed in this study was primarily concerned with determining the strength and horizontal scale size (or sizes) of the ionospheric irregularities believed to be present under quiet ionospheric conditions. Since the size range of possible irregularities was not known a priori, measurements were made at as wide a range of spacings as possible. The work of Bramley, carried out under quiet ionospheric conditions, indicated that the probable range of sizes of irregularities to be encountered would lie between 30 and 200 km. Making use of these observations, and considering some practical experimental limitations, a single stable-frequency CW transmitter was used,

and phase-path measurements were made simultaneously at two receiving points separated by distances which varied from 50 to 170 km. This provided two ray paths in the ionosphere which were separated horizontally by 25 to 85 km at the maximum height of the rays. One receiving system was located at the Stanford University Wide-Aperture Research Facility near Los Banos, California, while the other receiver was installed aboard a DC-3 aircraft. The aircraft was also equipped with an accurate tracking system which, in conjunction with two line-of-sight stable-frequency transmissions, allowed continuous (though not real-time) tracking of the plane's position. The equipment and data-processing method employed are described in detail in Appendix A. The resulting records show the variation in phase-path lengths between the transmitter (located in Bearden, Arkansas, 2600 km east of Los Banos) and each of the receivers. The records from the aircraft are corrected to compensate for the variation of the aircraft's position from a constant radial distance to the transmitter and from a constant altitude. For most of the experiments, the aircraft flew a course running from 50 to 170 km north of Los Banos. The course was flown in both directions.

The choice of this method of observation results in the ability to explore wave fronts at various receiving-antenna spacings without the necessity of establishing numerous field sites, and allows the detection of fixed irregularities. It does, however, suffer a decrease in the number of measurements that may be made at any given spacing, for the sake of an increase in the number of spacings that may be employed. The records show

$$P(t) - P_a \Big|_{\substack{r = \text{constant} \\ \theta = \text{constant}}} \quad \text{for the fixed receiver, and}$$

$$P(t,\theta) - P_b \Big|_{r = \text{constant}} \quad \text{for the aircraft receiver,}$$

where

P = phase-path length,

r = great-circle distance from the transmitter to the receiver,

θ = bearing from transmitter to receiver, and

P_a and P_b = unknown constants at the start of each measurement.

The slopes of these functions correspond to the observed frequency shift (doppler) of the signal and are given by

$$\frac{dP}{dt}, \quad \text{with} \quad r \quad \text{and} \quad \theta \quad \text{constant, for the fixed receiver,}$$

and

$$\frac{\partial P}{\partial t} + \frac{\partial P}{\partial \theta} \cdot \frac{d\theta}{dt}, \quad \text{with} \quad \frac{d\theta}{dt} \quad \text{and} \quad r \quad \text{constant, for the aircraft.} \quad (6)$$

The second term in the doppler expression for the aircraft arises from the aircraft velocity.

Two sources of error in interpretation of these data will now be mentioned with reference to their effect on our observations. The first is that the ray path joining the transmitter and the receiver does not lie in a plane containing the transmitter, the receiver, and the center of the earth, because of the tilts in the ionosphere produced by the irregularities we are studying. Therefore, the exact ray path is not known, and the measured doppler is that corresponding to a point in the ionosphere whose location is not precisely known. The error introduced by this deviation can be estimated by making use of angle-of-arrival measurements made by Sweeney ('70). He used a broadside antenna array which was 2.5 km long, and which received over the Arkansas-Los Banos path. He found root-mean-square (rms) angle-of-arrival fluctuations of about 1/4 deg, which implies that the ionospheric ray path has an rms deviation from the great-circle plane containing the transmitter and receiver of about 7 km at its maximum height.

The second source of error is introduced by the aircraft's motion (the $\partial P/\partial \theta$ term in Eq. 6). The effect of this error can also be determined from the known angle-of-arrival deviation. For a 15 m wavelength (20 MHz), a 1/4 deg change in angle of arrival will produce a phase variation normal to the nominal ray path of one cycle in 3 km. At the nominal aircraft velocity of 60 m/sec, this will result in a frequency shift of 0.02 Hz. As is indicated by the measured data presented in the next section, these zero-mean errors introduce only minor errors in the results for the values of frequency shift measured in these experiments, and for the number of points averaged in computing correlations.

Measurements using the aircraft receiver and the Los Banos receiver were made during April of 1969. A total of ten flights yielding satisfactory data were made. Frequencies between 20 and 25 MHz (wavelengths λ between 12 and 15 m) were used for these measurements. Each flight covered a path between a point 170 km north of Los Banos and a point 50 km north of Los Banos, and required between 20 and 40 minutes. On any given day, one or two flights over the path were made. If two flights were made on one day, they were made in rapid succession. (The data from two of the ten flights were later discarded because of interference on the tracking system frequencies in one case, and evidence on an ionogram and in the phase-path measurements of an ionospheric disturbance in the other.)

A typical pair of records from the fixed and airborne receivers is shown in Fig. 6. For each pair of records, a constant doppler (constant frequency shift, indicating a linear time rate of change of phase-path length) has been subtracted from both records. This removes the effect of large-scale ionospheric layer motions which do not influence the shape of the wave front. The most striking feature of the records is the quasi-periodic variation in phase-path length seen consistently in our observations. The time between peaks of these variations ranges from 15 to 25 min. The peak-to-peak phase-path length variations seen in these records ranged from about 8 λ (approximately 100 meters) to about 50 λ (approximately 600 meters). These length variations produced maximum frequency shifts ranging from about 0.05 Hz to 0.20 Hz. Analysis of these data

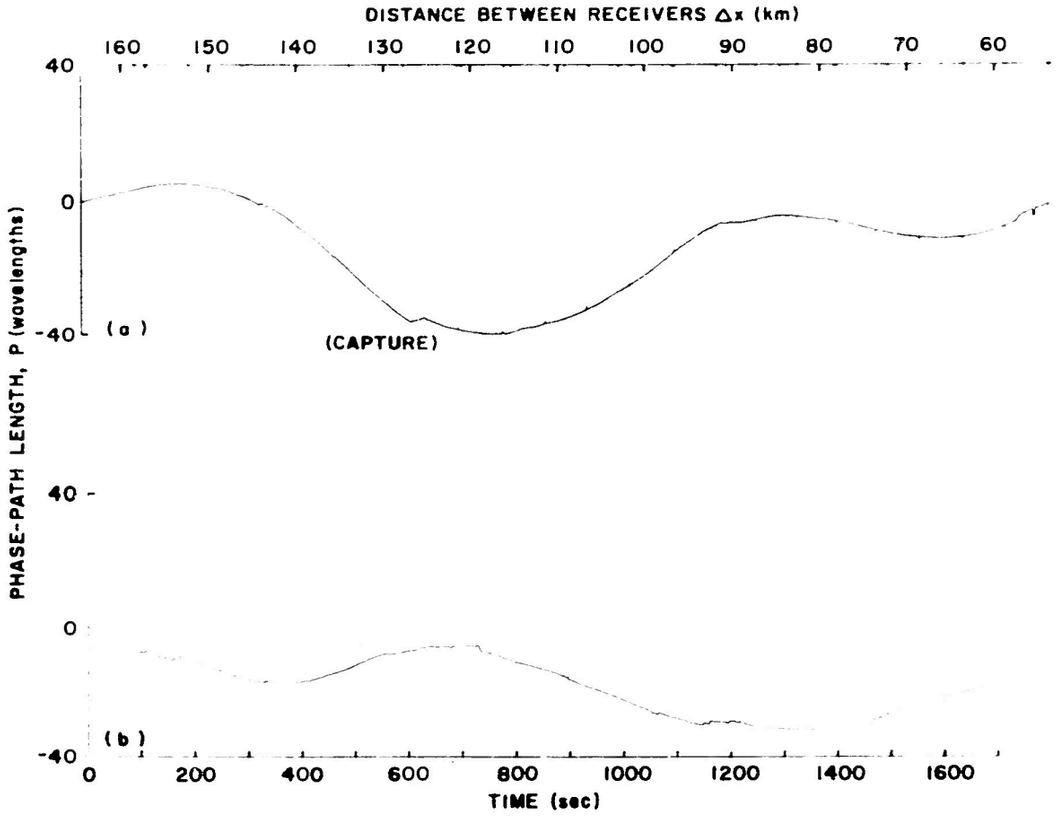

Figure 6. Two-point wide-spaced phase-path records.

(a) Fixed receiver--Los Banos, Calif.
(b) Airborne receiver.

f = 23.3 MHz, λ = 12.9 m

(see Section D of this chapter) indicated the presence of large, weak irregularities.

The small size of the measured frequency variations reveals some of the experimental difficulties which may be encountered in studying them. In order to make relative phase-path-length measurements at two separated points, the frequency standard at each point must be sufficiently accurate and stable that the desired measurement is not masked by variations in the standard. For variations of the order of 10 λ per 20 min, at an operating frequency near 20 MHz, we would like the standard to introduce errors no greater than 10 per cent of the desired measurement. This means one cycle per 20 min at 20 MHz, or a stability $(\Delta f/f)$ of about 4×10^{-11}. If the two measurements are made only a short distance apart, a common frequency standard may be used, making possible relative phase measurements that are as accurate as may be desired. However, if the effect being investigated produces only an insignificant difference in length of phase path at points separated by the small distances which may reasonably use the same frequency standards, independent standards of the above accuracy must be used in order to enable observation to be made at more widely separated receiving points. It is only recently that portable cesium-beam standards have been available which meet this requirement.

A second difficulty is encountered if doppler measurements are to be made using a Fourier analysis technique (instead of measuring the instantaneous slope of the phase-path variations). The smallest frequency interval Δf which may be resolved by Fourier analysis is $1/T$, where T is the length of the data sample. If ten independent frequency intervals are desired in the range of dopplers produced by weak irregularities, i.e., $f_d = 0.05$ Hz, then $\Delta f = 0.005$ Hz, and $T = 200$ sec. During this 200 sec interval, for the observed variations, the frequency will have shifted through several frequency-resolution cells, producing a poorly defined spectrum. If only a single signal component is present, we may use a shorter analysis time and interpolate between frequency intervals; however, this condition is rarely met for ionospherically propagated signals. When multiple, comparably strong (within an order of magnitude) components are present, the doppler method can separate them only when the frequencies change slowly enough to be resolved.

D. HORIZONTAL SCALE SIZE OF THE OBSERVED IRREGULARITIES

An estimate of the size (horizontal extent) of the irregularities being investigated was made from the above data by computing a correlation coefficient for the variation of the doppler from the mean, measured at various spacings of the two receivers. The doppler was measured graphically from the phase-path records. A total of eight pairs of records was found suitable for use in this correlation. For each pair of records,

$$\rho_i(\Delta x) = \frac{f_{d1} \cdot f_{d2}}{\overline{f_{d1}^2}} \tag{7}$$

was calculated, where

$\rho_i(\Delta x)$ is a sample of the correlation for the i^{th} flight at a receiver spacing of Δx,

f_{d1} is the scaled doppler value for the fixed receiver,

f_{d2} is the scaled doppler value for the airborne receiver, and

$\overline{f_{d1}^2}$ is the mean-squared doppler for the fixed receiver for the length of the record.

The estimate of correlation was then calculated as

$$\rho(\Delta x) = \sum_{i=1}^{8} \frac{\rho_i(\Delta x)}{8} \quad . \tag{8}$$

The calculated points are plotted in Fig. 7. The error bars indicate the estimated variance $(s')^2$ of the correlation [as defined by Eq. (7)] calculated from the measured values by

$$(s')^2 = s^2 \cdot \frac{n}{n-1} \quad ,$$

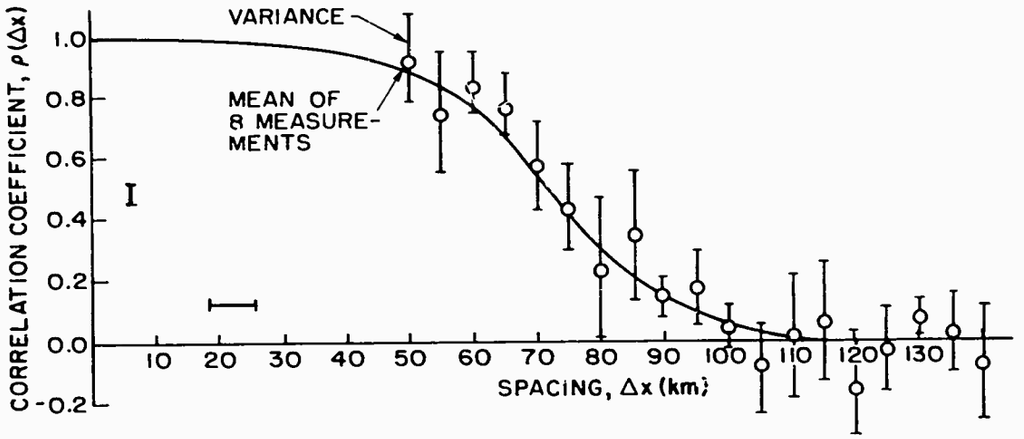

Figure 7. Doppler correlation coefficient for wide-spaced phase-path measurements.

I - Estimated error in ρ due to aircraft motion.

⊢⊣ - Estimaced error in Δx due to horizontal ray bending.

where $n = 8$ and s^2 is the sample variance.

Two sources of error in the measurements of ρ_i were mentioned in Section C. One is introduced by the motion of the aircraft, which was shown to introduce an rms error into the doppler measured by the aircraft (f_{d2}) of about 0.02 Hz. The rms measured doppler averaged over all flights was approximately 0.1 Hz. Therefore the expected error in ρ_i is 0.2 for this source. The expected error in ρ is then 0.2/ 8, or approximately 0.07.

The other source of error is introduced by the horizontal bending of ray paths by irregularities, which was shown to introduce an uncertainty in the location of the ray path of about 7 km near the reflection height of the rays. This can be represented as an error on the ground of 14 km for each ray. The error in Δx will depend on how the deviations of the two rays are correlated. At very small (compared to the size of the irregularities) spacings the deviations are positively correlated, decreasing the error in Δx. At very large spacings, the deviations will be independent. At some intermediate spacings, the two rays will be deflected oppositely by the two sides of each irregularity, causing the deviations to be negatively correlated, thus increasing the error in Δx. On the basis that the deviations are uncorrelated, the expected error in ρ is represented as an error in the location of $\rho(\Delta x)$. This error is approximately 7 km ($14\sqrt{2}/\sqrt{8}$). The effects of this error and the error due to aircraft motion are shown in Fig. 7.

The data of Fig. 7 show a correlation greater than 0.8 for the doppler measured at spacings of 60 km or less. At spacings greater than 90 km, the correlation is less than 0.3. This indicates that the irregularities producing the major component of the observed dopplers are of limited extent, and that the experimental configuration covered the size range of the major irregular structure. At a receiver separation of 70 km, the average correlation has dropped to about 0.5. This gives us a reasonable first estimate of 35 km for the horizontal extent of the irregularities in the ionosphere. This scale size will be used as a typical value in predicting the expected effects which these irregularities are expected to produce on wave fronts.

As was noted above, the doppler measured by the aircraft is a function not only of the time rate of change of ray path length at a fixed point, but also of the spatial variation of refractive index caused by the irregularities. The effect of the spatial structure of the irregularities of 20 min period, identified in the above doppler correlation study, was estimated earlier in this section using Sweeney's angle-of-arrival measurements, and was found to introduce only a small unbiased error term in the estimate of correlation. The possibility of the existence of a fixed irregular structure (or structure varying with a period much greater than the observed 20 min period) was examined by correlating the doppler measured on two pairs of consecutive flights over the path (spaced in time by about 30 min). Doppler correlations were computed from the data obtained on each pair of flights. The correlation coefficients of 0.13 and -0.05 for the two pairs of flights indicate that no fixed or semi-fixed structure was present with a magnitude comparable to that of the irregularities having the 20 min period variations.

A more accurate measure of the scale size of the irregularity structure could be obtained if it were possible to make prolonged measurements at fixed receiver separations. If multiple spacings were employed, some estimate of the spatial spectrum of irregularities could be obtained. Such a program could prove costly because of the large spacings needed and the high stability requirements of each receiving system. For the purposes of this work, the approximate scale size of the irregularity structure determined above will be used to study the effects to be expected in the presence of such irregularities.

E. VERTICAL SCALE SIZE

Having determined a reasonable estimate of the strength and of the effective horizontal scale size of the most significant irregularities for the oblique path, it was then necessary also to determine the approximate vertical extent of the irregularities in order to model their ray-beinding effects. The most convenient technique for probing the ionosphere at various heights, for a path joining two points, is to make use

of a range of radio frequencies which will penetrate to various heights into the ionosphere. Figure 8 shows the geometry of ray paths of various frequencies between two points, and gives the values of ray height at different points along the path, as computed by raytracing techniques (Croft '69), for an ionosphere typical of that over the path under study. These heights are used in estimating the vertical scale size of the irregularities.

During the winter and spring of 1969-1970 another series of experiments was performed over the same path used in the previous work, with the objective of determining the vertical scale size of the irregularities previously observed. Only the Los Banos receiver site was used for these measurements. Transmissions on two single-mode frequencies were made from Bearden and received at Los Banos. The two frequencies were received on a single whip antenna. One of the frequencies was also received on a whip antenna located 2.52 km north of the first antenna, for use in measuring the north-south velocity component of the irregularities. The outputs of the three receivers were recorded using the same phase-measuring technique used previously (see Appendix A). During the period from November 1969 to April 1970, measurements were made one or two days per week. Each day, from two to six hours of operation were possible (periods when single-mode propagation was possible and no irregularities were observable on ionograms over the path). The data collected in the course of these measurements were also analyzed to determine the vertical and north-south velocity components, seasonal occurrence, and signal-fading effects of these irregularities. These results are discussed in later chapters of this report.

Frequency separations in the range of 100 kHz to 6 MHz were used to achieve various ray spacings in the ionosphere. Doppler correlations similar to those employed in the determination of horizontal scale size were performed on pairs of frequencies using 1.2 hr segments of data. A considerably greater quantity of data were available for this work (75 segments of 1.2 hr each) than were available from the aircraft measurements.

Similar phase-path variations were observed at all frequencies used in these measurements. (Examples of the phase-path records are shown in

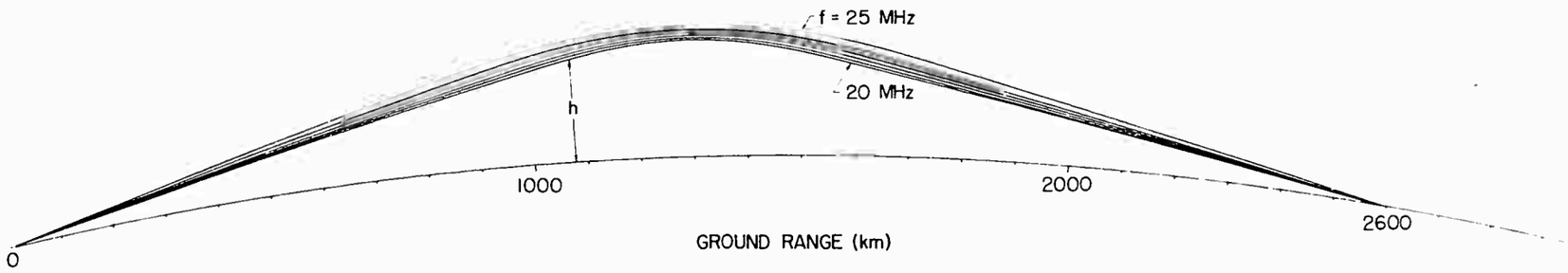

Figure 8. Ionospheric ray paths joining two points for several frequencies.

Frequency	Ray Height, h	
	At 800 and 1800 km Ground Range	At Midpath
20 MHz	131.1 km	224.84 km
21	135.5	228.94
22	140.0	233.33
23	146.0	238.34
24	154.7	243.56
25	166.6	252.83

Chapter III, Figs. 17-20.) Frequently, however, the amplitude of the phase-path changes decreased with increasing frequency. This information may be of use in determining the mechanism responsible for the observed variations; but for the present, only the vertical scale size of the irregularities is of interest. The form of the correlation computed was slightly modified in order to utilize the greater quantity of data available and to compensate for the general decrease in magnitude with frequency. The denominator used in calculating the correlation coefficient was changed from $\overline{f_{d1}^2}$ as in Eq. (7) to $\sqrt{\overline{f_{d1}^2} \cdot \overline{f_{d2}^2}}$. This form of the correlation function has the property that two functions differing only by a constant factor will have a correlation coefficient of 1.0. For each sequence of data, taken at a fixed frequency spacing, a correlation was calculated from 64 doppler measurements during the 1.2 hour period. In Fig. 9, the correlations are plotted against the frequency separation used. On the assumption (supported in the next chapter) that the irregularities have their maximum effect near the maximum altitude of the rays, spatial separations are also assigned to the frequency axis in Fig. 9 by using an average value of 4 km per MHz. The error in this average spacing as determined by raytracings in several representative model ionospheres (see Fig. 8) is indicated on the figure.

Again, a smoothly decreasing correlation is observed as the spacing increases. The average vertical distance required for the doppler correlation to drop to 0.5 is about 15 km, based on the assumed ray separations. This considerably smaller vertical scale size of the irregularities, in comparison to horizontal scale size, will be of importance in determining the effects produced by these irregularities.

F. CONCLUSIONS FROM PHASE-PATH MEASUREMENTS

The important parameters of the irregularities observed will now be summarized in a form which will allow an investigation in the following chapters of the expected effect of these irregularities on wave front characteristics and antenna performance. All of the observations of irregularities during the course of this work were made under undisturbed winter daytime conditions over a 2600 km path at frequencies for which

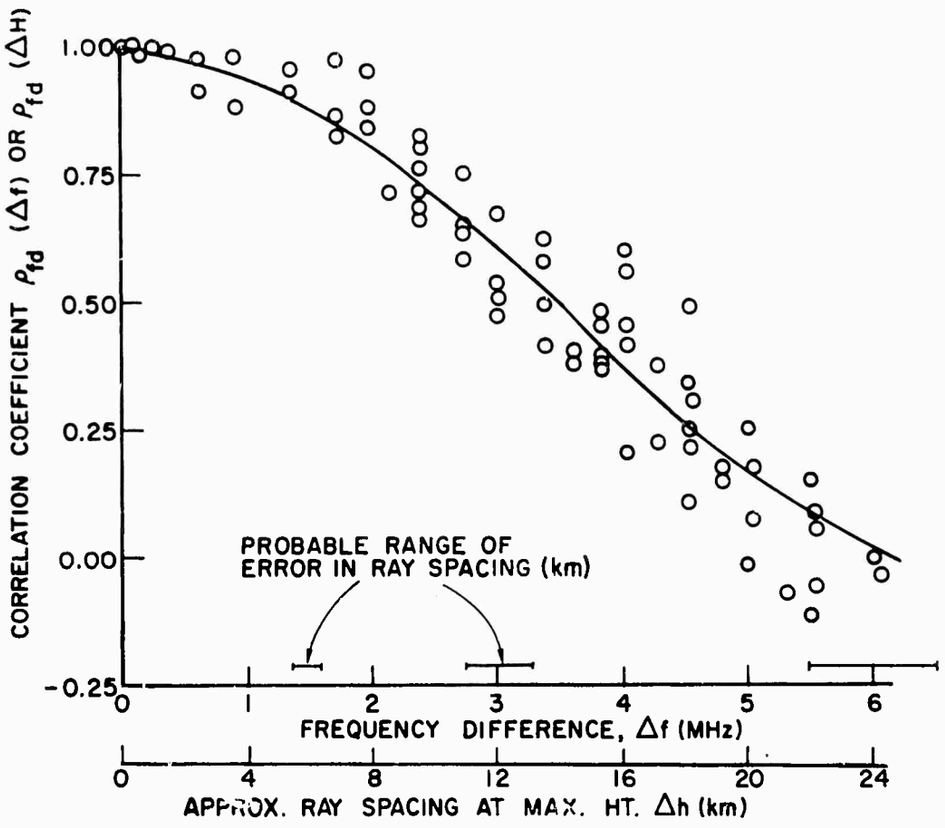

Figure 9. Doppler correlation coefficient for multiple-frequency phase-path measurements.

only the one-hop lower-ray F-layer mode was propagating. No data were taken during periods when larger irregularities (which are visible as "kinks" in the ionogram--Fig. 3b) were present. The conditions represent the most promising conditions for high-performance HF propagation, and are therefore of great practical interest. Such conditions also allow the use of the most direct measurement methods. Furthermore, the application of the knowledge gained under these conditions will help to clarify the results of observations made under more complex conditions.

During about 100 hours of observation in the spring of 1969, and in the winter and spring of 1969-1970, phase-path variations having a distinct period of 15 to 25 min were always observed. The amplitude of these variations ranged from about 8 λ to 75 λ peak to peak. The horizontal spatial correlation of the doppler produced by these variations indicates a correlation of 0.5 for receiver spacings of about 70 km on the ground. This implies a horizontal scale size for the irregularities of about 35 km. (If scale size is defined for a correlation of 1/e, where e is the base for natural logarithms, the scale size would be about 43 km.) A similar calculation of vertical scale size indicates a vertical extent of about 15 km, assuming the effects are produced at the maximum height of the rays. Also, for a fixed ionosphere, a decrease in magnitude of the phase-path variation with increasing radio frequency has been noted.

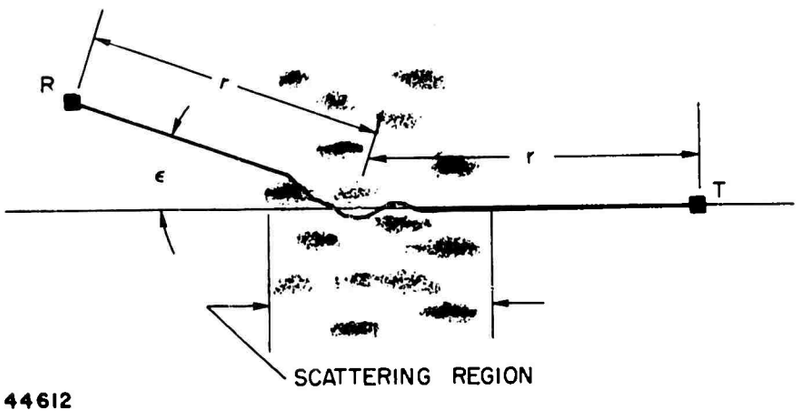

Figure 10. Two-dimensional scattering geometry.

III. MODEL OF THE IONOSPHERIC IRREGULARITIES

The phase-path-length measurements described in the preceding chapter were used to determine the strength and spatial extent of the irregularities producing the measured variations in phase-path length. The measurements do not, however, provide a complete description of the received wave field. In fact, the measuring technique intentionally rejects amplitude fluctuations and small phase fluctuations in order to provide measurements which describe the causative mechanism (the irregularities) most directly. In this chapter, irregularity models are used to determine the nature of the total wave field expected in the presence of the weak, medium scale irregularities.

A two-dimensional representation of ray bending, as shown in Fig. 10, will be used. In the figure, r is the distance from the scattering region to the point of observation, and ϵ is the angular deviation imposed on the ray by the irregularities. This representation will be applied to diffraction in both the vertical and horizontal planes.

A. THE RAY-THEORY APPROXIMATION

The spatial extent of an irregularity strongly influences its effect on waves which propagate through it. In particular, the relation between the transverse scale size (Λ_T) of the irregularities (measured transversely to the ray path) and the length of the first Fresnel zone (F) determines the suitability of a ray-theory treatment ($\Lambda_T \gg F$) or a diffraction theory treatment ($F \gg \Lambda_T$). If it is assumed that parallel rays are incident on the scattering region, then

$$F = \sqrt{r\lambda} \quad , \tag{9}$$

where r is the distance from the receiver to the scattering region and λ is the wavelength. For the parameters of the measurements in this work, $r \approx 1300$ km and $\lambda \approx 12$ m. Therefore, $F \approx 4$ km. Since the scale size of the irregularities in question was determined in the previous chapter to be considerably larger than 4 km, a ray-theory treatment is appropriate.

B. THE EFFECTS OF A SINGLE IRREGULARITY

In this section it is assumed that the observed variations in phase-path length are caused by single isolated circular irregularities. The refractive index within the irregularity is given by

$$\mu = \mu_b + \frac{\Delta\mu_{max}}{\mu_b} \exp\left(-\frac{z^2}{\Lambda_T^2}\right) ,$$

where μ_b is the ambient (background) refractive index of the ionosphere, $\Delta\mu_{max}$ is the refractive index change at the center of the irregularity (the strength of the irregularity) and z is distance from the center of the irregularity.

1. Nature of the Wave Field Produced by a Single Irregularity

Computed ray paths through a single circular irregularity are shown in Fig. 11 for three different values of irregularity strength. Figures 11a, b and c illustrate the effect of successively stronger irregularities. The scales are greatly compressed in the direction of propagation in order to provide a convenient format.

The angle ϵ through which rays are bent when passing through such an irregularity is a function of the phase change, φ, produced by the irregularity and of the transverse scale size Λ_T of the irregularity. The wave field at the receiver plane is determined by the angular deviations of the rays and by the distance from the irregularity to the receiver. If the phase change of a ray passing through the center of an irregularity is defined as φ_{max}, the nature of the received wave field is determined by the ratio of φ_{max} to Λ_T/F. If φ_{max} is small compared to Λ_T/F, only a single ray will arrive at a given point on the ground (Fig. 11a). However, if φ_{max} is large compared with Λ_T/F, rays will cross before reaching the receiver (Fig. 11c), thus producing a field at the receiver plane which may be composed of three separate waves having slightly different arrival angles.

By calculating points of constant phase-path length (i.e., $\int \mu\, ds$ = constant) along each ray path, the shape of the resulting wave

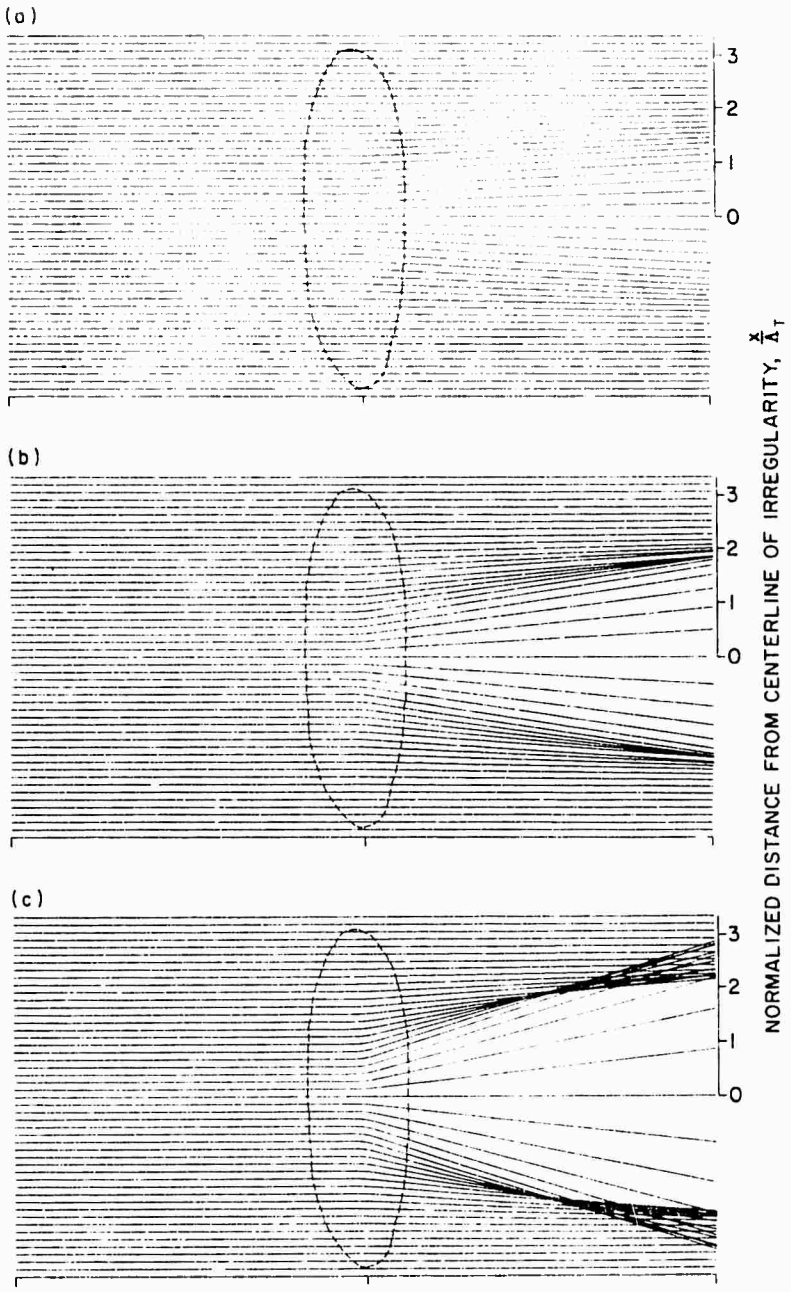

Figure 11. Computed raypaths through a gaussian irregularity.

(a) $\varphi_{max} < \Lambda_T/F$.

(b) $\varphi_{max} \approx \Lambda_T/F$.

(c) $\varphi_{max} > \Lambda_T/F$.

fronts may be determined. By computing the change in area of each flux tube (an arbitrary volume bounded by rays), the resulting distributions of field amplitude may be determined (with some restrictions in regions where rays are focused). Examples of the results of such calculations are shown in Figs. 12 and 13 for irregularities which produce maximum phase changes, φ_{max}, of φ_1, $4\varphi_1$, and $6.5\varphi_1$, where φ_1 is chosen arbitrarily simply to illustrate the effects of varying irregularity strengths. Note that the wave-front plots, Fig. 12, could be plotted on the ray tracings, Fig. 11; but the scale of interest is drastically different. For the irregularities we are studying, the total ray-path length is over 2600 km, while the maximum wave-front deviation is about 1 km.

In the presence of a single irregularity, the field at the receiver will be composed of one or three waves, depending on the strength and position of the irregularity. If multiple waves are present, the amplitudes of the waves will be similar, differing by only a few dB. As the strength or position of the irregularity changes with time, deep fades will be observed as the relative phase of the similar amplitude waves changes with time.

2. Relation of Variations in Phase-Path Length to Variations in Refractive Index and Electron Density

The two-dimensional single-irregularity model just described will now be used to estimate the variations in refractive index and electron density required to produce the experimentally observed variations in phase-path length. The calculations ignore the ray curvature produced by the slowly varying background refractive index. However, it is shown in Appendix B that these calculations nevertheless provide a valid relation between observed changes in phase-path length and changes in refractive index. Since the simple model assumes that all observed phase-path variation is caused by one individual irregularity, this calculation will set an upper bound on the electron-density variation. The peak-to-peak variations in P observed experimentally were in the range of 100 to 1000 m. Assuming that the irregularities are roughly circular in plan view (as was assumed in the raytracing), the length of the ray path in

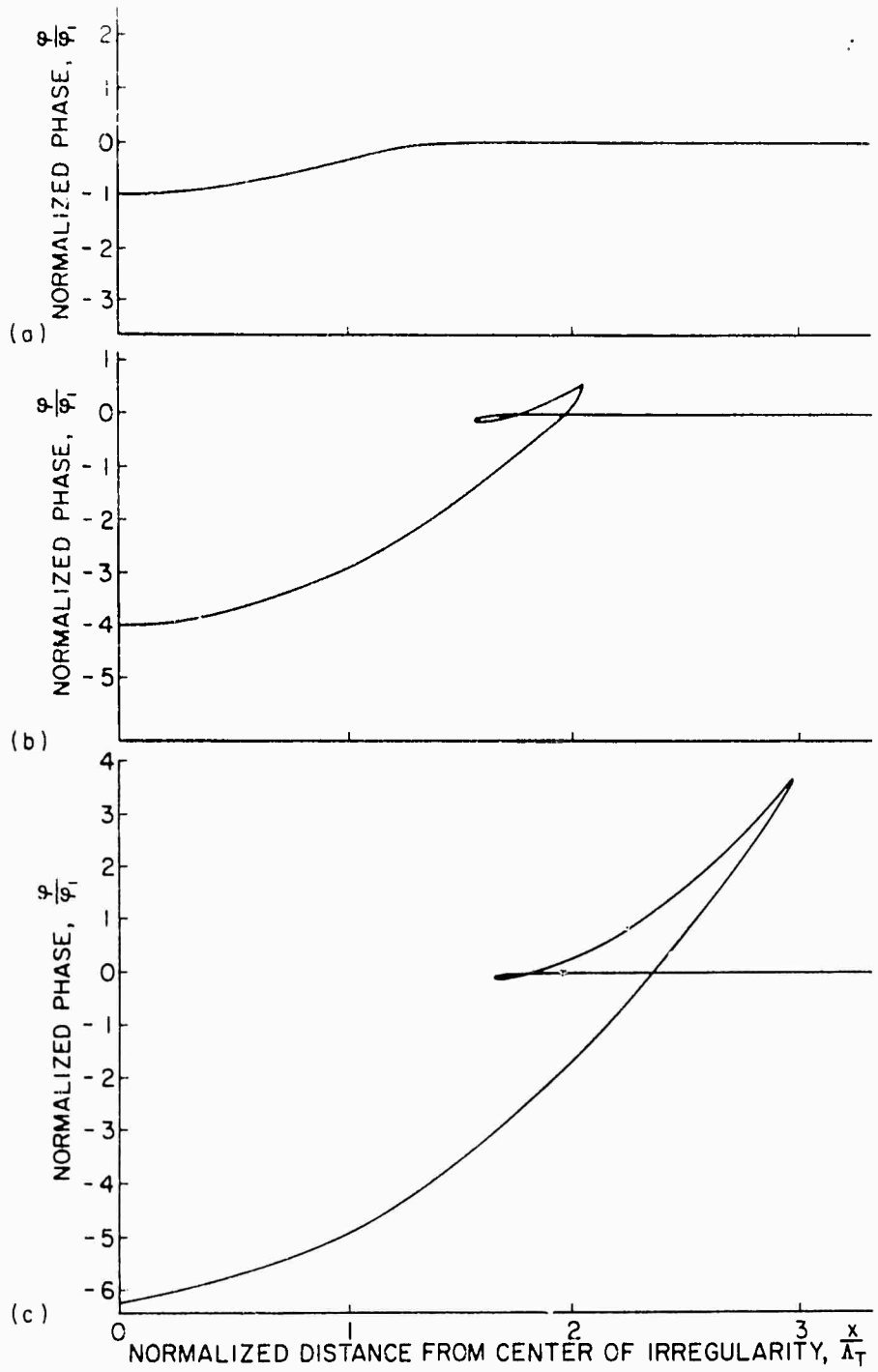

Figure 12. Computed received wavefronts for waves propagating through a gaussian irregularity.

(a) $\varphi_{max} = \varphi_1$ $(\varphi_{max} < \Lambda_T/F)$

(b) $\varphi_{max} = 4\varphi_1$ $(\varphi_{max} > \Lambda_T/F)$

(c) $\varphi_{max} = 6.5\varphi_1$ $(\varphi_{max} \gg \Lambda_T/F)$

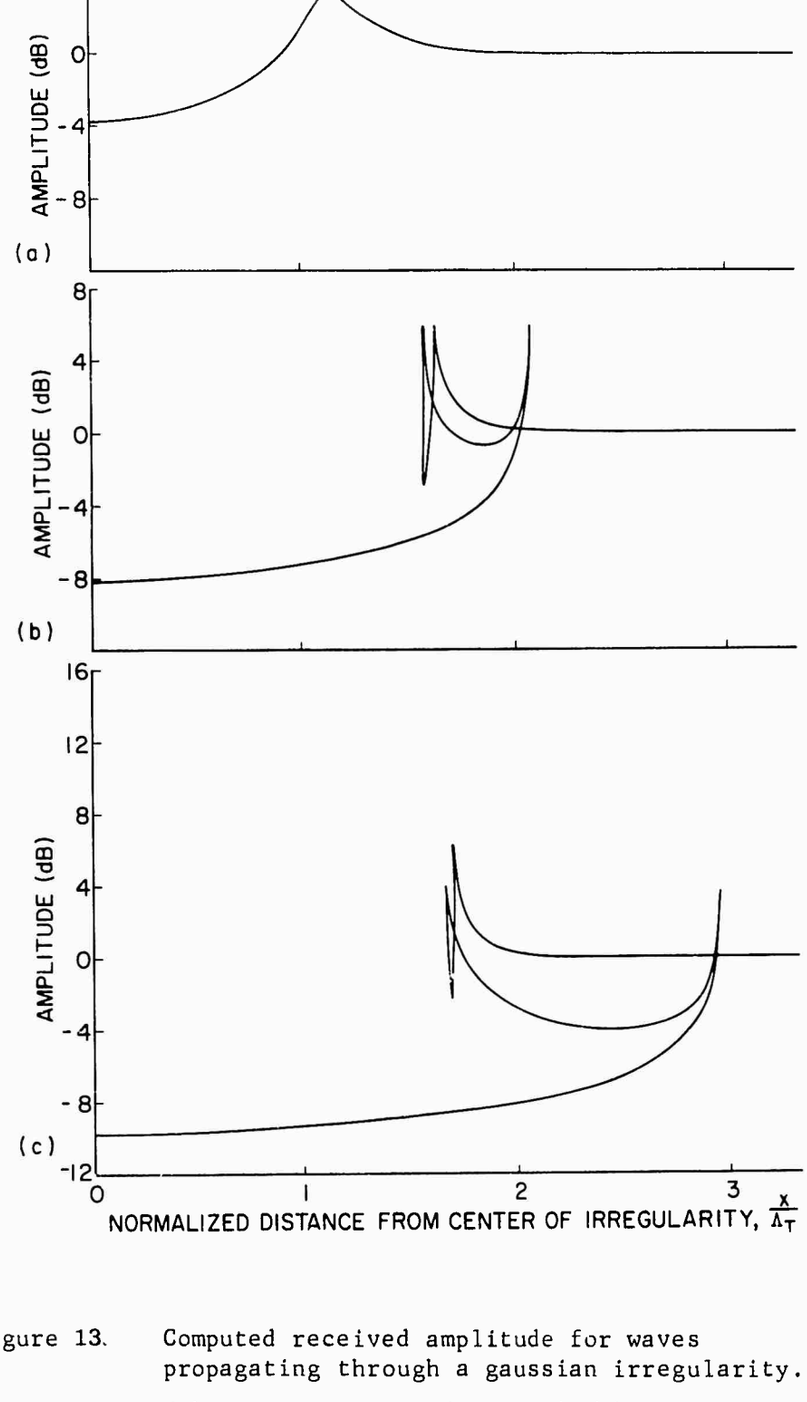

Figure 13. Computed received amplitude for waves propagating through a gaussian irregularity.

(a) $\varphi_{max} = \varphi_1$ $(\varphi_{max} < \Lambda_T/F)$

(b) $\varphi_{max} = 4\varphi_1$ $(\varphi_{max} > \Lambda_T/F)$

(c) $\varphi_{max} = 6.5\varphi_1$ $(\varphi_{max} \gg \Lambda_T/F)$

the irregularity is about 35 km. Therefore, the ray path is modified by about 100 to 1000 m in a distance of 35 km. From the defining equation of the ray-path length, Eq. (1), it is seen that $\Delta P/P$ is proportional to $\Delta\mu/\mu$. Therefore, the variations of refractive index are in the range of 0.3 per cent to 3.0 per cent. The relation between the electron density variation, $\Delta N/N$, and the refractive-index variation, $\Delta\mu/\mu$, is a function of the background refractive index, μ.

For the ionosphere, neglecting electron/ion collisions and the effect of the magnetic field (which are unimportant for this calculation) the refractive index is given by

$$\mu = \sqrt{1 - \frac{80.6\ N}{f^2}} \quad , \tag{10}$$

where N = electron density in electrons per cubic meter, and f = frequency in MHz.

Figure 14 is a plot of the per unit change in electron density, $\Delta N/N$, required to produce a one per cent change in refractive index, plotted against the background refractive index, μ. For the path and frequencies under investigation, the refractive index along the ray path varies from 1.0 to a minimum of about 0.7 at the maximum height of the ray. At a background refractive index of 0.7, a one per cent change in refractive index requires about a two per cent change in electron density. At points of lower height along the ray path, the refractive index is greater, and larger changes in electron density are required to produce the same modification of refractive index and hence of the ray path length. For the changes in refractive index observed in the present studies, electron density variations of 0.6 per cent to 6.0 per cent are required at the reflection height. Considerably greater changes would be required at other points on the ray path.

The calculated changes in electron density may be compared with the variations observed by others. A great deal of the information available on ionospheric irregularities has been acquired with vertical-incidence pulse sounders. However, ionospheric dispersion limits the time delay (range) resolution of measurements made with these sounders. Also, antennas

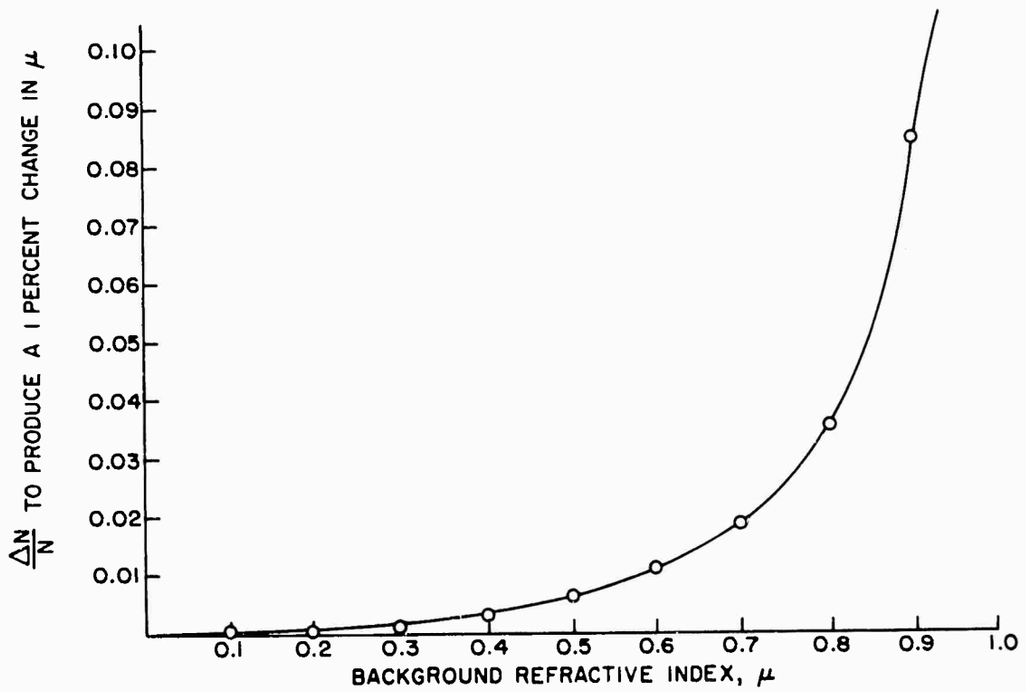

Figure 14. Change in electron density required to produce a one per cent change in refractive index.

having little directivity are usually employed with such sounders, causing their sensitivity to decrease for spatially small irregularities because of the spatial averaging effect of the antenna. According to Munro ('58), the lower limit for detection of medium-scale irregularities with vertical-incidence pulse sounders is "a few per cent" of the background electron density. It is therefore reasonable to assume that if the irregularities most prominent in our measurements are located near the ray reflection height, they would not be seen by vertical-incidence sounders, or at best would be at the lower limit of resolution for vertical-incidence techniques. We have already noted the difficulties involved in observing such irregularities using doppler Fourier analysis methods, and we have concluded that the irregularities we observe are at or below the lower resolution limit of this method.

The use of satellite signals in measuring small or weak irregularities is also limited. Satellite measurements indicate variations in the total electron content of the ionosphere between the observation point and the satellite, and hence are somewhat less sensitive in detecting irregularities of limited vertical extent than are ground-based measurements. Also, satellite measurements do not directly yield the altitude at which irregularities occur. Titheridge ('63) observed variations in total electron content in the range of 0.05 per cent to 7.0 per cent, which for the size, shape and altitude (somewhat below the F-layer peak) of the irregularities we observe, would require variations in electron density, with reference to the ambient background, of 0.5 per cent to about 25 per cent. It is likely that some of the smaller irregularities observed by Titheridge were the same type observed in the present work. However, satellite methods do not frequently observe irregularities as small (horizontally) as those observed here, because of the low probability that a ray path between a satellite and a ground station will pass through a given irregularity.

In summary, then, it appears that the irregularities whose existence and characteristics are proposed from the two-dimensional, single-irregularity model are of a size and strength range not readily observed using other techniques. Such irregularities are, however, very significant in their effect on HF oblique-incidence radio communication, as will be seen in Chapter IV.

3. Modifications of the Simple Two-Dimensional Model to Account for Background Variation in μ

So far, the effects of the curvature of the ionospheric ray paths in the vertical plane (vertical focusing), arising from the slowly varying refractive index of the background as the ray travels upward have not been considered. The simple model of Fig. 10 is directly applicable to horizontal (azimuthal) ray bending, if the value of F is modified appropriately for rays diverging from a point source. In this case $F = \sqrt{r\lambda/2}$, ignoring a minor error due to the curvature of the earth and the ionosphere. However, a realistic model for vertical ray beinding should include vertical focusing effects caused by the smooth variation with height of the ionospheric refractive index.

While ray bending effects may be determined for any specific irregularity distribution using computerized raytracing methods, it is of greater value in the present research to develop an analytical description of these effects. The correction for ionospheric focusing in the vertical plane may be made by determining the length of the first Fresnel zone (F) in the vertical plane for the region where the ray paths are affected by irregularities.

The fundamental definition of F is the distance along a wave front at which two ray paths to a receiving point differ by one-half wavelength (Born and Wolf, '64). The parameter F therefore describes the effect that phase changes introduced at different points across the wave front will have on the field at large distances from the phase-changing region. By computing wave fronts produced by radiation from a transmitter on the ground, using rays traced through a typical ionosphere, the distance F may be determined at various points along the ray paths. This was done to determine the value of F near the reflection height for a number of ranges and frequencies typical of long-distance HF communication. In Fig. 15 the ratio of the actual value of F to $\sqrt{r\lambda}$ at the reflection height is plotted for various ranges and frequencies. For the conditions of our measurements, the ratio of F to $\sqrt{r\lambda}$ is less than 2.0. The use of the actual value of F will allow the inclusion, in the following calculations, of the focusing effects produced by the smooth variation with height of refractive index in the ionosphere.

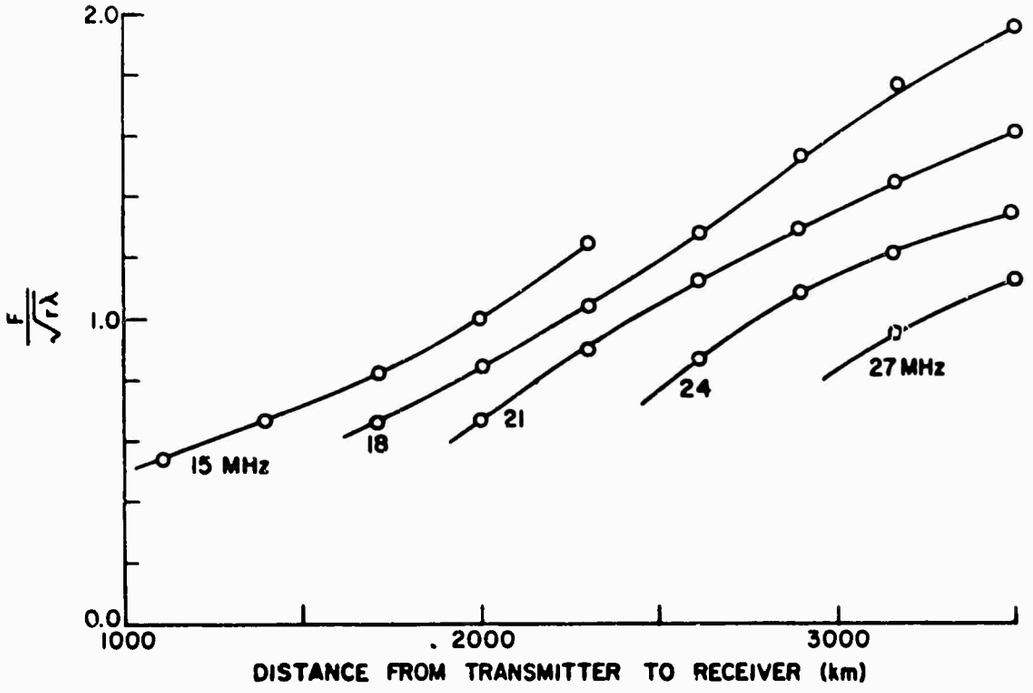

Figure 15. Computed Fresnel zone length at the reflection height for rays in the ionosphere.

C. THE EFFECTS OF MULTIPLE IRREGULARITIES IN THREE DIMENSIONS

The two-dimensional representation of propagation and as affected by irregularities (as in Fig. 10) will now be applied to both the horizontal and vertical axes of the irregularities, including the corrections for focusing determined in the previous section. The effects of multiple irregularities will also be included.

1. The Effect of the Presence of Multiple Irregularities on the Calculated Change in Electron Density

The raytracings shown in Fig. 11 are the results of raytracing through a single irregularity. There may be more than a single irregularity that influences wave field at the receiver. However, the number of such irregularities is probably not large, as the region where the ray path is most susceptible to irregularities of a given percentage deviation in electron density is limited to the region near the maximum height of the ray. In the presence of an isolated two-dimensional gaussian irregularity, the number of rays at the receiver will be one or three, depending on the strength and size of the irregularity (see Fig. 11). In the presence of more than one irregularity, a larger number of rays is expected to reach the receiver.

Chernov ('60) calculates the mean squared phase fluctuation $\overline{\varphi^2}$, due to propagation through an irregular medium described by a spatially stationary gaussian correlation of refractive index with distance, as

$$\overline{\varphi^2} = \sqrt{\pi}\ \overline{(\Delta\mu)^2}\ k^2 \Lambda_L L \quad , \tag{11}$$

where

$\Delta\mu$ = the change in refractive index,

$k = 2\ \pi/\lambda$,

L = the length of the scattering region,

Λ_L = the longitudinal scale size of the irregularity.

From the measurements made in this work, $\overline{\varphi^2}$ may be calculated. Using this estimate in (11), $\overline{(\Delta\mu)^2}$ can be estimated, assuming that the longitudinal and transverse scale sizes of the irregularities are known. For the single-irregularity model used previously, it was assumed that $\Lambda_T = \Lambda_L = L$. While these assumptions cannot be verified with the experimental geometry used, they do however produce reasonable values for $\Delta\mu$. If more than one irregularity affects a single ray path $(L > \Lambda_L)$, or if the irregularities are elongated in the direction of propagation $(\Lambda_L > \Lambda_T)$, smaller values of $\Delta\mu$ result. This would be acceptable in terms of known ionospheric characteristics.

2. The Range of Phase Changes Produced by the Observed Irregularities

Ray bending effects caused by irregularities are determined mainly by the phase change produced by the irregularities and the transverse (to the ray path) scale size Λ_T of the irregularities (horizontal and vertical). A variety of data taken during the experiments of this work, which is representative of the range of phase-path variations observed, is presented here. Figure 16 is an example of data representing quiet conditions. Phase-path length changes are expressed in wavelengths. The record shows a maximum change in phase-path length of about 20 wavelengths peak-to-peak. The trace is smooth, indicating that a single ray was dominating the measurement throughout the period of the observation. Figure 17 is a similar record, but with a greater observed deviation in phase-path length. The record is still dominated by a single ray throughout.

Some other effects occasionally appear in the records. Figure 18 shows the effect of alternate capture of the measurement by two rays having different doppler shifts. The record which would be produced by either of these rays separately is shown by the dotted lines. In this record, the measurement is still yielding a useful description of the changes in phase-path length for the rays. Finally, Fig. 19 is an example of a record taken under conditions in which the usefulness of the measuring technique has broken down because of the presence of a number of rays of different doppler shifts, each of which dominates the measurement for short periods of time.

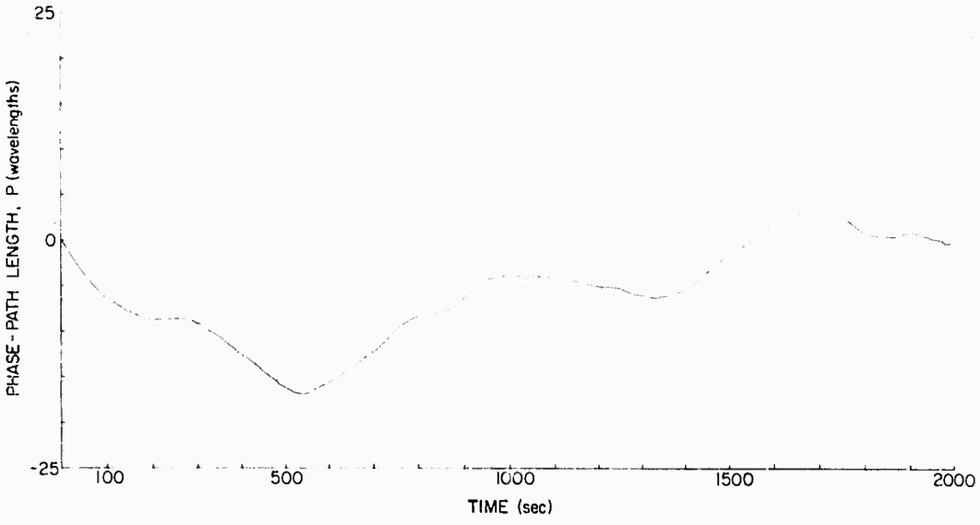

Figure 16. Phase-path length measurement for very quiet ionospheric conditions.

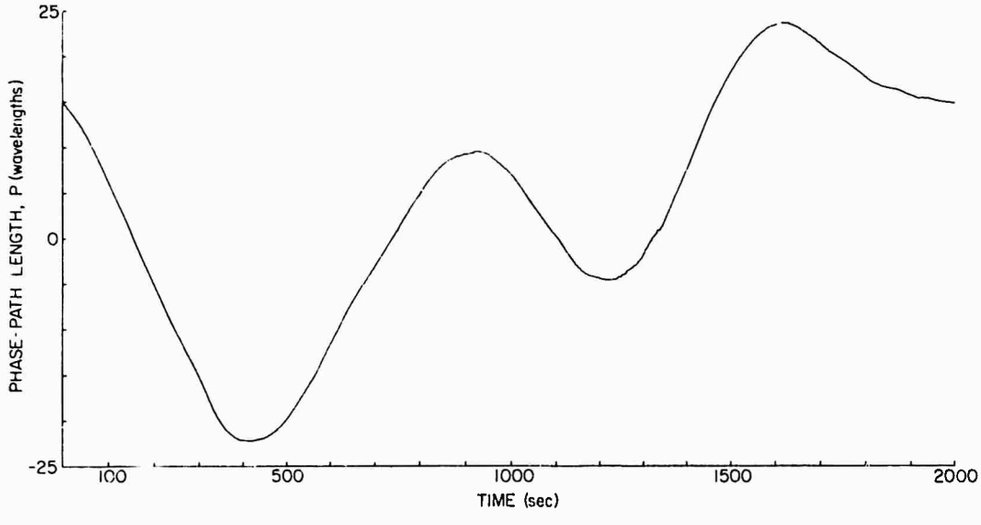

Figure 17. Phase-path length measurement for fairly quiet ionospheric conditions.

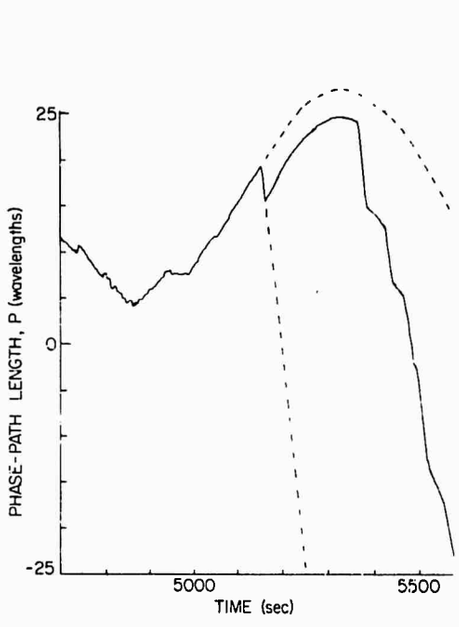

Figure 18. Phase-path length measurement alternately captured by two rays of comparable amplitude.

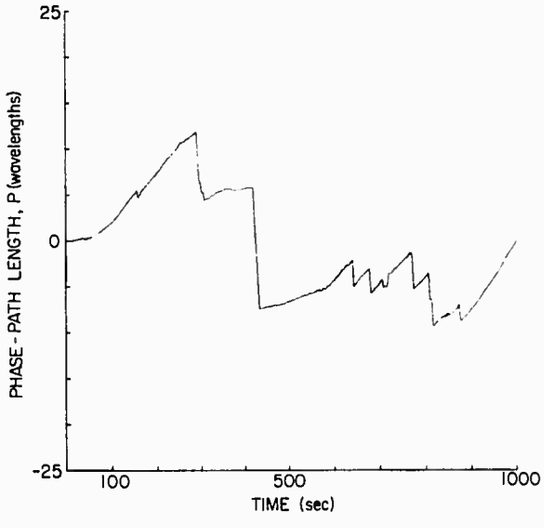

Figure 19. Phase-path length measurement for disturbed ionospheric conditions.

3. The Effects of the Observed Phase Changes

With the observed range of phase variations, $\overline{\varphi^2}$, in mind, the theoretically predicted wave-front effects in the presence of multiple irregularities can be determined. Chernov calculates the mean squared angular ray deviations $\overline{\epsilon^2}$ as a function of $\overline{\varphi^2}$ and of Λ_T, the transverse scale size of the irregularities.

$$\overline{\epsilon^2} = \frac{1}{\pi^2}\left(\frac{\lambda}{\Lambda_T}\right)\overline{\varphi^2} \quad . \tag{12}$$

Rays emerging from the scattering region are unchanged in amplitude or position, but have a change in angle imposed upon them. As the wave propagates through space to the receiving location, the rays converge or diverge (Fig. 11). Also, as the wave propagates, the amplitude at various positions across the wave will change due to the convergence and divergence of the rays. Manning ('68) describes two classes of wave fields which result from this process. The distinction is based upon the number of rays which are expected to arrive at one point on the ground. For weak, large or nearby irregularities, only a single ray will be expected to arrive at any one point on the ground. For stronger, smaller or more distant irregularities, rays will cross before reaching the plane of the receiver, and multiple rays will arrive at least some points on the ground. Manning calculates the expected number of rays at a given point (for the two-dimen ional geometry) as

$$E[R] = 1 + \frac{\sqrt{2}}{\pi^{3/2}}\frac{F}{\Lambda_T}\sqrt{\overline{\varphi^2}} \quad , \tag{13}$$

where $E[\cdot]$ denotes expectation. The factor $(\pi^{3/2}/\sqrt{2}) \approx 4$. So, if $\overline{\varphi^2} \ll 16(\Lambda_T/F)^2$, it is probable that only one ray will arrive at a given point on the ground; whereas if $\overline{\varphi^2} \gg 16(\Lambda_T/F)^2$, more than one ray can arrive at the same point.

For the case where the scattering region contains irregularities which have variations in two dimensions transverse to the ray path, Manning further shows that

$$E[R] = E[R_V] \cdot E[R_H] \quad , \tag{14}$$

where $E[R_V]$ = the expected number of rays produced by vertical bending, and $E[R_H]$ = the expected number of rays produced by horizontal bending.

As was previously pointed out, the effective value of F is modified in the case of vertical ray deviations by the focusing effect of the smooth variation in μ with height in the ionosphere. By using the corrected value of F for vertical bending as plotted in Fig. 15, and $F = \sqrt{r\lambda/2}$ for horizontal bending, the calculations of the expected number of rays, as well as the signal strength calculations (Fig. 13), can be corrected for the effect of vertical bending in the ionosphere.

For the observations made in this work, $\overline{\varphi^2}$ was found to vary over the range of approximately 100 to 10,000 radians squared. For a horizontal scale size of 45 km and a vertical scale size of 20 km, $E[R]$, $E[R_V]$ and $E[R_H]$ are plotted against $\sqrt{\overline{\varphi^2}}$ in Fig. 20. It can be seen that the major contribution of the ionosphere to the multiple rays arriving at the receiver is refraction in the vertical plane, and that for all but the quietest conditions seen during our observations, $E[R]$ is greater than 1, but usually less than 10. The value of $E[r]$ from Fig. 20 can be regarded as an upper limit on the expected number of rays reaching the receiver. Therefore it is expected that wave fields such as those of Figs. 11b and 11c will be common, and in the presence of more than a single irregularity, somewhat more complex.

The total amplitude and phase of the wave field at a point on the ground can now be described in terms of the summation of R waves. The relative amplitudes of the waves will be in the range shown in Fig. 13. The resulting total amplitude and phase fluctuations are described in Chapter IV.

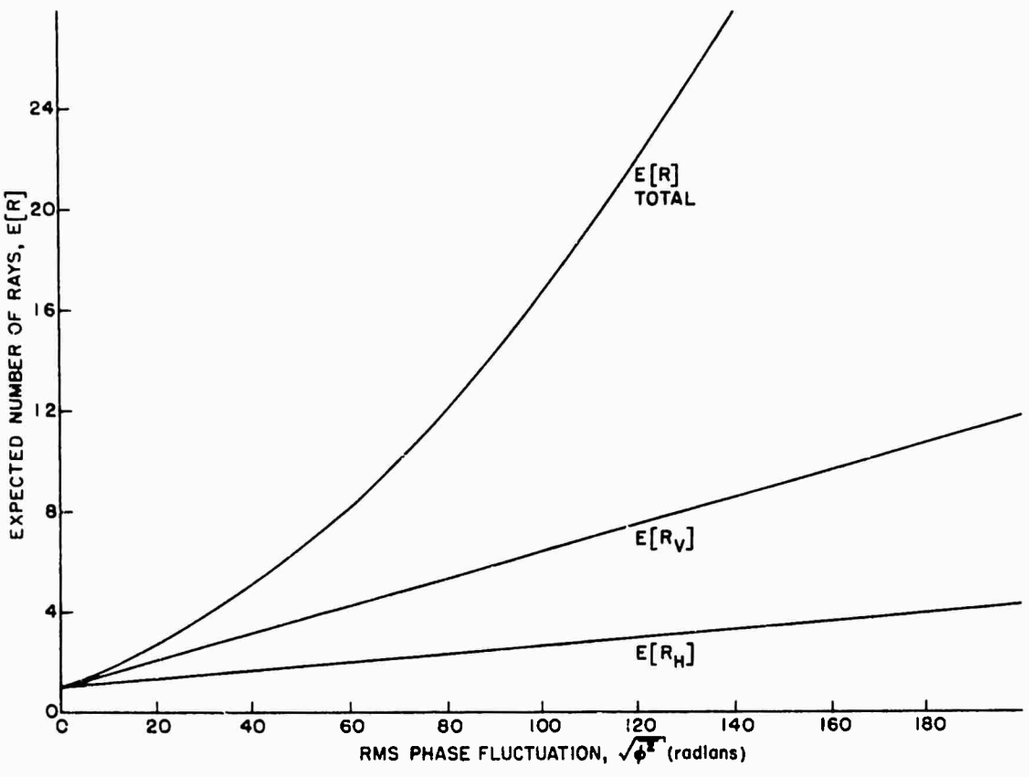

Figure 20. Expected number of rays for the given path and measured irregularity scale sizes.

D. EFFECT OF THE EARTH'S MAGNETIC FIELD

Thus far the effect of the earth's magnetic field on oblique-incidence HF ionospheric propagation has been ignored. This effect may be described either in terms of the rotation of the plane of polarization of a linearly polarized wave (Faraday rotation) or in terms of splitting of the wave incident on the ionosphere into two components, each of which exhibits one of two possible characteristic polarizations for a wave of that direction and frequency in the ionosphere, and propagates over a slightly different path. The field produced by the combination of these two component waves at any point on the path produces the linearly polarized wave described by the first method.

The concept of Faraday rotation is frequently valid for oblique-incidence ionospheric propagation. As a wave propagates through the ionosphere its plane of polarization (assuming that the transmitted wave is plane-polarized) rotates slowly with distance in the refracting region of the ionosphere. This rotation causes the wave arriving at the receiver to have a plane of polarization determined by the amount of Faraday rotation which occurred in the ionosphere. If the receiving antenna is linearly polarized, the received signal strength will vary as the plane of polarization of the received wave rotates. For the path used in our experiments, the total number of rotations of the plane of polarization along the path of the ray is calculated by raytracing (Croft '69) to be about 20 turns under typical daytime conditions.

It is not possible to develop a simple relation between variations in the total phase-path length and changes in the number of Faraday turns, for a ray in the ionosphere. Therefore, various assumed ionospheric electron density profiles, representative of various times of day, were used for tracing rays, while calculating both the total phase path and the total number of Faraday turns. A variation of 50 to 100 wavelengths in P produced a change of one turn in Faraday rotation. This implies that for smooth changes in the ionosphere, only one or two nulls in received signal strength should occur for each 50 to 100 wavelengths of observed change in P.

When considering the effects of irregularities, it is more revealing to consider the model consisting of two component rays propagating over

slightly different paths, than it is to use the concept of Faraday rotation. The two rays are customarily denoted as ordinary (O) and extraordinary (X). If these rays have phase-path lengths P_o and P_x, a change in the difference between the two phase-path lengths $(P_o - P_x)$ of one wavelength will cause one Faraday-turn null at the receiver. By tracing rays using the ESSA three-dimensional ray-tracing program (Jones '68), it was determined that for the conditions of our measurements, the O and X components will be separated vertically by a maximum of 0.5 km to 1.0 km at their greatest height in the ionosphere. Laterally, they will be separated by no more than 200 m. These numbers represent the ray spacings under undisturbed ionospheric conditions, i.e., with no irregularities present. If an irregularity causes the phase-path length of one of the rays to change with respect to that of the other ray by one wavelength, one null will be observed at the receiver. Based on the measured irregularity scale sizes, and assuming gaussian irregularities, the changes in phase-path length for two rays spaced by about 1 km vertically are highly correlated--of the order of 0.98. Therefore, for irregularities such as those studied and modeled in this work, about one Faraday null is expected for each 50 wavelengths change in P due to irregularities. Based on the above calculations, then, both irregularities and smooth variations in the ionosphere are expected to produce variations in the received polarization which will cause one receiver null for each 50 to 100 wavelengths change in P. This sets an upper limit to the number of such nulls which can be explained on the basis of the measured irregularity sizes.

IV. SIGNAL-STRENGTH FLUCTUATIONS

In Chapter II a series of measurements of the phase characteristics of HF obliquely propagated ionospheric waves was described. These measurements allowed a determination of the size and strength range of irregularities which are present in the ionosphere under quiet conditions. In Chapter III the effects which would be anticipated for waves propagating through such irregularities were examined. The expected number of rays which would be produced by these irregularities was determined and the expected relative magnitudes were found. In the present chapter, the amplitude variations which are observed under quiet ionospheric conditions are examined to verify that observed amplitude fluctuations are explained in terms of interference of rays. In addition, other possible causes of the observed amplitude fluctuations are discussed.

The envelope-amplitude fluctuations of a received signal can be described by their statistical distribution. The probability density function for the envelope-amplitude, $\Phi(E)$, will be calculated for various assumptions about the received waves. These calculated distributions will be compared with histograms of observed envelope-amplitude fluctuations. The histograms are plotted so that the densities of the measured values of envelope-amplitude, $W(E)$, are directly comparable with the computed probability-density functions. The mean envelope amplitude $\bar{E}$ is used as a scale factor in plotting both the computed and observed envelope-amplitude distributions.

In addition to the density functions themselves, the normalized variance of the envelope amplitude, σ^2, will be calculated for both predicted and observed amplitude fluctuations. The value of σ^2 is given by

$$\sigma^2 = \frac{\overline{E^2}}{(\bar{E})^2} - 1 \quad .$$

A second statistic, $\overline{\varphi^2}$, is also calculated for each of the assumed forms of the received wave field. Here φ is the difference between the phase of the received signal at any instant of time and the phase

of the strongest of the signal's component waves. The values of σ^2 and $\overline{\varphi^2}$ may be used to determine the efficiency of receiving antennas under certain conditions. This subject will be discussed briefly in the next chapter.

A. MULTIPLE WEAK-SCATTERING INTERPRETATION OF AMPLITUDE FLUCTUATIONS

Booker, Ratcliffe and Shinn ('50) applied diffraction theory to the ionospheric propagation problem by describing scattering in the ionosphere in terms of a scattering region composed of a thin screen of small, weak phase-changing irregularities. The signal which emerges from such a scattering region can be characterized in terms of a specular component and a cone of scattered rays. The "coherence ratio", β, is used to describe the ratio of the energy of the specular component to the energy of the scattered rays. The width of the cone of scattered rays is determined by the size of the irregularities in relation to the wavelength employed. The cone of rays is made up of a large number of rays having random amplitudes and phases. If the number of scattered rays reaching the receiver is statistically large, the expected envelope-amplitude distributions for the sum of a sine wave and narrow-band random noise, as derived by Rice ('45), may be used to predict analytically the amplitude fluctuations produced by the specular and scattered components of ionospherically propagated waves. Rice derives the probability density for the envelope-amplitude of such a signal as

$$\Phi(E) = \frac{2E}{E_n^2} \exp\left(-\frac{E^2 + E_S^2}{E_n^2}\right) I_o\left(\frac{2E_S E}{E_n^2}\right) \qquad (15)$$

where (in the notation used in the present report):

E = the envelope amplitude of the received signal,

E_S = the amplitude of the specular component,

E_n = the amplitude of the scattered component,

and

I_o is the zero-order Bessel function of imaginary argument.

Curves of $\Phi(E)$, using the normalizations employed by Rice, are shown for different values of the parameter $s = \sqrt{2\beta}$ in Fig. 21. Before an experimental amplitude density distribution may be compared with these curves, the parameter β must be determined. β is related to the measureable quantity $\overline{E^2}/(\bar{E})^2$, the ratio of the mean squared amplitude to the squared mean of the amplitude, by the relation

$$\frac{\overline{E^2}}{(\bar{E})^2} = \frac{4(1+\beta^2)\exp(\beta^2)}{\pi\left[(1+\beta^2)I_o\left(\frac{\beta^2}{2}\right) + \beta^2 I_1\left(\frac{\beta^2}{2}\right)\right]^2}, \qquad (16)$$

where I_o and I_1 are Bessel functions of imaginary argument. This function is plotted in Fig. 22. $\overline{E^2}/(\bar{E})^2$ must lie in the range $1 < \overline{E^2}/(\bar{E})^2 < 4/\pi$.

Experimentally determined amplitude distributions may be compared with the Rice distributions in order to determine the applicability of the multiple weak-scattering theory proposed by Booker, Ratcliffe and Shinn. Because of the necessity for calculating β before plotting the experimental distributions, Rice's method of displaying amplitude distributions (Fig. 21) is not suitable for conditions where Eq. (15) may not apply. Therefore, the Rice distributions are replotted in Fig. 23 for various values of β, using the mean amplitude $\bar{E}$ as a scale factor. These graphs were computed using a random-number generator and the Monte Carlo method. This computation method will be used later in connection with other models of amplitude fading. Note that for β equal to 0 (a random component only), the distribution is the Rayleigh distribution.

The results of applying the multiple weak-scattering theory to oblique F-layer ionospheric propagation have not provided a consistent picture of the ionospheric mechanism responsible for the observed signal fluctuations. Al'pert ('63) discusses some of the results of such measurements and some of the problems encountered in their interpretation.

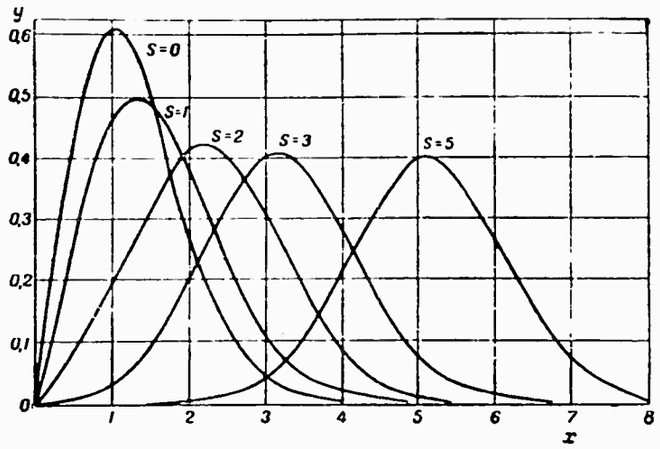

Conversion:

$$s = \sqrt{2\beta}$$

$$x = \sqrt{2}\left(E/E_n\right)$$

$$y = \Phi\left(E\right) \cdot \left(E_n/\sqrt{2}\right)$$

Figure 21. Amplitude distributions as derived by Rice for a specular ray and a cone of scattered rays.*

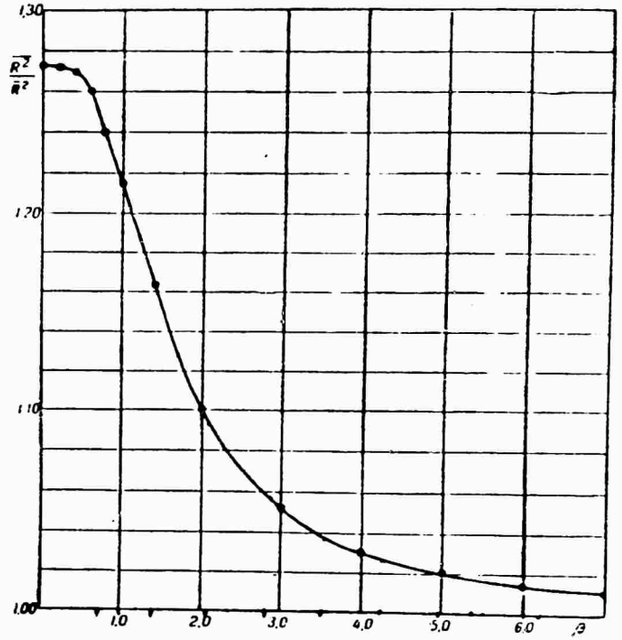

Conversion: $\dfrac{\overline{R^2}}{\overline{R}^2} = \dfrac{\overline{E^2}}{\left(\overline{E}\right)^2}$.

Figure 22. The relation of wave coherence, β, to amplitude fluctuation, $\overline{R^2}/\overline{R}^2$, for the small scattering model.*

*From Radio Wave Propagation and the Ionosphere, Ya. L. Al'pert, (translation from the Russian), Consultants Bureau, New York, 1963.

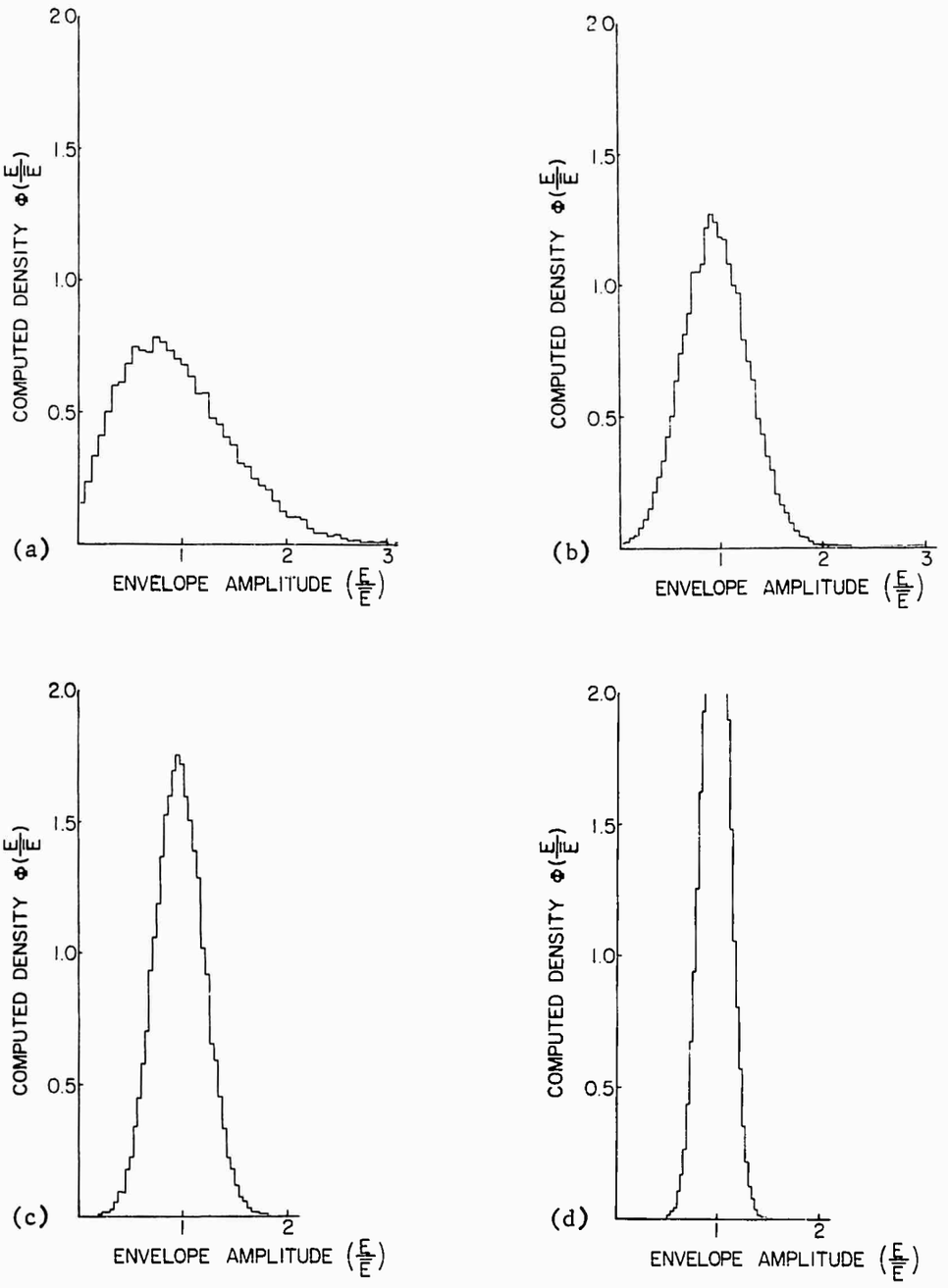

Figure 23. The Rice amplitude distribution computed using the Monte Carlo method and plotted with the mean envelope amplitude $\bar{E}$ as a scale factor.

(a) $\beta = 0$, $\sigma^2 = 0.272$.

(b) $\beta = 2$, $\sigma^2 = 0.101$.

(c) $\beta = 3$, $\sigma^2 = 0.054$.

(d) $\beta = 5$, $\sigma^2 = 0.024$.

Measurements of β are reported in the range from 0 to 10, with usual values in the range of 2 to 4. No numerical evaluation of how well the observed data fit the predicted results of the multiple weak-scattering theory is presented. However, Al'pert notes that in about 30 per cent of the observations, the value of $\overline{E^2}/(\overline{E})^2$ exceeds $4/\pi$, the maximum value permitted by the theory. Also, in about 20 per cent of the observations, distributions with more than one maximum are observed. These discrepancies lead Al'pert to conclude that some other mechanism must be contributing to the observed signal-strength fluctuations.

The same ionospheric scattering model used in the amplitude fluctuation studies discussed above has been applied by others in analyzing the phase fluctuations observed on pairs of spaced antennas. Whale and Gardiner ('66) derive unique probability distributions for the difference in phase measured at two spaced antennas as a function of β and the spatial autocorrelation function of the scattered component alone. Whale and Boys ('68) and Boys ('68) use this method and find for one-hop propagation, that β is usually quite high with measured values of 10 or more, indicating that the received wave is highly specular. The results of these phase measurements are not compatible with those commonly obtained from amplitude measurements using the Rice theory.

B. INTERPRETATION ON THE BASIS OF LARGE IRREGULARITIES

The signal-strength fluctuations which are expected in the presence of large irregularities will now be examined in terms of the amplitude distributions which could be produced by such irregularities. Computed envelope-amplitude probability-density distributions $\Phi(E/\overline{E})$ will be used to gain some insights into the effect of varying parameters on the shapes of these distributions. Also, the normalized variance of the amplitude fluctuations will be computed for comparison with the known limits for this statistic under the random-noise (multiple weak-scattering) representation. Measurements of the density distribution of observed amplitude fluctuations, $W(E/\overline{E})$, will be compared with the computed probability-density distributions. Four different possible sources of signal amplitude variation will be discussed. These are focusing, multipath interference, polarization mismatch, and absorption.

1. Focusing

The spatial variations in refractive index produced by ionospheric irregularities cause changes in the convergence or divergence of rays. This in turn causes variations in the energy density between adjacent rays. This change in energy density will produce variations in the observed strength of a given wave at a distance from the refracting region. As can be seen from the raytracings in Fig. 11, the variations in amplitude increase with distance from the scattering region. These variations are in the range of a few decibels for the irregularities which we have proposed. (See Fig. 13.) In cases where only a single ray is present at any point in the receiver plane, we would therefore expect to see signal-strength variations of this order of magnitude. In the case of multiple rays, it is noteworthy that the difference in amplitudes for the various components is again only a few dB. This fact will be of considerable importance in considering multipath interference.

If changes in received amplitude are attributable only to variations in the strength of a single component due to focusing, the expected fluctuations in signal strength would be a few dB. This is observed at times on HF paths. It has also been noted in ground backscatter radar observations. Figure 24a is a record of signal-strength variations of the type observed over the path used for the phase measurements of this report. However, signal-strength fluctuations as small as these are much more the exception than the rule. Figures 24b and 24c show examples of more typical signal-strength records over this path. Variations such as these cannot be explained on the basis of focusing due to irregularities.

2. Multipath Interference

Inasmuch as the irregularity model developed in Chapter III predicts that because of the effect of even a single irregularity, the expected number of rays at the receiver location will frequently be greater than one, the effects on total signal strength which will be produced by the summation of several rays must be considered. As can be seen from the amplitude plots in Fig. 13, the amplitudes of multiple rays are not very different from one another. Considering the vector addition of rays, as was done in Chapter II, it can be seen that the

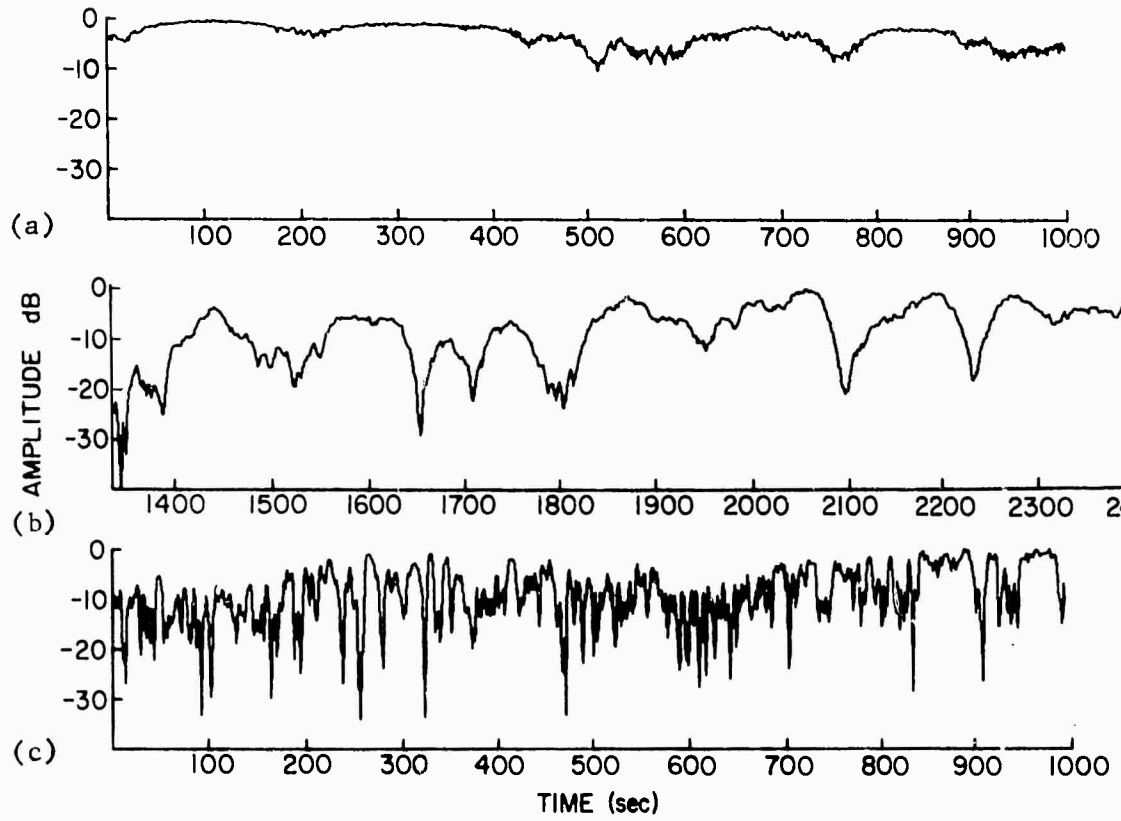

Figure 24. Observed signal-strength fluctuations for the Arkansas--Los Banos path.

(a) Little fading.
(b) Moderate fading.
(c) Severe fading.

possible range of amplitudes for the sum will be bounded by the summation of the ray amplitudes as an upper limit, and by the difference between the largest ray and the summation of the remaining rays as a lower limit. If the lower limit is negative, then all values from zero to the upper limit are possible (as we are interested in the envelope amplitude). The phases of the multiple rays vary sufficiently that in performing the vector summations, it will be assumed that the phase of each ray is uniformly distributed in the range of zero to 2π. This assumption is usually valid for the measurement periods used in this work, which span a number of signal minima. Computed amplitude probability-density distributions calculated for two rays and three rays having amplitude differences of a few dB (such as we expect to encounter based on the work of the previous chapter) are shown in Figs. 25a and b. Note that these amplitude distributions are quite different in appearance from those calculated using the random-noise representation for a large number of small scatterers and a strong specular component (see Fig. 23).

3. Polarization Mismatch

As was pointed out in Chapter III, the ionosphere is birefringent because of the presence of the earth's magnetic field. Therefore, if a linearly polarized wave is incident on the ionosphere, it will be split into two components of differing elliptical polarization, and each component will travel a slightly different path through the ionosphere. Upon emerging from the ionosphere, these two components (the ordinary and extraordinary rays) will add to produce some resultant polarization which is a function of the difference in path lengths for the components, and of the difference in strength of the components. At the end of Chapter III, it was shown that very little differential in path length or signal strength between the ordinary and extraordinary rays was expected to be introduced by ionospheric irregularities. If this is the case, the emerging waves will sum to form a linearly polarized wave (still assuming that the incident wave was linearly polarized). However, the plane of polarization will no longer be the same as that of the incident wave; and furthermore, it will be time-varying. If a circularly polarized antenna is used to receive such a wave, its response will be constant,

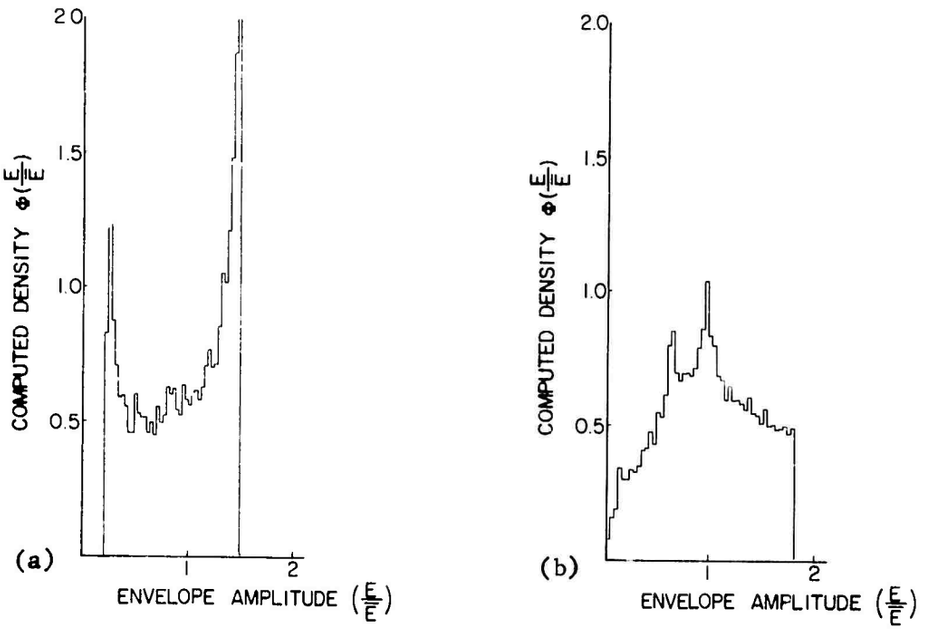

Figure 25. Computed amplitude distribution for the random vector sum of rays.

(a) Two rays, amplitudes = 1.0, 0.7. - $\sigma^2 = 0.175$, $\overline{\varphi^2} = 0.53$.

(b) Three rays, amplitudes = 1.0, 0.7, 0.5. - $\sigma^2 = 0.200$, $\overline{\varphi^2} = 0.80$.

regardless of the plane of polarization of the wave. In practice, it is difficult to construct and test an antenna designed to be sensitive to circular polarization for the frequencies and low radiation angles used for long-range HF communication. If a linearly polarized receiving antenna is used, a polarization mismatch will result, producing variations in response depending upon the instantaneous plane of polarization of the received wave. The signal amplitude from such an antenna will be proportional to $\cos \alpha$, where α is the angle between the planes of polarization of the incident wave and the antenna. The two components (O and X) arriving at a linearly polarized receiving antenna may be represented by two linearly polarized waves having amplitudes equal to the fraction of each wave's energy which lies in the plane of polarization of the receiving antenna. The amplitudes will remain fixed over long periods of time, since the polarization of the received components is determined primarily by the ray direction and the earth's magnetic field. Figure 26 shows the calculated amplitude distributions which would be expected for two waves of differing relative amplitudes. The distributions show sharp upper and lower limits in amplitude, corresponding to the sum and difference of the two rays.

4. Absorption

Waves propagating in the ionosphere also suffer losses due to absorption of energy associated with particle collisions. With the exception of periods of severe solar storm activity, the loss due to absorption is very small for frequencies above a few megacycles. Variations in loss from this mechanism are neglected in this work.

C. SURVEY OF AMPLITUDE DISTRIBUTIONS

We shall now examine a number of computed amplitude probability-density distributions in order to understand the characteristics imparted to such distributions by various signal combinations. We have already seen some distributions in the discussion of fading mechanisms.

A single ray of constant amplitude will naturally produce an impulse in amplitude probability density at the mean value (Fig. 27a). Combinations

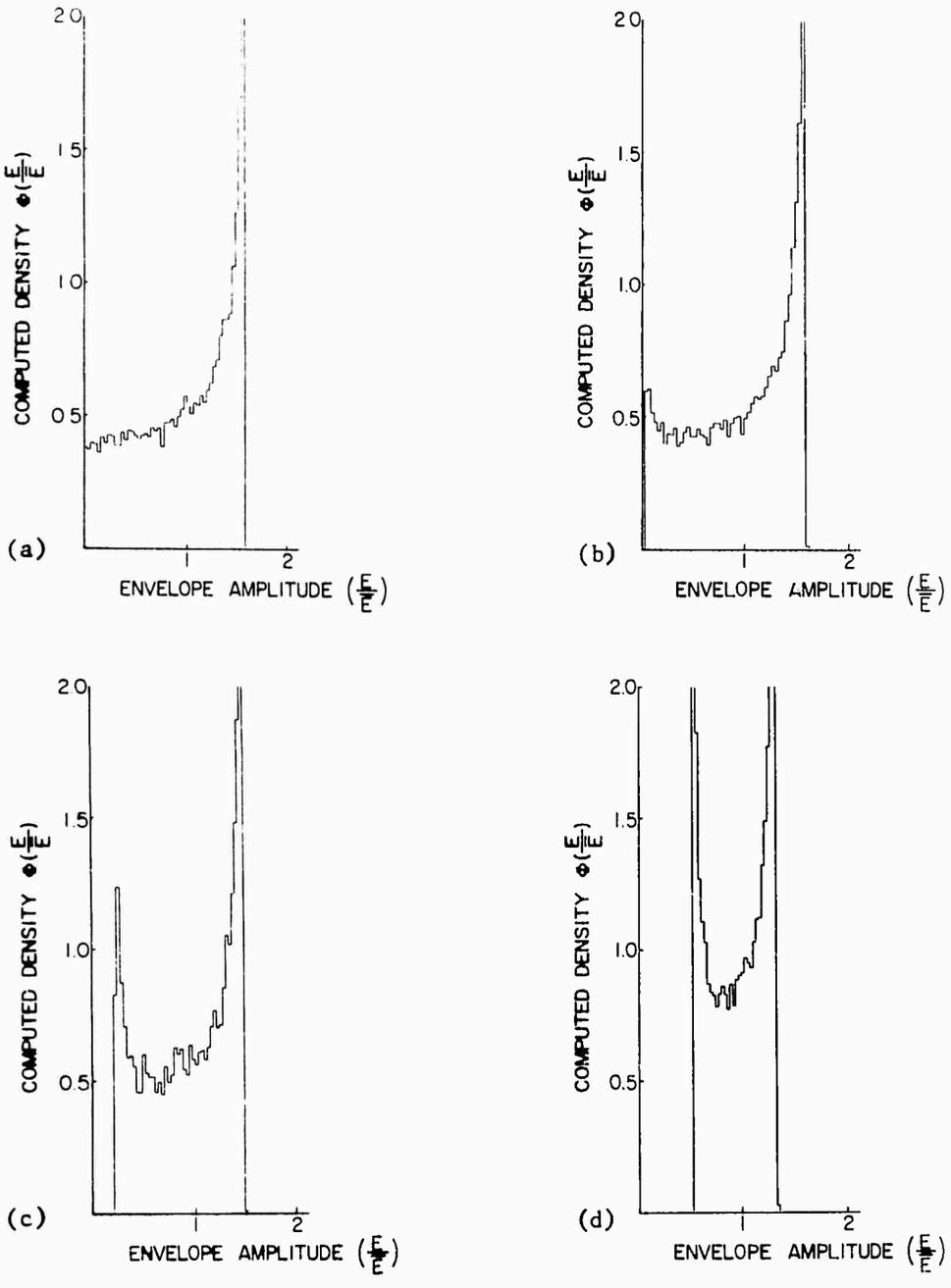

Figure 26. Computed amplitude distribution for the random vector sum of two rays.

(a) Amplitudes = 1.0, 1.0. - $\sigma^2 = 0.233$, $\overline{\varphi^2} = 0.90$.

(b) Amplitudes = 1.0, 0.9. - $\sigma^2 = 0.231$, $\overline{\varphi^2} = 0.74$.

(c) Amplitudes = 1.0, 0.8. - $\sigma^2 = 0.205$, $\overline{\varphi^2} = 0.63$.

(d) Amplitudes = 1.0, 0.4. - $\sigma^2 = 0.073$, $\overline{\varphi^2} = 0.29$.

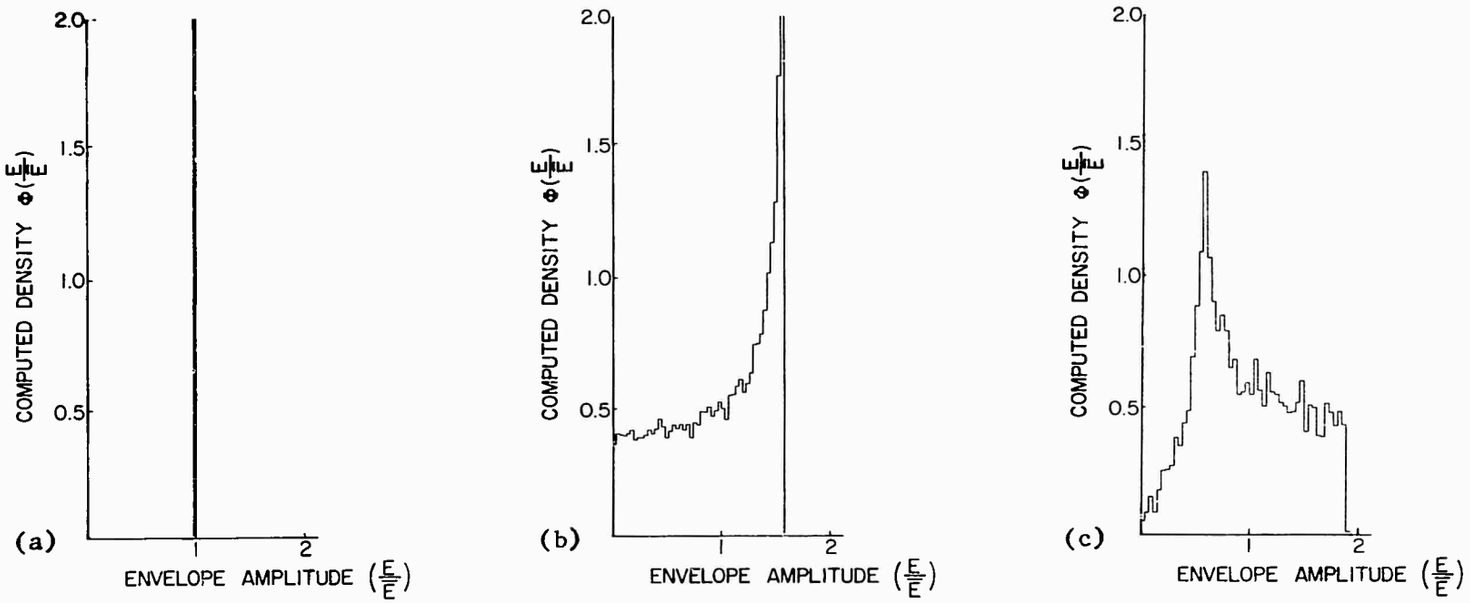

Figure 27. Computed amplitude distribution for the random vector sum of rays.

(a) One ray, amplitude = 1.0. - $\sigma^2 = 0.00$, $\overline{\varphi^2} = 0.00$.

(b) Two rays, amplitudes = 1.0, 1.0. - $\sigma^2 = 0.233$, $\overline{\varphi^2} = 0.93$.

(c) Three rays, amplitudes = 1.0, 1.0, 1.0. - $\sigma^2 = 0.233$, $\overline{\varphi^2} = 0.93$.

of two or three rays of equal amplitude produce the distributions shown in Figs. 27b and 27c. The case of two unequal rays has already been seen in connection with the discussion of polarization effects (Fig. 26). The two-ray distributions exhibit a double peak, with the spacing between the peaks inversely related to the difference in the strengths of the two rays.

In Fig. 28, the amplitude distributions produced by three rays of various relative magnitudes are plotted. They tend to exhibit the double peaked nature of the two-ray distributions, but are considerably smoother, and do not have the sharp upper and lower amplitude limits of the two ray distributions. The spacing of the two peaks is seen to increase as the relative strength of the middle amplitude component increases, or as the weakest component decreases. The clarity of the peaks is affected by the strength of the weakest component and by the separation of the peaks.

As more components of comparable magnitude are added, the characteristic features of the distributions decrease, approaching the Rayleigh distribution. Figure 29a shows a distribution produced by six rays. When the number of rays becomes large, it is not possible to interpret a measured amplitude distribution in terms of known distributions, other than to say that a large number of rays appears to be present. An exception occurs if the distribution is dominated by a few strong rays, but other rays of considerably lower amplitude are present. The weaker components then may not mask the features of the distribution, but only smooth out the features. Several distributions of this type are shown in Fig. 29.

In the discussion of polarization mismatch, amplitude distributions which would be expected if only one ordinary and one extraordinary ray should arrive at the receiver were discussed. If multiple ray paths exist, each composed of an ordinary and an extraordinary component, then at least four rays will arrive at the receiver. This circumstance will increase the likelihood of having distributions which resemble the Rayleigh distribution. Figures 30a and 30b show examples of this type of distribution for equal ordinary and extraordinary component strengths. The representation used in calculating these distributions for multi-ray propagation with both ordinary and extraordinary components assumes that the polarization of each of the paths is independent. Because of the

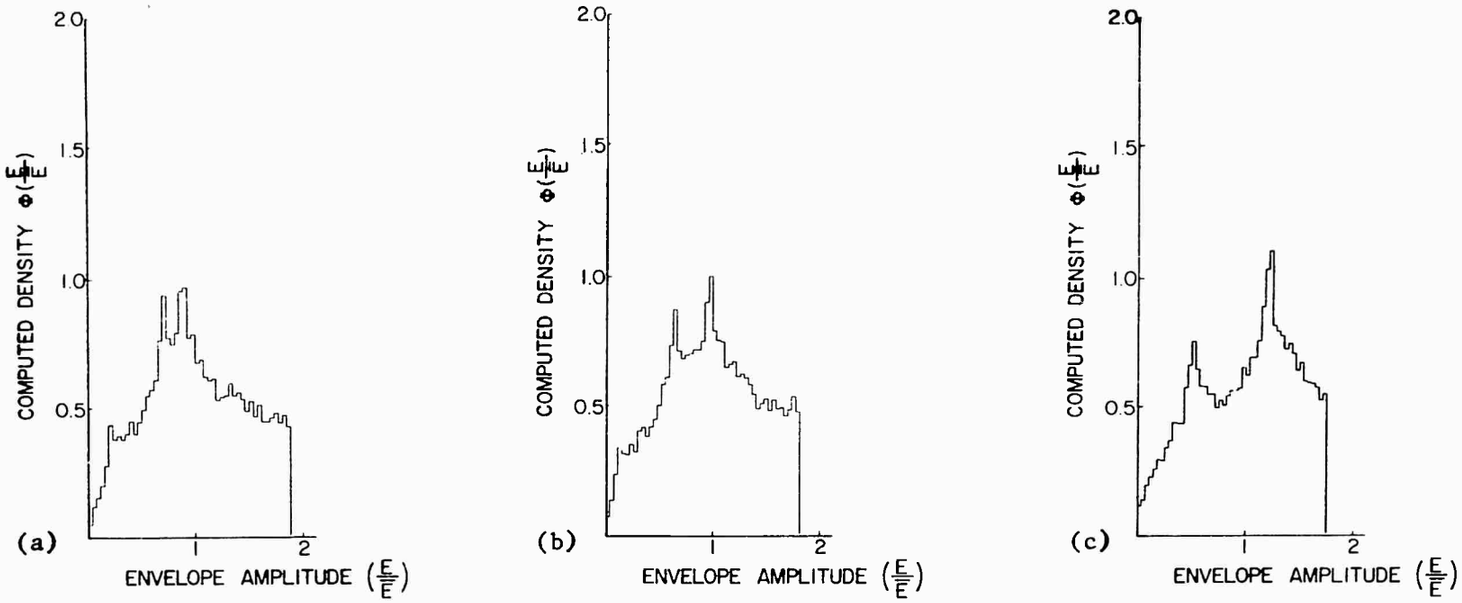

Figure 28. Computed amplitude distribution for the random vector sum of three rays.

(a) Amplitudes = 1.0, 0.7, 0.6. - $\sigma^2 = 0.201$, $\overline{\varphi^2} = 0.87$.

(b) Amplitudes = 1.0, 0.7, 0.5. - $\sigma^2 = 0.196$, $\overline{\varphi^2} = 0.79$.

(c) Amplitudes = 1.0, 0.7, 0.3. - $\sigma^2 = 0.189$, $\overline{\varphi^2} = 0.62$.

Continued on next page.

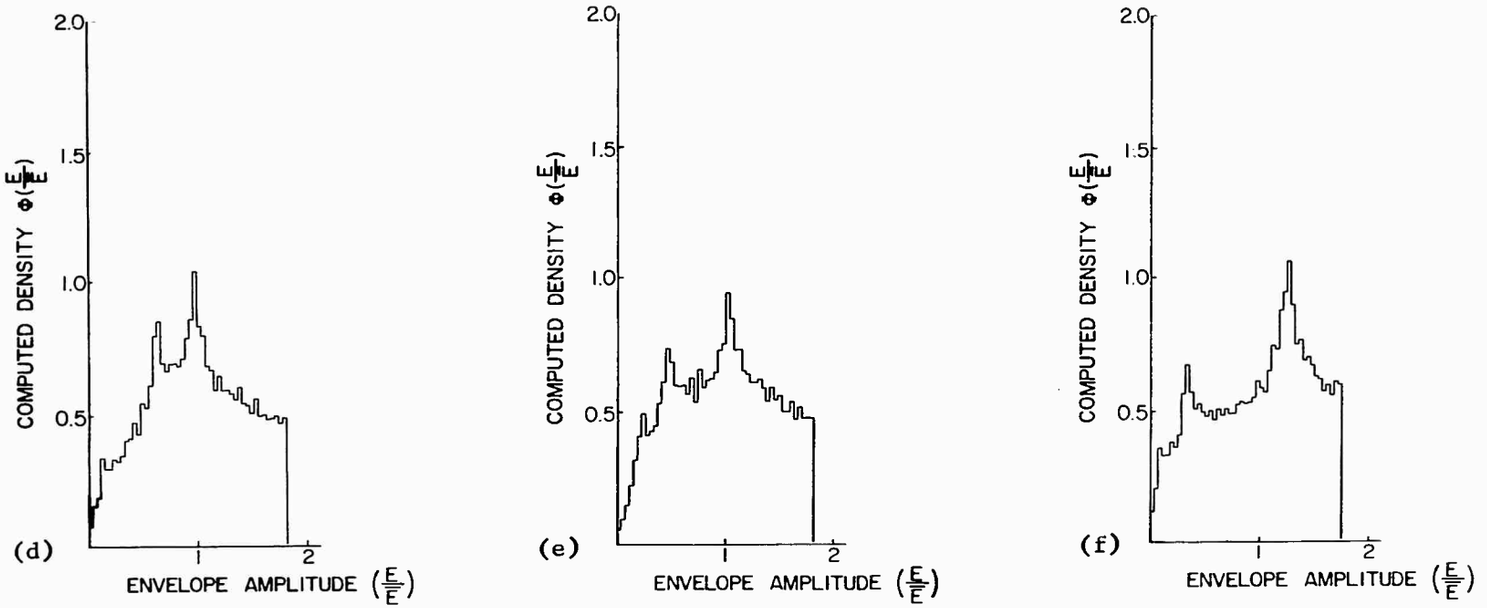

Figure 28. Continued.

(d) Amplitudes = 1.0, 0.85, 0.7. - $\sigma^2 = 0.210$, $\overline{\varphi^2} = 1.01$.

(e) Amplitudes = 1.0, 0.85, 0.5. - $\sigma^2 = 0.211$, $\overline{\varphi^2} = 0.93$.

(f) Amplitudes = 1.0, 0.85, 0.3. - $\sigma^2 = 0.216$, $\overline{\varphi^2} = 0.82$.

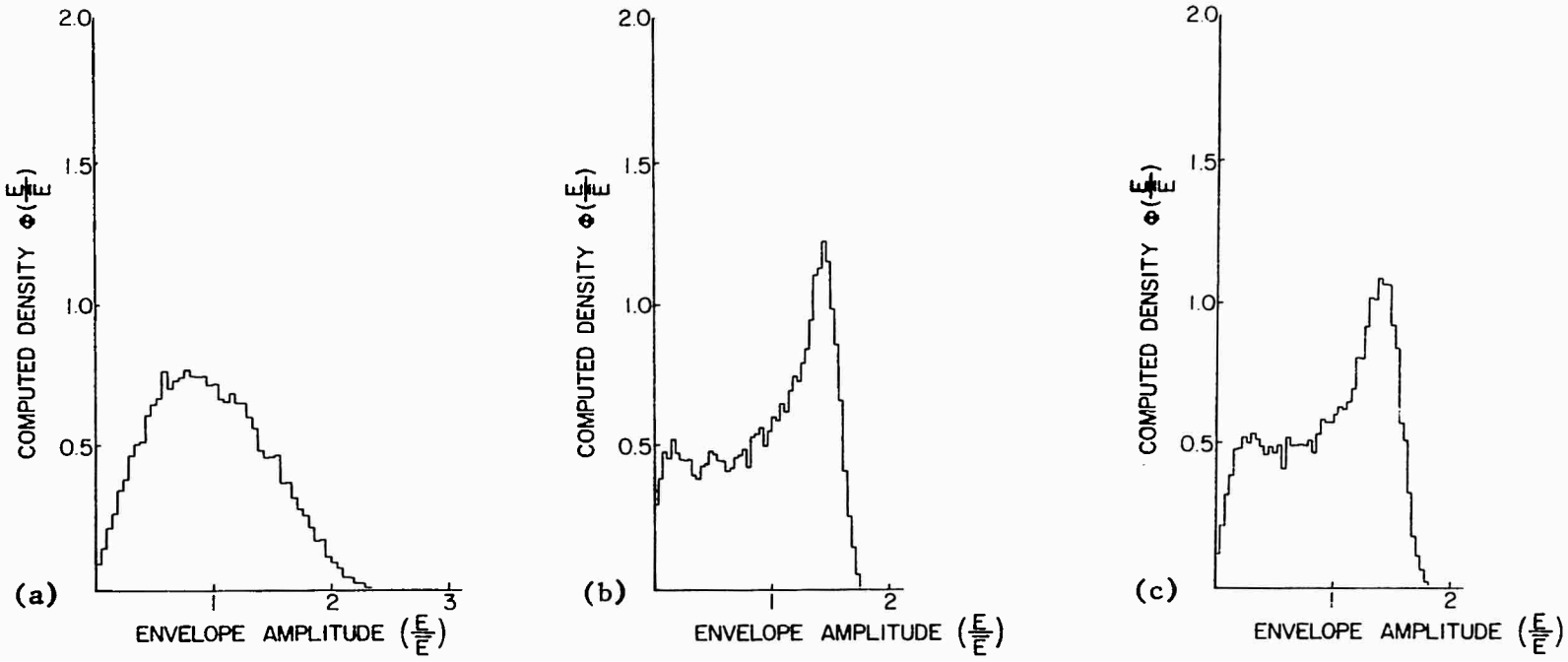

Figure 29. Computed amplitude distributions for the random vector sum of five or more rays.

(a) Six rays, amplitudes = 1.0, 0.85, 0.7, 0.4, 0.3, 0.2. - $\sigma^2 = 0.22$, $\overline{\varphi^2} = 1.05$.

(b) Five rays, amplitudes = 1.0, 1.0, 0.1, 0.1, 0.1. - $\sigma^2 = 0.23$, $\overline{\varphi^2} = 0.95$.

(c) Six rays, amplitudes = 1.0, 0.85, 0.1, 0.1, 0.1, 0.1. - $\sigma^2 = 0.21$, $\overline{\varphi^2} = 0.58$.

Continued on next page.

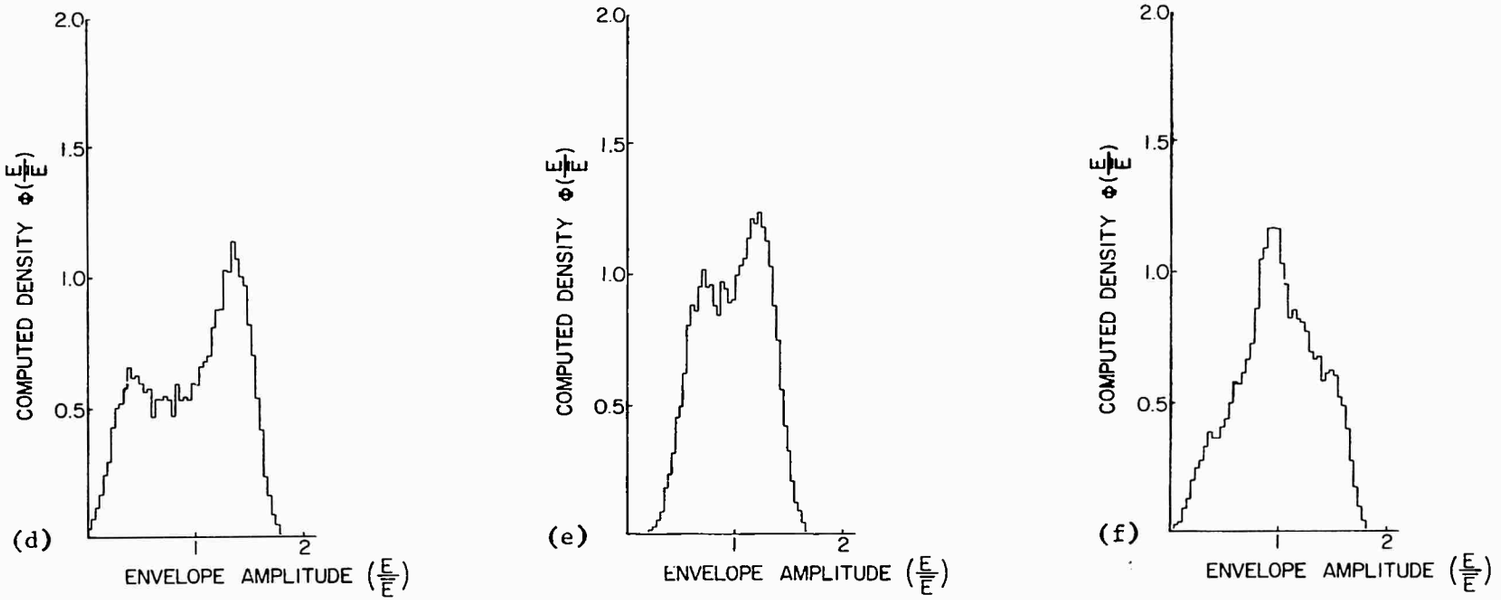

Figure 29. Continued.

(d) Six rays, amplitudes = 1.0, 0.7, 0.1, 0.1, 0.1, 0.1. - $\sigma^2 = 0.18$, $\overline{\varphi^2} = 0.58$.

(e) Six rays, amplitudes = 1.0, 0.4, 0.1, 0.1, 0.1, 0.1. - $\sigma^2 = 0.09$, $\overline{\varphi^2} = 0.33$.

(f) Eight rays, amplitudes = 1.0, 0.4, 0.4, 0.05, 0.05, 0.05, 0.05, 0.05. - $\sigma^2 = 0.13$, $\overline{\varphi^2} = 0.44$.

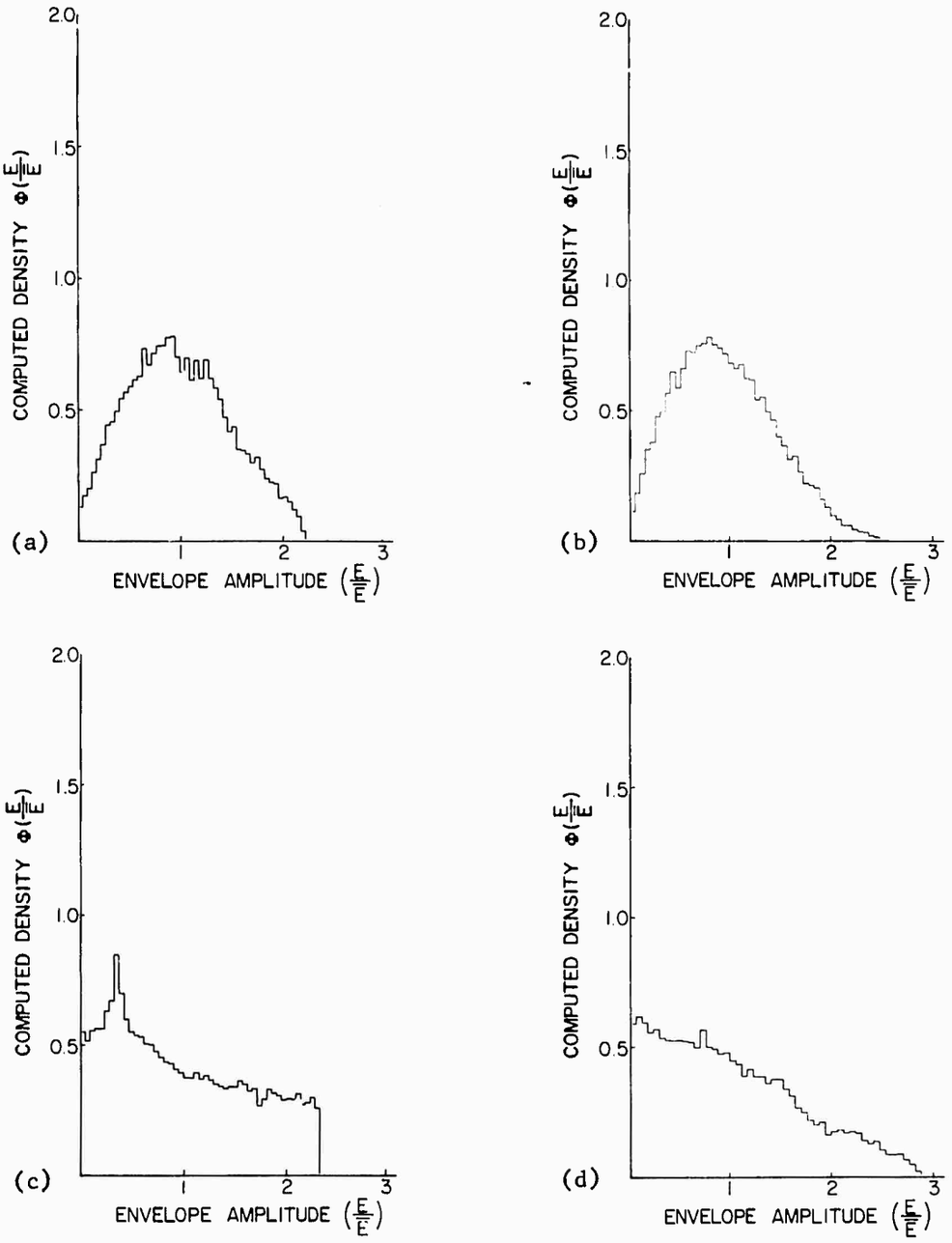

Figure 30. Computed amplitude distributions for the random vector sum of rays, including the effect of polarization mismatch.

(a) Ray polarization-independent, two rays, amplitude = 1.0, 0.7, $\sigma^2 = 0.232$, $\overline{\varphi^2} = 0.89$.
(b) Ray polarization-independent, three rays, amplitude = 1.0, 0.7, 0.4, $\sigma^2 = 0.239$, $\overline{\varphi^2} = 0.97$.
(c) Ray polarization-equal, two rays, amplitude = 1.0, 0.7, $\sigma^2 = 0.453$, $\overline{\varphi^2} = 0.53$.
(d) Ray polarization-equal, three rays, amplitude = 1.0, 0.7, 0.4, $\sigma^2 = 0.470$, $\overline{\varphi^2} = 0.71$.

differences in path lengths suggested by our model for the rays, it is anticipated that the resulting polarizations would be independent. If this is not the case, the polarization mismatch for the various paths will be related. If this assumption is used in computing the expected amplitude distribution, the curves of Fig. 30c and 30d result. These distributions have a very distinctive appearance when compared with the other distributions we have examined, in that they are almost always monotonically decreasing. Another characteristic of these distributions is that the normalized variance usually exceeds $(4/\pi) - 1$.

The amplitude probability-density distributions computed above give an idea of what can be expected of measured amplitude distributions under various conditions. These computed distributions will be compared with experimentally observed amplitude variations in the following sections.

D. RELATION OF SIGNAL-STRENGTH FLUCTUATIONS TO PHASE-PATH FLUCTUATIONS

In this section a relation between the occurrence of phase-path variations and fluctuations in the strength of the received signal is established. This relation is to be expected on the basis of the irregularity model and its prediction of multipath interference during periods of high irregularity activity. Using measured signal-strength and phase-path data acquired during the winter and spring of 1969-1970, about ninety hours of data were examined for this purpose. For each 1.2 hr segment of data, the rms phase fluctuation $\sqrt{\overline{\varphi^2}}$ (with mean and linear trend removed) was computed. These segments were grouped into ten intervals according to the computed value of $\sqrt{\overline{\varphi^2}}$. For all of the data segments in each interval, the measured normalized variance $\sigma^2 = \left[\overline{E^2}/(E)^2\right] - 1$ of the observed signal-strength fluctuation was calculated for 200 sec periods (this period includes a number of signal-strength minima under most conditions). The mean and the standard deviation of the amplitude variance were computed for each interval of $\sqrt{\overline{\varphi^2}}$. These values, and the number of data segments in each interval, are shown in Fig. 31. Although a wide range of signal-strength fluctuation is observed at any measured value of phase fluctuation, a strong dependence between phase fluctuations and amplitude fluctuations is seen. This indicates that the presence of the

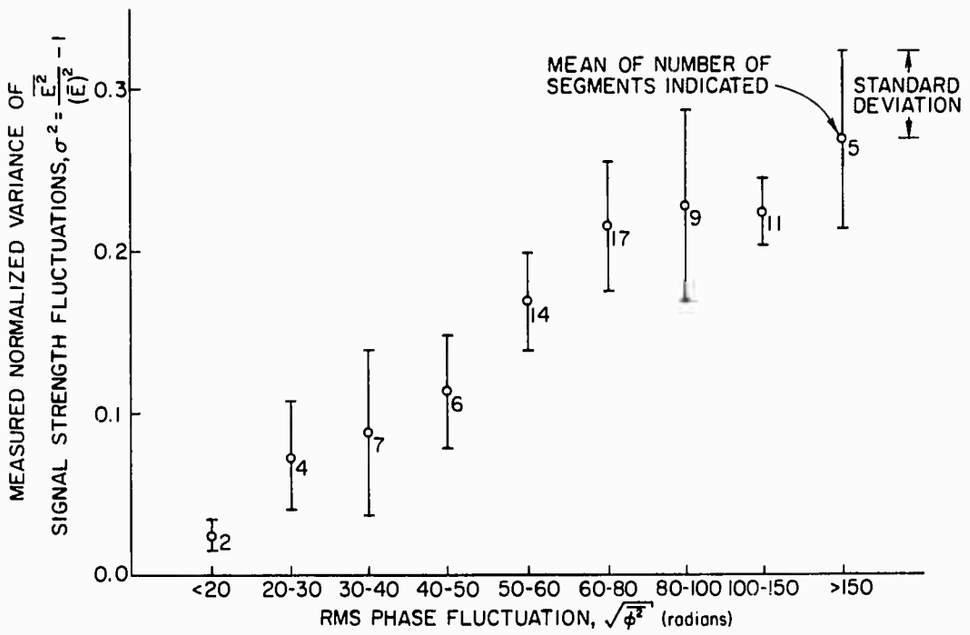

Figure 31. Observed signal-strength fluctuations vs. observed phase fluctuations.

irregularities which produce the observed phase fluctuations strongly influences the fading observed.

In order further to verify the predicted effect of phase fluctuations on observed signal strengths, a few measurements were made over a shorter path. It is expected that for shorter paths, the effect of irregularities of a given size and strength on signal-strength fluctuations should not be as great. This can be seen from Eq. (13), which shows that the expected number of rays reaching a point on the ground is a function of F/Λ_T. By decreasing the range, we reduce F. In addition, the focusing arising from smooth ionospheric variations (Fig. 15) will be less, further reducing the effective value of F.

Simultaneous observations were made over the path used for the other measurements of this work, and over the path from National Bureau of Standards Station WWV at Fort Collins, Colorado to Los Banos, California, in order to compare the influence of path length on signal-strength fluctuations. Changes in phase-path length were also recorded simultaneously. The distance from Fort Collins to Los Banos is about 1430 km. The difference in distance, plus ionospheric focusing, should produce an effective Fresnel-zone size for the WWV path about half that for the Arkansas path. This would be expected to produce a significant decrease in amplitude fluctuation effects.

Because no sounder was available over the WWV-Los Banos path, it was not possible to determine positively that only one mode was propagating over this path. However, ionograms over the Arkansas path were examined to determine the most likely times and frequencies for single-mode propagation from Fort Collins. This type of propagation occurred most frequently for WWV at 15 MHz. A single-mode frequency for the Arkansas path was chosen to provide a reflection height which was comparable to that on the WWV path based on nominal ionospheric conditions. This was usually about 24 MHz. (The difference in frequencies will cause the Fresnel-zone length for WWV to be slightly larger than half the Fresnel-zone length for Bearden.)

In all observations, fading on the WWV path was significantly less than on the Arkansas path. At times the WWV path exhibited almost no

noticeable fading. Figure 32 is typical of the data obtained under such conditions. The phase-path variations are similar in magnitude, although uncorrelated. The signal fluctuations on the WWV path are considerably weaker. In addition, the measured amplitude density distributions for the period of the records (Fig. 33) shows that the WWV signal is much more constant in amplitude. Again, this verifies our interpretation of the phase fluctuations observed.

E. MEASURED AMPLITUDE HISTOGRAMS

We shall now examine a number of amplitude histograms calculated from the measured signal-strength records, and attempt to infer some characteristics of the rays producing the observed distributions. A major difficulty in this task is presented by the discreteness of the irregularities and the small number of rays. Under these conditions, the number and amplitudes of the rays are expected to vary significantly with time. For irregularities having a 20 min period, it is not likely that the situation will remain stationary for more than a few minutes. For observations to represent conditions at any one particular time, the conditions should remain relatively constant for the period of the measurement. The measuring period will therefore be a compromise between a period short enough to provide stationarity and a period long enough to permit obtaining the reasonably large number of samples required to produce valid distributions.

Measurements of amplitude were made at intervals of 0.1 to 1.0 sec. There is a limit to the amount of information to be gained by sampling more rapidly. If the observed distribution is to be valid, the rays must have doppler shifts sufficiently large and sufficiently different from each other that a random phasor sum of the rays will be observed. The effects of different sampling intervals will be discussed together with the observed amplitude distributions. Also, the variance σ^2 of the observed amplitude fluctuations will be noted for comparison with those predicted in the computed distributions. The values of σ^2 are indicated in the captions for each of the computed and measured distributions. If the distributions result from a random phasor sum of sine waves whose

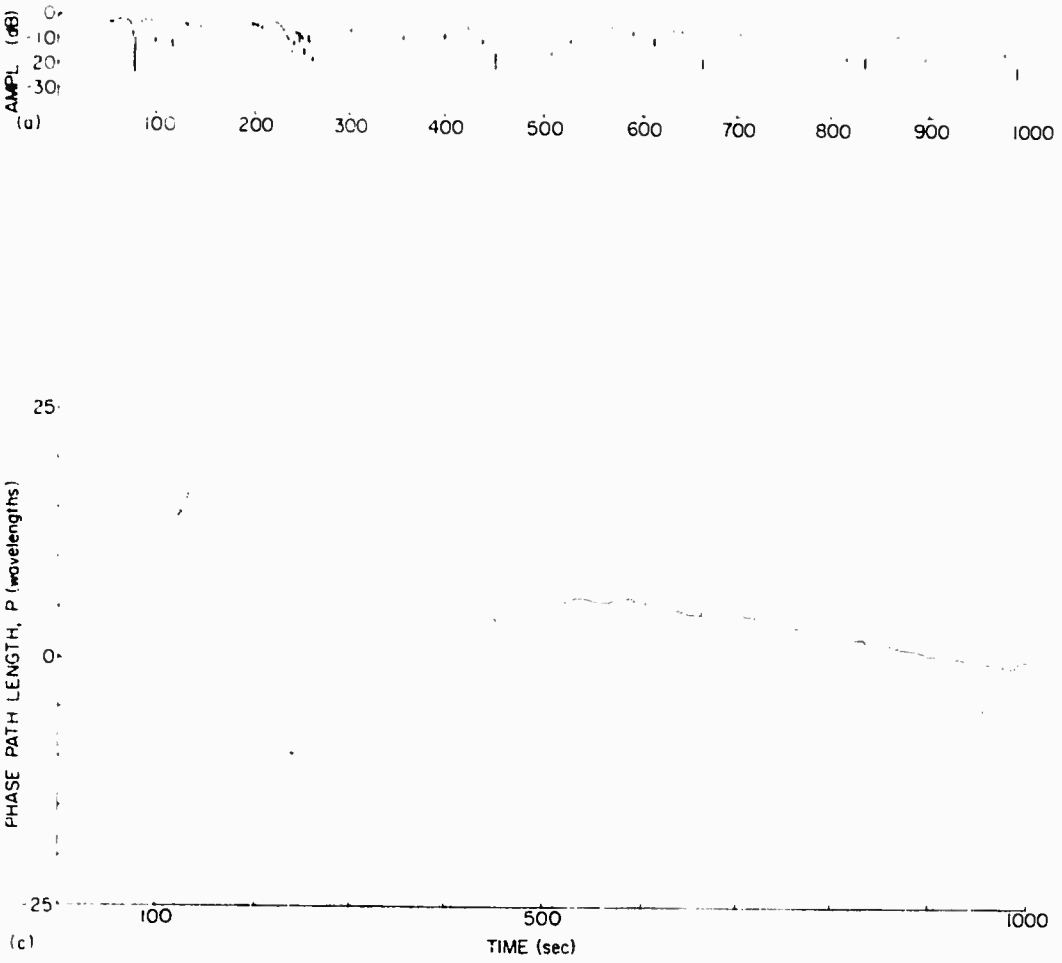

Figure 32. Observed signal-strength and phase-path-length fluctuations over two paths at the same time.

(a) Signal strength, WWV-15, Fort Collins, Colorado to Los Banos, Calif. (1430 km).

(c) Phase-path-length fluctuations--Fort Collins.

Continued on next page.

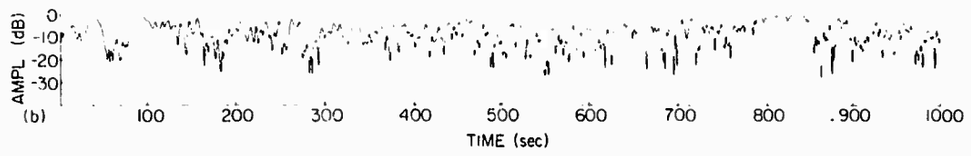

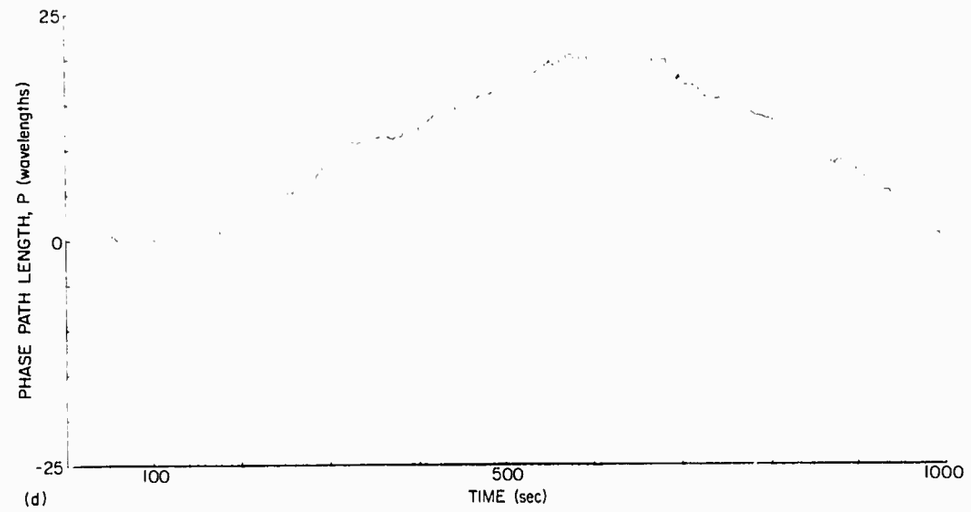

Figure 32. Continued.

(b) Signal strength--22.81 MHz, Bearden, Arkansas to Los Banos, Calif. (2600 km).
(d) Phase-path-length fluctuations--Bearden.

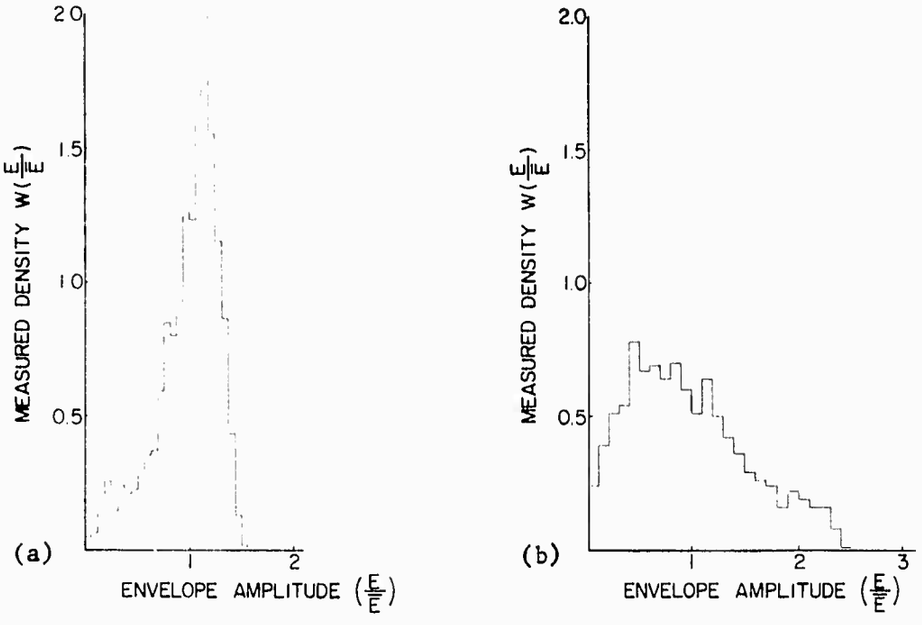

Figure 33. Observed amplitude density distributions $W(E/\bar{E})$ for the period shown in the records of Fig. 33.

(a) Fort Collins path. - $\sigma^2 = 0.081$.

(b) Bearden, Arkansas path. - $\sigma^2 = 0.204$.

amplitudes do not vary, the variance σ^2 is restricted to lie in the range from 0 to 0.273 $[(4/\pi) - 1]$. Greater values may occur if the signal energy changes during the analysis interval. Such variations in energy would be expected, based on our irregularity model.

The examination of a large number of measured amplitude distributions reveals some general characteristics. First, no distribution curve shape may be said to be typical. The shape of the distributions is a strong function of the analysis interval and the nature of the signal fluctuations during the analysis interval. The second general characteristic of the data is that σ^2 frequently exceeds 0.273, indicating that for analysis times long enough to produce valid random phasor sums, significant energy changes occur. Finally, only when fading is quite rapid and severe do the measured distributions resemble any of the Rice distributions shown in Figs. 21 and 23, and then only the $\beta = 0$ distribution, which is equivalent to the computed distributions for more than a few rays of comparable magnitude.

A frequently noted characteristic of the observed amplitude distributions is a double-peaked form. Three such distributions are shown in Fig. 34, which displays the observed amplitude density, $W(E/\overline{E})$, versus $E/\overline{E}$. These distributions are measured from data taken during 10 to 15 min intervals. These double-peaked curves resemble the 2-ray and 3-ray distributions of Figs. 26 and 28. They differ from the latter distributions in having more elongated high-amplitude "tails". Such long tails are frequently observed, and are assumed to be caused by changes in the amplitudes of the rays being received.

In an effort to verify this assumption, some data were analyzed for a 2.5 min period. These data were sampled at 10 samples per sec, so that enough points to produce a smooth distribution could be obtained. Records such as shown in Fig. 35a were produced under these conditions. This distribution has a sharp upper limit. It does not, however, appear to be a satisfactory random vector sum, and while ray amplitudes are probably relatively constant for this interval of 2.5 min, the frequency shifts of the various rays are apparently not sufficient to produce the desired random vector sum. Figure 35b shows the distribution produced by analyzing a 5 min period which included the period used for Fig. 35a.

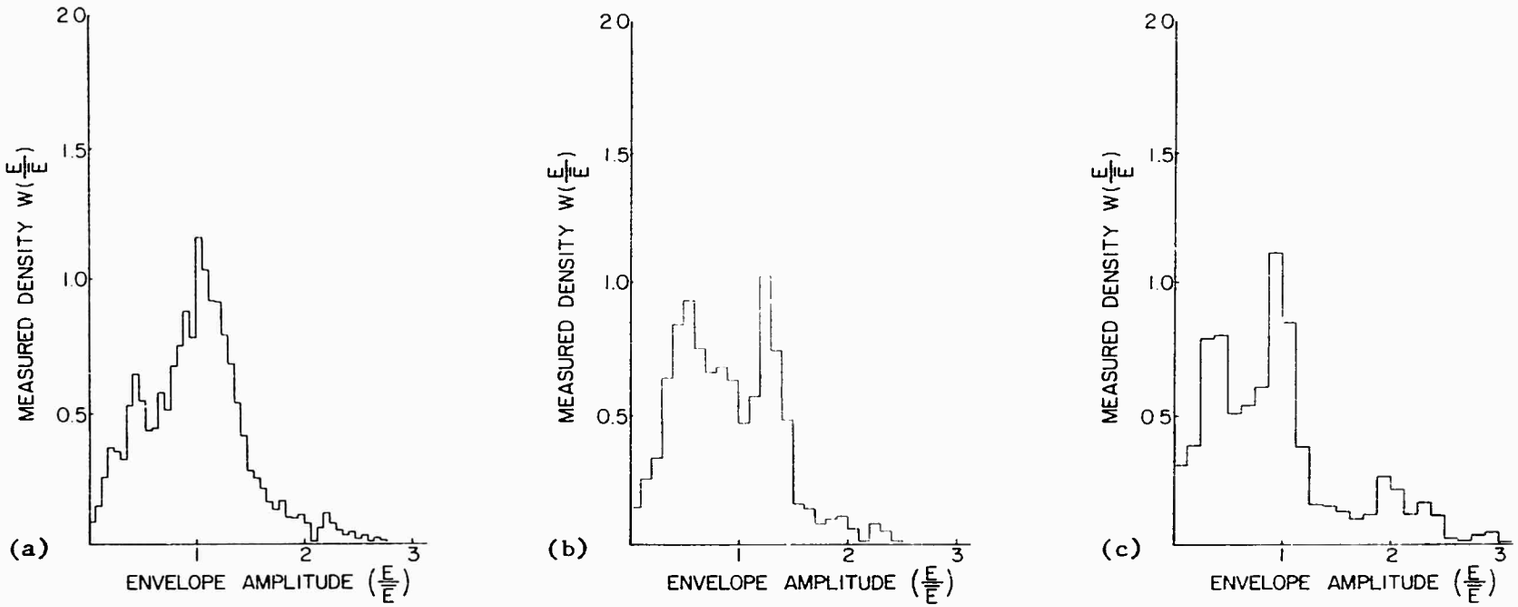

Figure 34. Observed amplitude density distributions exhibiting multiple peaks.

(a) Analysis time = 15 min. - σ^2 = 0.213 .

(b) Analysis time = 10 min. - σ^2 = 0.223 .

(c) Analysis time = 14 min. - σ^2 = 0.247 .

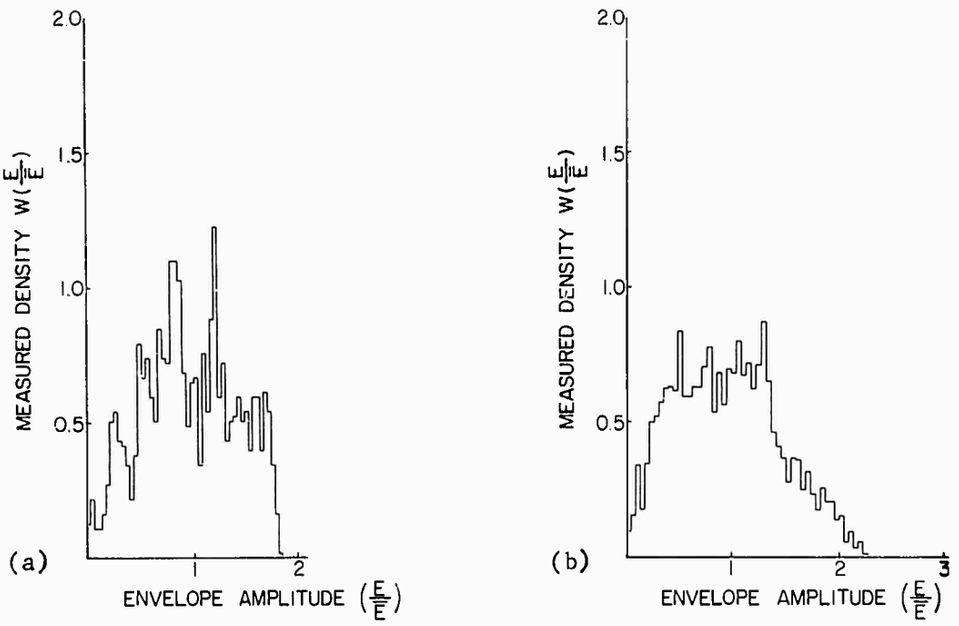

Figure 35. Observed amplitude density distributions for short analysis times.

(a) Analysis time = 2.5 min. - $\sigma^2 = 0.194$.

(b) Analysis time = 5.0 min. - $\sigma^2 = 0.238$.

Note that the tail of the distribution is growing, indicating a change in the amplitudes of some of the component rays.

To further investigate the effect of changing ray amplitudes, a distribution was computed for which one ray was present for half of the samples and three rays were present for the other half. Such a stepwise change is not realistic, but the resulting computed distribution, shown in Fig. 36a, gives an insight into the effect of changing energy. A measured distribution exhibiting a similar effect is shown in Fig. 36b.

All of the above measured distributions were taken during periods of relatively rapid fading, as observed on the signal-strength records. If the observed fading were the result of interference between two rays of about equal amplitude, such as would be the expected result of magnetoionic splitting, distributions similar to those of Figs. 26, 30a and 30b should be observed. Records such as these, however, are not observed during periods of rapid signal-strength fluctuation, indicating that Faraday rotation is not the dominant mechanism in producing these fades. Observations made over long periods of time when little fading is present, do however appear quite similar to the computed distributions for two rays of similar strength. Figures 37a and 37b show two such measured distributions, where the analysis time is 20 min. This indicates that the effects of Faraday rotation are seen over longer time intervals, but not for short intervals. This is consistent with predicted behavior for the ordinary and extraordinary rays.

Additional examples of some observed distributions are shown in Fig. 38. These distributions were measured during three consecutive 10 min periods under conditions of moderate fading. They show the change in the dominant rays during the interval. In all cases σ^2 is less than 0.273, indicating that energy was relatively constant during each 10 min period. Figure 38d shows the amplitude distribution for the entire period, indicating the loss of information due to changes in the ray structure. Also, for this record, σ^2 is greater than 0.273.

Finally, we show three more measured distributions in Fig. 39. These are the result of analyzing 20 min segments of data during a one and a half hour period. The signal-strength record for this period is shown in Fig. 39d. The three distributions correspond to periods of time when

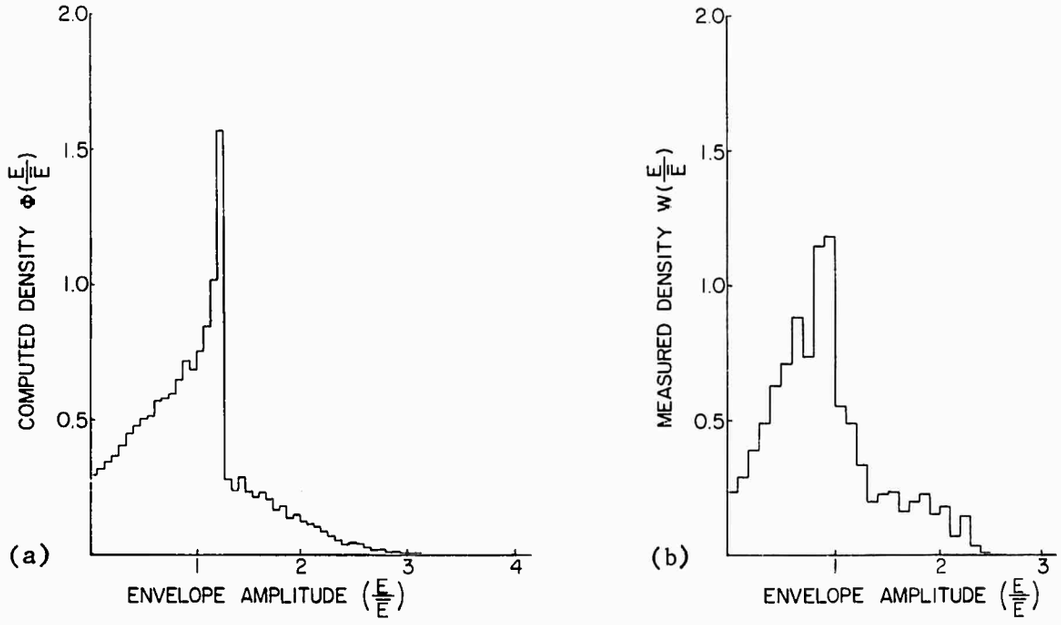

Figure 36. Amplitude distributions exhibiting the effect of changing signal energy.

(a) Computed distribution with one ray (amplitude = 1.0) present for half of the analysis interval and three rays (amplitude - 1.0, 0.85, 0.7) present for the other half of the analysis interval. - $\sigma^2 = 0.288$, $\overline{\varphi^2} = 0.79$.

(b) Measured distribution. - $\sigma^2 = 0.26$.

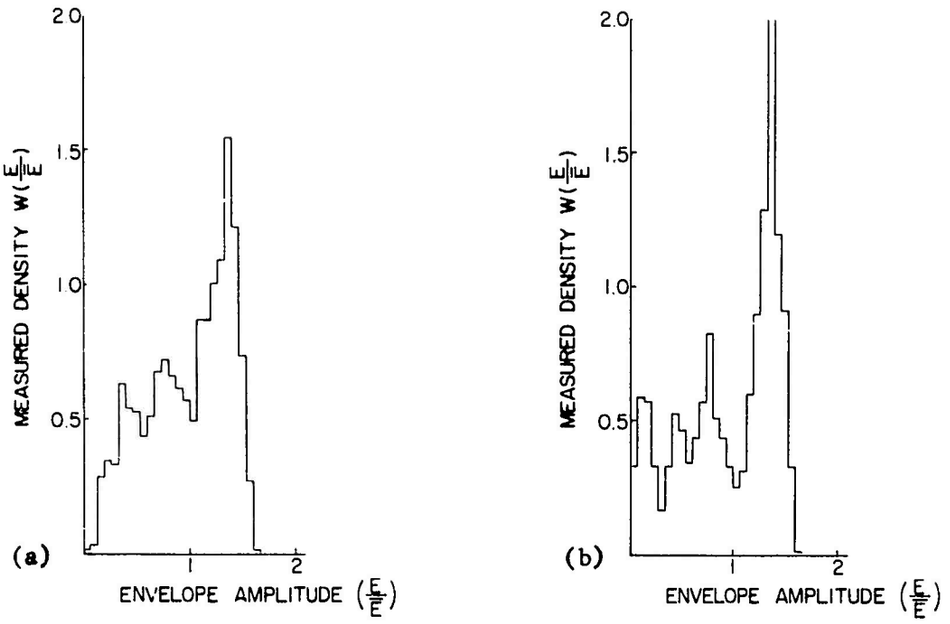

Figure 37. Measured amplitude distributions showing the effects of Faraday rotation.

(a) Analysis time = 20 min. - $\sigma^2 = 0.14$.

(b) Analysis time = 20 min. - $\sigma^2 = 0.20$.

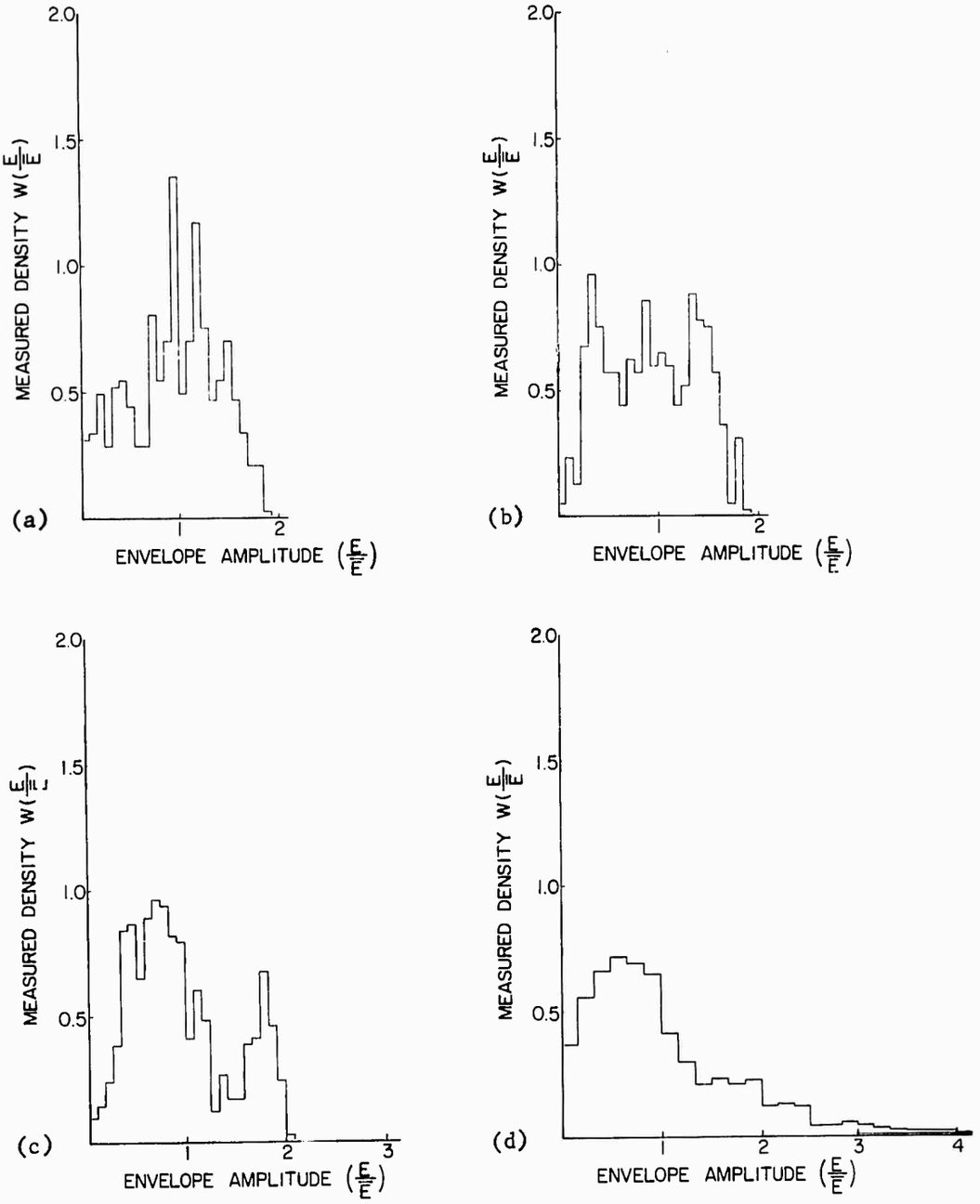

Figure 38. Measured amplitude distribution for three consecutive 10-min intervals, and for the whole 30-min interval, showing the effect of analysis time on observed distributions.

(a) First 10 min. - $\sigma^2 = 0.238$.

(b) Second 10 min. - $\sigma^2 = 0.206$.

(c) Third 10 min. - $\sigma^2 = 0.197$.

(d) Total 30 min. - $\sigma^2 = 0.433$.

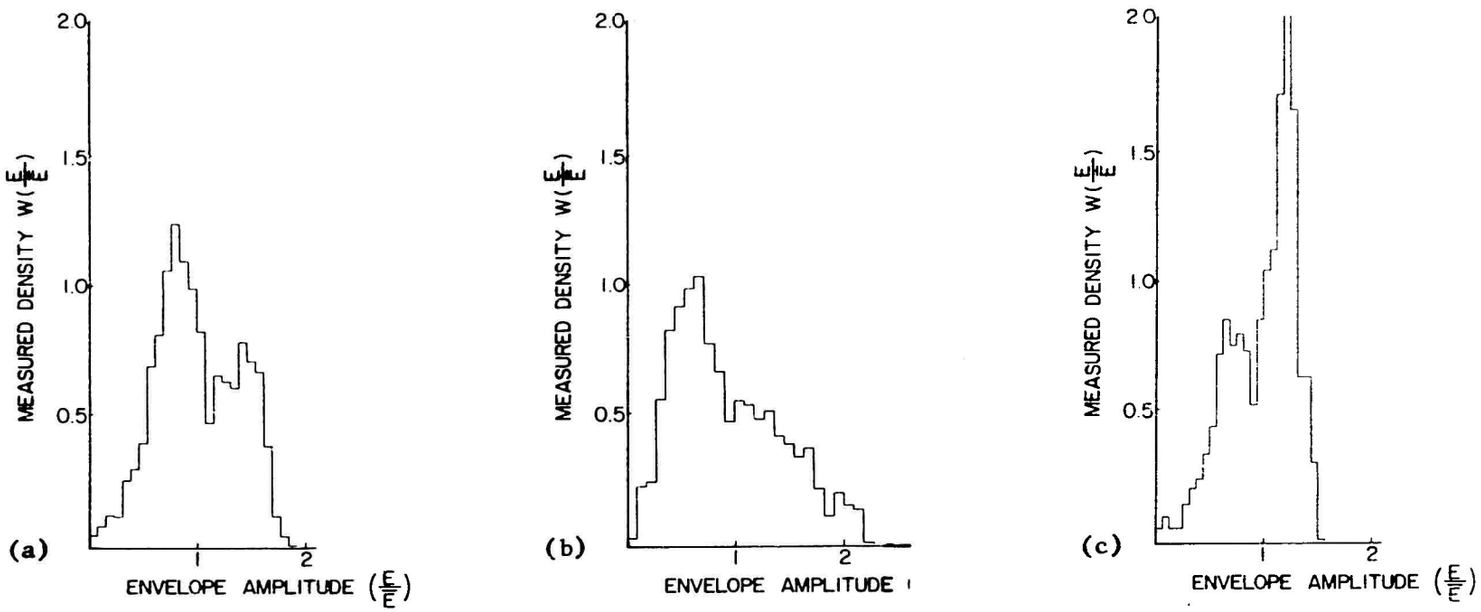

Figure 39. Measured amplitude distributions and signal-strength record relating amplitude distribution to observed signal fluctuations.

(a) 20-min period of moderate fading. $-\sigma^2 = 0.125$.

(b) 20-min period of severe fading. $-\sigma^2 = 0.232$.

(c) 20-min period of little fading. $-\sigma^2 = 0.086$.

Continued on next page.

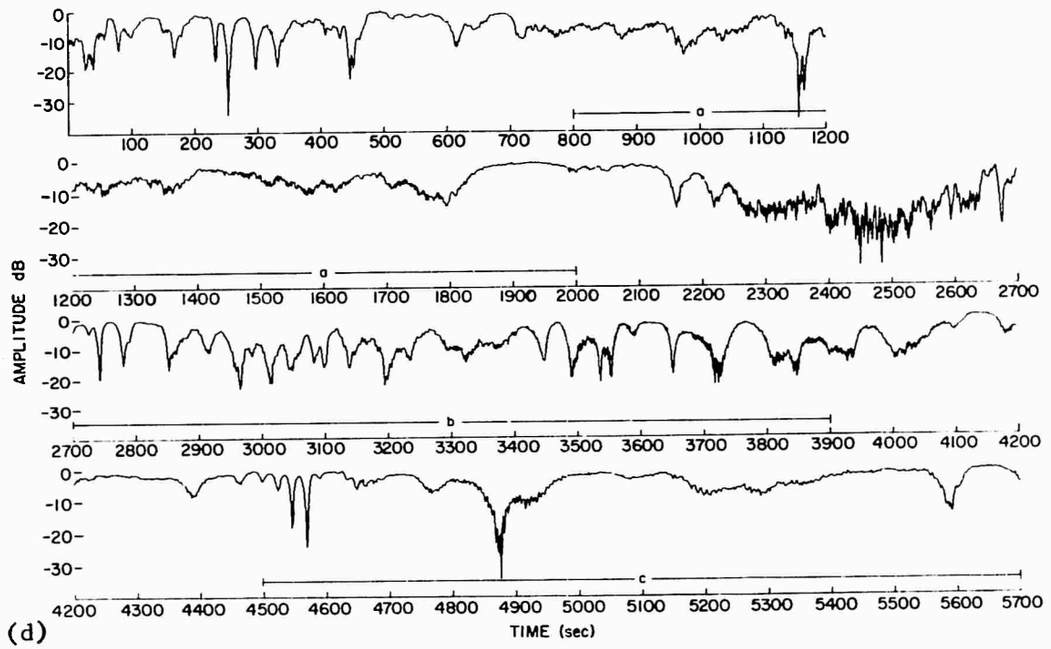

Figure 39. Continued.

(d) Signal-strength record. - The periods analyzed for the amplitude distributions of parts a, b and c of this figure are indicated by bars above the time axis.

the signal-strength record had different appearances. Figure 39a appears to resemble the amplitude distribution produced by two or three rays (Fig. 26). During the corresponding interval the signal-strength record shows a moderate amount of fading. Figure 39b, the distribution for a more disturbed period on the signal strength record, more closely resembles computed distributions for a larger number of rays. Figure 39c shows a very strong component indicating that a single ray was prominent during this period. The signal strength during this latter time was very stable.

F. CONCLUSIONS FROM SIGNAL-STRENGTH ANALYSIS

The observed amplitude distribution data presented in the above examples are similar to a majority of the observed amplitude distributions examined. Analysis times were chosen to emphasize certain features of the data. For all data taken during the course of the experiments, similar distributions were produced when analysis intervals were chosen long enough to give reasonably smooth distributions, and short enough to avoid encompassing widely varying situations which produce distributions approaching the Rayleigh. From these analyses, the following conclusions are drawn:

1. Signal-strength fluctuations observed for single-mode ionospheric propagation under quiet ionospheric conditions are adequately described in terms of the multipath interference resulting from vertical ray bending caused by large, weak ionospheric irregularities.

2. Under most conditions, fading due to O-X interference is not significant compared with that arising from the vertical ray bending caused by the irregularities being investigated.

3. Measured amplitude histograms for ionospherically propagated rays are highly time-dependent because of the variability of the causative mechanism.

4. Weak scattering caused by a large number of small scatterers does not produce the major portion of the fading observed on single-mode one-hop ionospheric propagation. We do not know whether such weak scattering occurs in some smaller degree which is masked by the multipath-interference effects. Experiments to answer this question must consider the effects

of multipath such as we observe. Such experiments would promise most success if performed for shorter paths, where multi-ray interference is less, and during periods of low fluctuation in phase-path length.

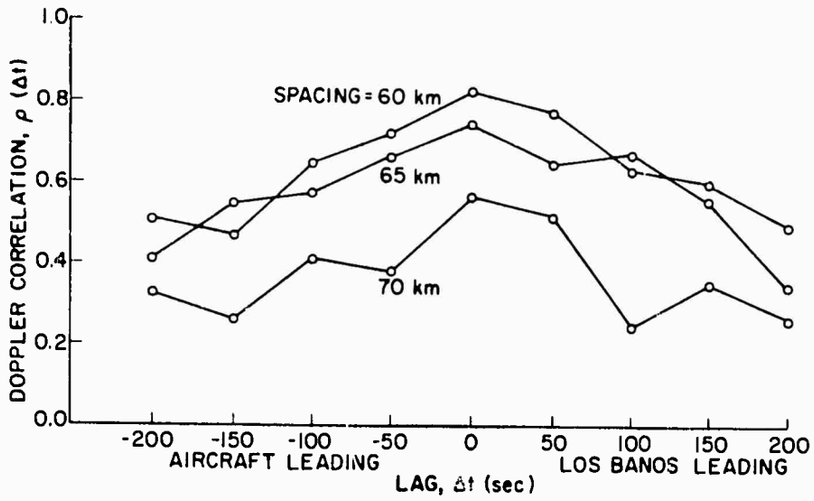

Figure 40. Doppler correlation versus time lag for wide-spaced phase-path measurements made with receiving antennas at Los Banos, Calif. and on an airplane.

V. OTHER CHARACTERISTICS OF THE IRREGULARITIES

A. HORIZONTAL MOTION OF IRREGULARITIES

Some of the phase-path data acquired in this work have been examined with the object of determining whether the observed irregularities exhibit any preferred direction and velocity of motion. The observational geometry used in this work was sensitive to horizontal motions in the north-south direction, and also to vertical motions (when more than one radio frequency was used simultaneously).

The records obtained from the wide-spaced CW measurements, using receivers at Los Banos and on an airplane, were examined in an attempt to identify a consistent horizontal velocity component of the irregularities. The aircraft doppler measurements taken at spacings of 60, 65 and 70 km were correlated [as in Eqs. (7) and (8)] with the fixed receiver-site measurements using time lags of ±50 sec to ±200 sec for the fixed site, to determine whether the highest correlation occurred at a time lag other than zero. The results of these correlations are shown in Fig. 40. In all cases, the correlation decreased for time lags other than zero, indicating no preferred horizontal motion.

The above test involved averaging data over eight observations, and therefore would sense only a preferred direction of motion. It is possible that each of the irregularities is moving, but that the directions of motion vary widely. In order to observe the motion of individual irregularities, use was made of the data gathered during the winter and spring of 1969-1970. Changes in phase-path length measured on two vertical monopoles spaced 2.5 km apart were cross-correlated to determine the time shift of maximum correlation. Figure 41a shows a typical result of this correlation. The phase of the signals at this spacing was highly correlated (greater than 0.97 in all cases). The maximum phase-path correlation $\rho_p(\Delta t)$ occurs for a time shift of 0 ± 5 sec for all records examined. Because of the slow decorrelation of phase with time, it is difficult to assign a value of north-south velocity component from these records, and no attempt was made to do so.

Similar correlations were performed on the amplitude data available from the experiments. As shown in Fig. 41b, the amplitude correlation

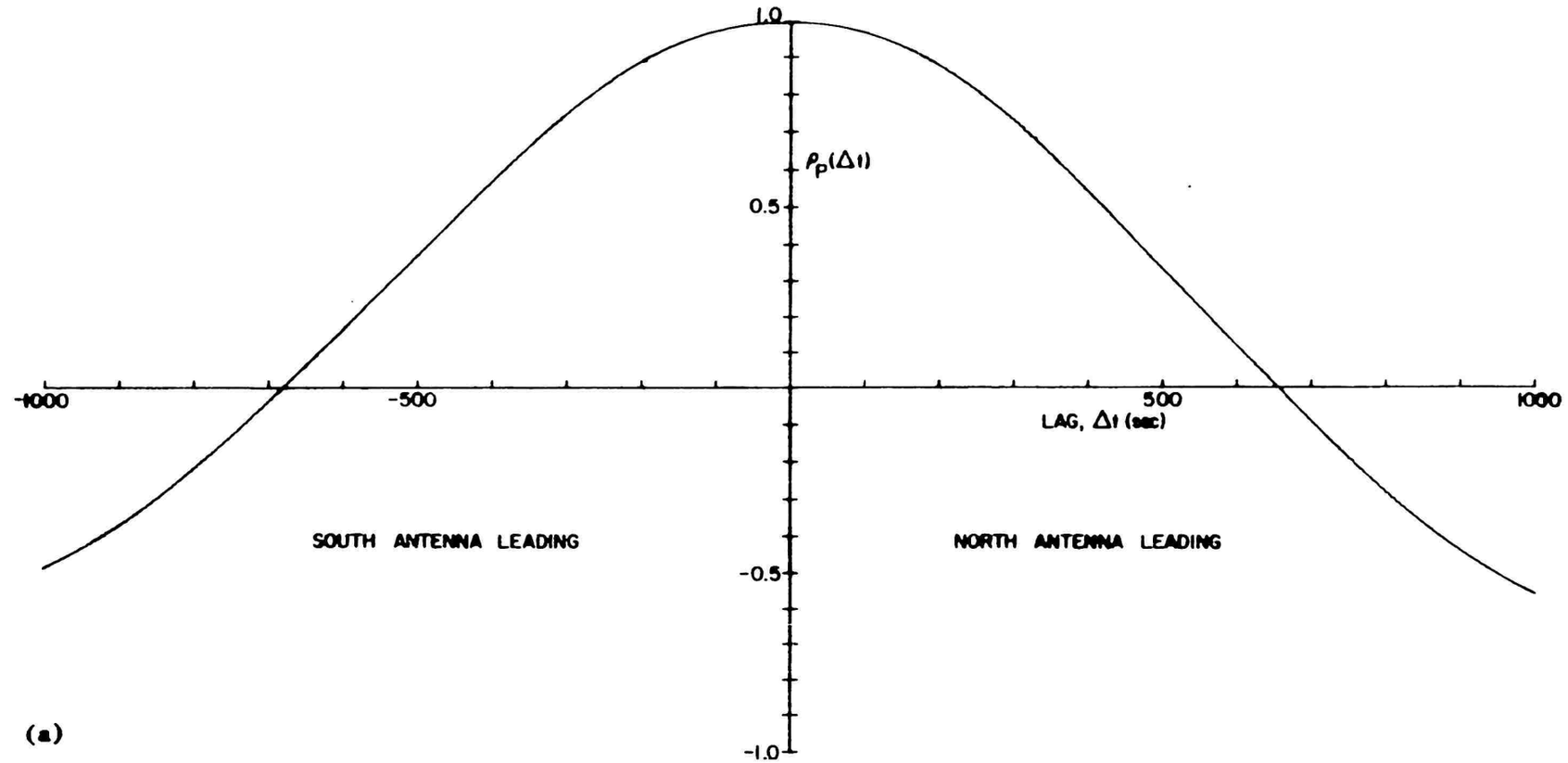

Figure 41. Cross correlation of signals on antennas spaced 2.5 km apart.
(a) Phase-path correlation, $\rho_p(\Delta t)$.

Continued on next page.

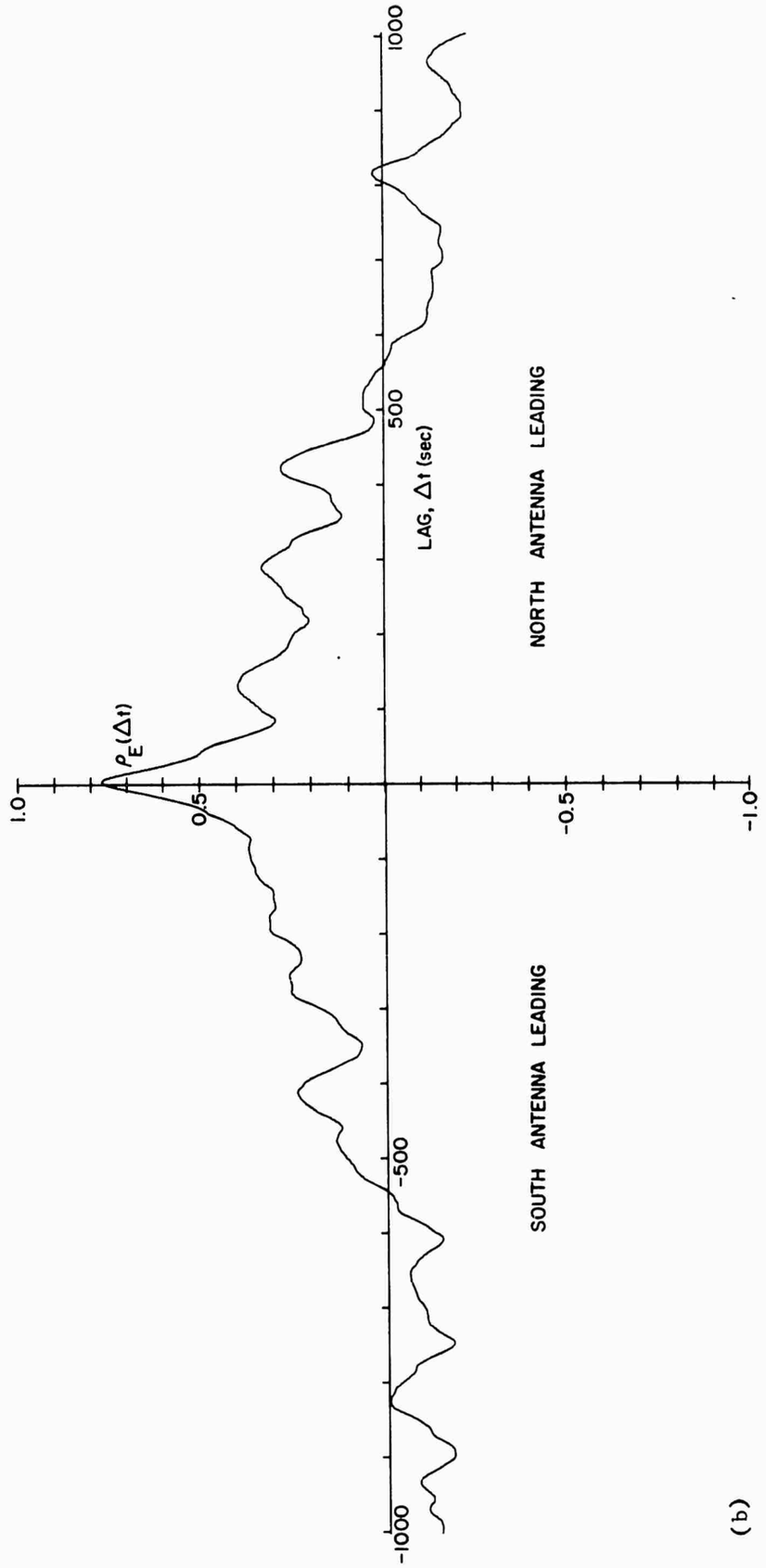

(b)

Figure 41. Continued.

(b) Envelope amplitude correlation, $\rho_E(\Delta t)$.

$\rho_E(\Delta t)$ decreases much more rapidly with time than does the phase-path correlation. Offsets of the peak amplitude correlation (from zero lag) ranged from 0 sec to ±20 sec. The interpretation of these time lags is difficult for two reasons. First, only one component of the velocity is observed. This allows us only to place a lower limit on the velocity of the fading pattern. Second, horizontal motion of the fading pattern can result from vertical motion and deformation of the irregularities as well as from their horizontal motion.

If we assume that horizontal irregularity motion, rather than vertical motion or deformation, is responsible for the motion of the fading pattern, we find (based on the antenna spacing and time lag given above) a lower limit for the horizontal velocity of the irregularity of about 65 m per sec.

B. VERTICAL MOTION OF IRREGULARITIES

By making use of simultaneous transmissions on two frequencies over the Arkansas-Los Banos path, changes in phase-path length could be measured on two vertically separated paths simultaneously. Approximately thirty hours of such two-frequency data taken during the winter-spring 1969-1970 period were analyzed to determine whether the observed irregularities moved vertically. The analysis was performed by cross-correlating the phase-path variation records for the two paths. Data segments of 1.2 hours were used for each correlation. Frequency separations between 100 kHz and 5.1 MHz were used. A typical record for a 2 MHz frequency spacing is shown in Fig. 42. The peak correlation occurs at a time lag of 240 sec for the lower-frequency path. Assuming the vertical ray spacings given in Fig. 8, this corresponds to a downward velocity of about 33 m/sec. All of the data analyzed in this manner (shown in Fig. 43) indicated a downward velocity of between 30 and 40 m/sec. We therefore have considerable confidence in this measurement.

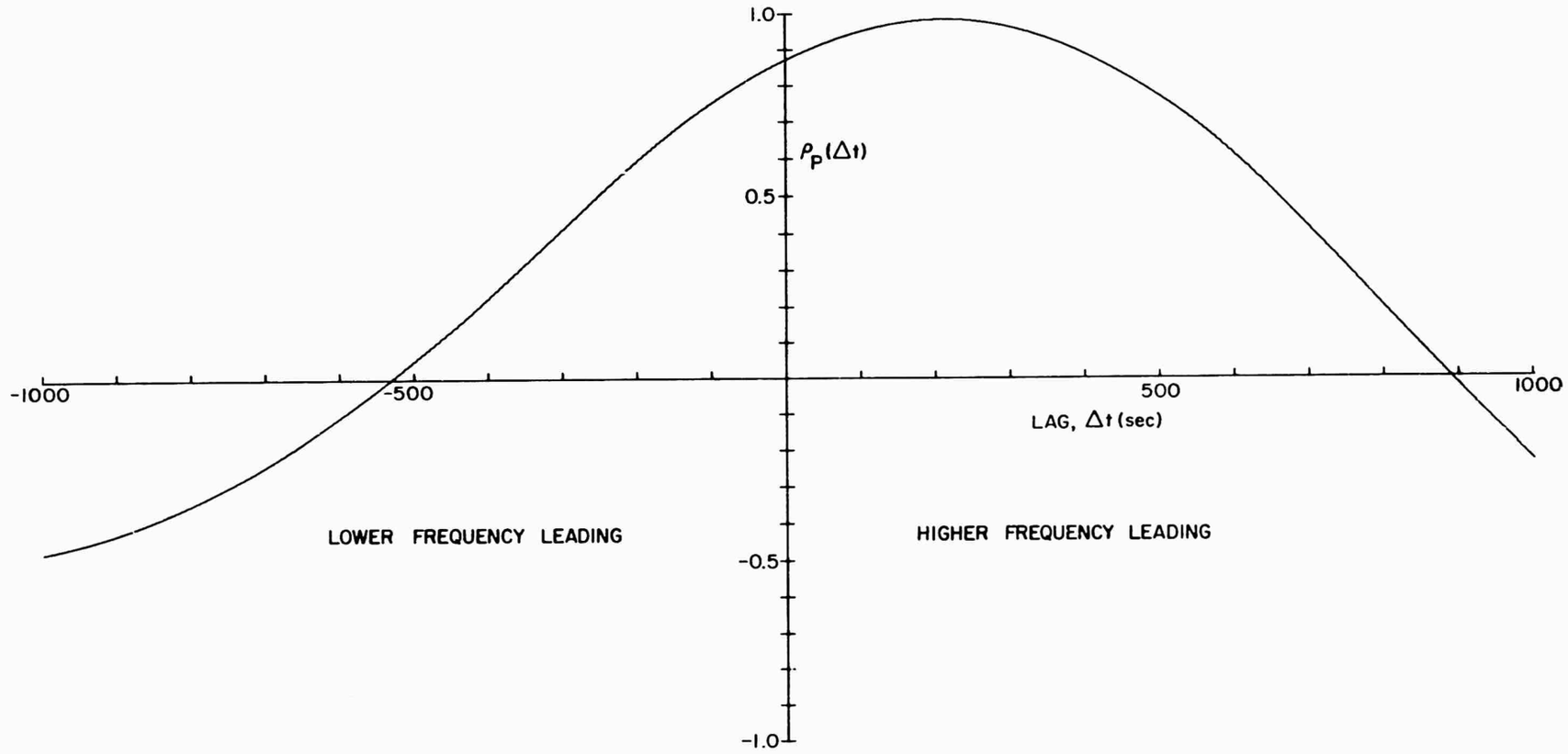

Figure 42. Cross correlation of phase-path length changes observed on the Bearden-Los Banos path for two frequencies separated by 2 MHz.

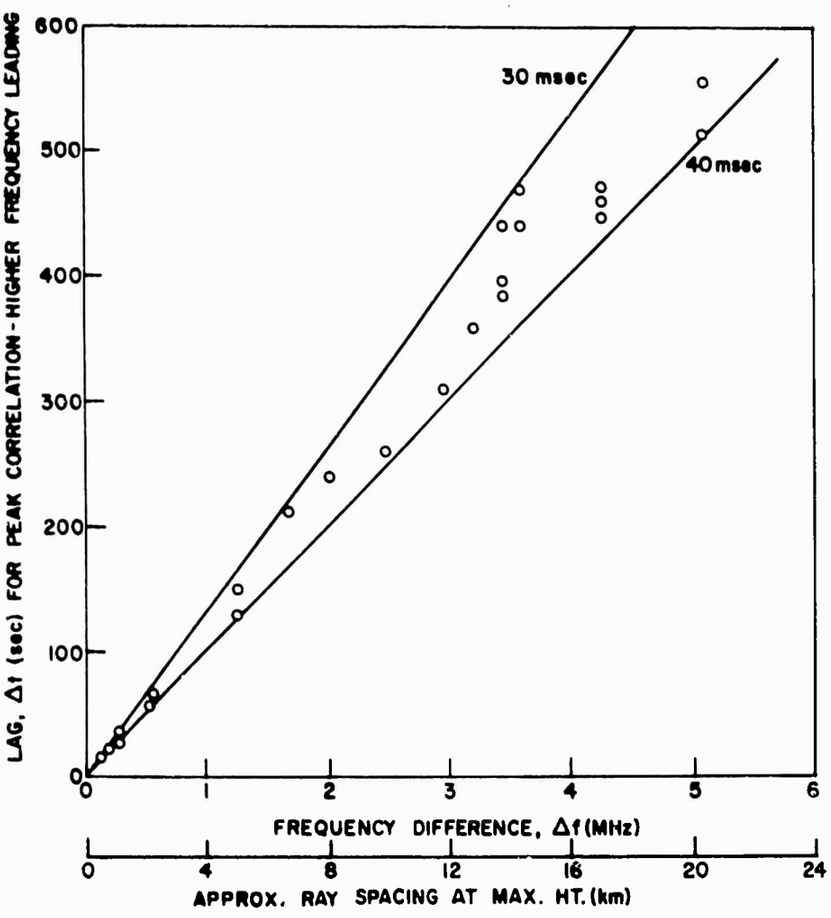

Figure 43. Time lags required to produce maximum cross correlation of phase-path length changes for spaced frequencies.

C. DIURNAL AND SEASONAL VARIATIONS

The measuring technique used in the course of this work could be regularly employed only during winter daytime periods for the path involved. To determine any diurnal variation which might be observable during these limited periods (about 10:00 am to 4:00 pm local time at midpath) the rms phase fluctuations observed for each 1.2 hr segment of data analyzed in Chapter III, Section D (Fig. 31) are grouped into 1 hour intervals (according to the time of day at the middle of the segment) and an average is calculated. These averages and their standard deviations are shown in Fig. 44. They indicate that large phase fluctuations are most common in the morning, and least common near noon.

To examine the seasonal variations of $\sqrt{\overline{\varphi^2}}$ this quantity is averaged for each day of available data. These averages are shown in Fig. 45, for the period from November 1969 through April 1970. Single-mode phase-path measurements are not possible on a regular basis over the Bearden-Los Banos path at other times of the year. For the period of the data, a small decrease in the magnitude of the phase-path-length fluctuations is observed during the latter portion of the period.

D. ANTENNA PERFORMANCE

If it is desired to make use of very large apertures (greater than one km) for HF communication systems, in order to increase antenna gain and reduce interference, the irregularities described in this work will strongly influence the design and performance of such antennas. The strength and horizontal scale size of the irregularities will determine the wave-front curvature for rays arriving at the receiving antenna. This will limit the length of antennas which may be employed without compensation for the varying curvature of the wave fronts. It is found, however, that antennas having lengths up to about 20 km will be useful under many circumstances without compensation for wave-front curvature. Such antennas must, however, be able to track the changing apparent azimuthal angle of arrival of incoming rays.

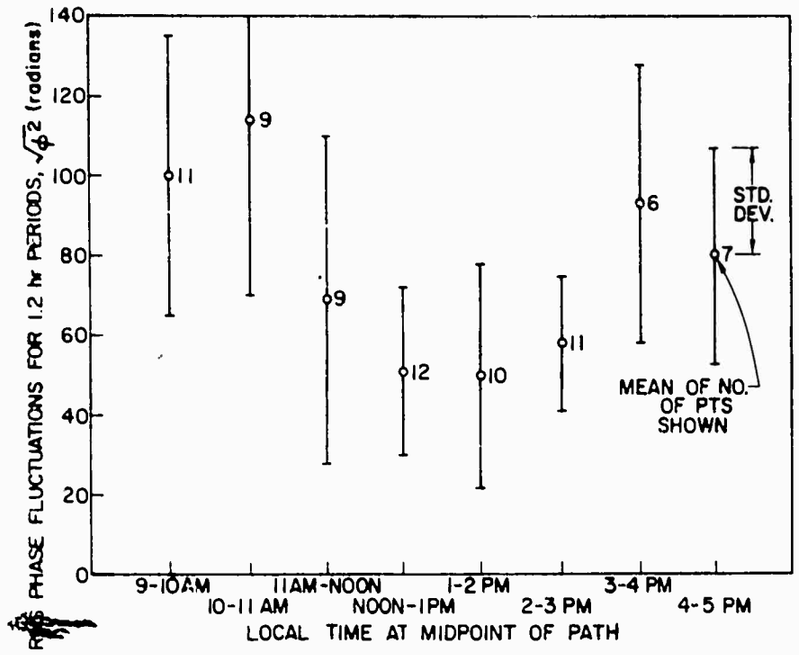

Figure 44. Variation of phase fluctuations with time of day.

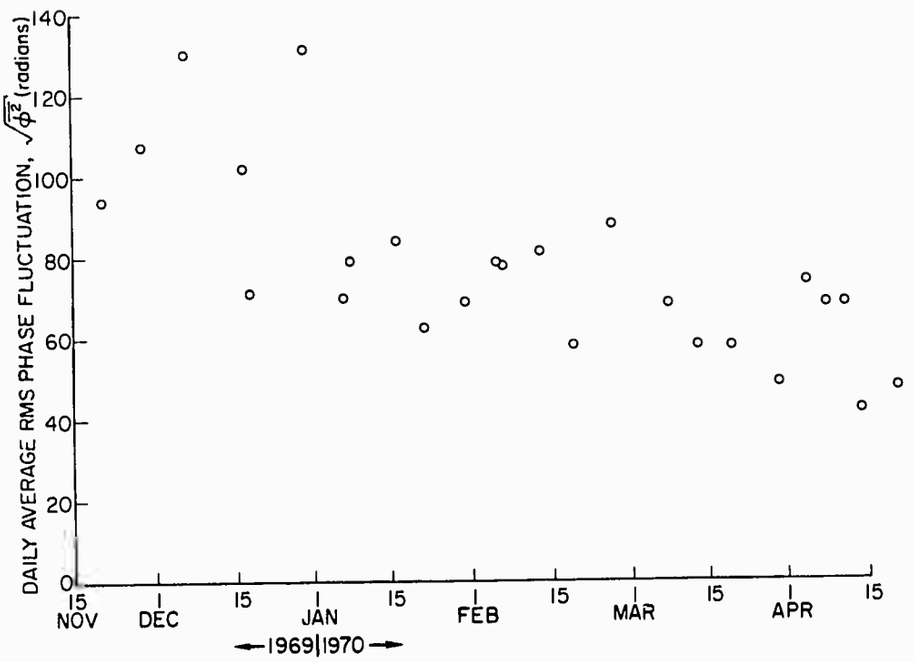

Figure 45. Variation of phase fluctuations with time of year.

Signal-strength fluctuations will produce fading on any antenna that is short compared with the dimensions of the ray interference pattern on the ground. Measurements made during the course of this work show that the correlation coefficient for amplitude fluctuations on two spaced antennas perpendicular to the ray path is 0.8 to 0.95 at spacings of 360 m and 0.4 to 0.8 at spacings of 2.5 km (Fig. 41b). Larger horizontal spacings, vertical spacings, or spacings which are not normal to the ray path may provide more rapid decreases in the amplitude correlation with distance. If the antenna can be made large enough so that it is composed of a number of cells (subdivisions) each of which observes amplitudes independent of those observed by the other cells, the antenna performance may be predicted using the methods of Bracewell ('60). With this method, the field at the receiving antenna, E, is represented as the sum of the strongest ray arriving at the antenna, E_m, and a superimposed random component, ξE_m, where ξ is the complex deviation factor of the field from its average value. The efficiency of the antenna is then given by

$$\eta = \frac{1}{1 + \text{var } \xi} \quad . \tag{20}$$

In Chapter III the variance of the amplitude fluctuations (σ^2) for each measured and computed distribution, and the variance of the phase fluctuations $(\overline{\varphi^2})$ for the computed distributions were calculated. These variances may be used to predict the efficiency of large antenna systems if the antenna is large enough that the required independent cells are present. Fading would not be observed with such an antenna, although its efficiency would be reduced by the multiple incident rays.

E. BANDWIDTH LIMITATIONS

The multiray representation of the field resulting from propagation through ionospheric irregularities may also be used in describing the bandwidth characteristics of the channel. At any given frequency,

the channel transfer function is described by the relative amplitudes of the rays and by their differential time delay, $\Delta P/c$. The manner in which these quantities vary with frequency has not been investigated in this work.

If the directivity of an antenna can be made high enough so that only one ray is accepted, the interfering rays will not be admitted to the receiver. This would eliminate the fading and the bandwidth limitations described above. In the vertical (elevation) plane, rays will originate at heights which differ by about 15 km at the reflection height. For a path of the length used in our measurements, these rays will arrive at the receiving antenna with a separation in elevation angle of about a half degree. A vertical aperture of over 1 km would be required to separate these rays. Therefore, it does not appear practical to reject interfering rays by the use of large vertical apertures. However, large horizontal antennas might be able to reject multipath rays, if the rays have sufficiently different azimuthal angles of arrival.

VI. SUMMARY AND RECOMMENDATIONS

A. SUMMARY

High-frequency ionospheric radio propagation over a one-hop lower-ray F-layer path has been studied under "quiet" ionospheric conditions, i.e., during periods when high-resolution oblique-incidence soundings over the path showed no evidence of ionospheric irregularities. Changes in the phase-path length of rays propagating over the path were measured using a technique which is sensitive to changes occurring as slowly as ten meters per hour. Under quiet conditions, the technique allows measuring ionospheric refractive-index irregularities with a sensitivity about an order of magnitude better than that of other methods, e.g., pulse sounders, satellite Faraday rotation measurements and doppler spectrum analysis.

Analysis of the data produced in these measurements revealed a class of weak slowly-varying irregularities which were present during all of the observations. The data were taken during daylight hours in the spring of 1969 and the winter and spring of 1969-1970, over a 2600 km mid-latitude east-west path. A variety of experimental configurations were employed. The major physical characteristics of the irregularities are:

1. Horizontal scale size of about 35 km.
2. Vertical scale size of about 15 km.
3. Electron-density changes of 0.6 to 6.0 per cent.
4. Horizontal velocity of 65 m/sec (lower limit)--no preferred direction.
5. Vertical phase velocity of 35 m/sec--downward.

Using these parameters, we may classify the new irregularities as smaller, weaker, and somewhat slower-moving than those studied by Munro, Titheridge and others. Their continuous presence and comparatively large effects make them quite significant in ionospheric radio propagation over long one-hop F-layer paths.

A model was developed, and was shown to predict correctly the amplitude fluctuations most commonly observed for long-distance single-mode HF propagation. These fluctuations had not been satisfactorily explained previously. The irregularities also impose fundamental limits on the spatial resolution and bandwidth which may be achievable in HF ionospheric propagation.

No attempt has been made to determine the origin of these irregularities, but their characteristics are consistent with effects which might be produced by internal gravity waves. Georges ('67) in studying large- and medium-scale traveling ionospheric disturbances points out that preferred periods for gravity waves in the F-region are close to 20 minutes. He also shows that for internal gravity-wave energy propagating vertically upward, the phase velocity of the resulting disturbances is vertically downward. If the irregularities observed in this investigation result from internal gravity waves, there is reason to believe that the source of energy producing them lies below the F region, and possibly within the upper atmosphere. Georges notes that thundercloud tops are observed to oscillate with periods of about 20 min, and that attempts have been made by others to detect ionospheric effects which might be produced by these oscillations. The phase-path measurement method used in this work offers considerable potential for observing such a relation if it exists.

B. RECOMMENDATIONS

The bandwidth limitations imposed by weak ionospheric irregularities are not yet fully understood. They are, however, an important result of propagation through such irregularities. Additional information concerning the characteristics and occurrence of these irregularities is needed in order to form a complete description of their effect on HF propagation under varying circumstances. The stable-frequency phase-path measuring system employed in this work would be particularly suitable for additional investigations of the motion, the solar-cycle dependence, and the seasonal, diurnal and global frequency of occurrence of these irregularities. For use in potential development of large antenna systems, more detailed information on the azimuthal-angle distribution of multiple rays is needed.

The major degradation of HF communication-system performance produced by these irregularities is multipath interference within a single mode. Since the extent of this interference is a function of the distance from the scattering region to the receiver, it may be possible to optimize the design of a high-performance communication system by selecting paths sufficiently short that such interference is minimized to the greatest possible extent. More data is required on the occurrence and global distribution of the irregularities if such an optimization is to be used in practice.

APPENDICES

APPENDIX A

CW PHASE-PATH MEASUREMENTS

A. THE BASIC MEASUREMENT

The phase-path measurements of this work were made using CW transmissions from stable-frequency transmitters. The transmitted frequencies were synthesized from a cesium-beam frequency standard (or in some cases, from a highly stable crystal frequency standard). The signals were received using standard HF receivers. All of the conversion injection frequencies of these receivers were synthesized from cesium-beam frequency standards. The audio-frequency output of the receivers was sampled by a computer with an analog-to-digital converter. Zero crossings of the audio signal were counted continuously from the start of each data-gathering run. At each "sampling interval" the computer subtracted a number, n, from the running total of zero crossings. The value of n was

$$n = 2f_a t \quad ,$$

where f_a is the nominal audio output frequency of the receiver, as determined by the receiver conversion frequencies used, and t is the sampling interval used. Sampling intervals between 1/10 and 1 sec were used. The sampling rate and the length of the sampling interval were controlled by pulses derived from digital dividers clocked by the cesium-beam frequency standard.

In addition, at the end of each sampling interval the instantaneous phase of the audio signal was calculated by measuring the fractional part of a half-cycle as

$$\text{fract.} = \frac{t_1}{t_2} \quad ,$$

where t_1 is the time between the end of the interval and the zero crossing immediately prior to the end of the sampling interval, and t_2 is the time between the zero crossings immediately preceding and immediately

following the end of the sampling interval. The sum of the running total of zero crossings and the measured fraction is the desired measurement of phase-path length in units of $\lambda/2$, where λ is the wavelength of the transmitted frequency. Using this technique, errors in the measurement of the fractional part of a half-cycle do not accumulate, as the output at each sampling interval is the running total of zero crossings for the entire measurement period (an integer number) plus the fraction measured at the end of the specific interval.

The envelope amplitude of the signal was determined by measuring the slope of the audio signal at the zero crossings immediately preceding and following the end of the sampling interval. For narrow-band signals, this slope is directly proportional to the envelope amplitude of the signal.

Errors in these measurements are introduced by instabilities in the frequency standards and in the other equipment (e.g., receiver phase drift, digital-circuit jitter). As stated in the body of the report, errors in the frequency standards introduce an error of about 10 m/hr in the measurement of phase-path length. Tests were made to determine the total system error by introducing synthesized standard frequencies directly into the input of the receivers. The long-term phase drift observed was less than 10 m/hr (equivalent phase-path length) when the receiver input was derived from the same frequency standard used to synthesize the receiver injection frequencies, or from another independent cesium-beam frequency standard. When a stable crystal frequency standard was used to supply the receiver input, a linear long-term drift was observed due to the frequency error of the crystal standard. Departures from a linear drift were less than 20 m/hr.

Short-term phase errors, arising primarily from noise and digital circuit jitter, were less than 2 deg at the maximum receiver input level, and less than 10 deg ($\sim$ 1/3 m) at a receiver input 40 dB below the maximum level. The amplitude measurement was accurate to within 1 dB over the 40 dB range of input levels.

During the first series of measurements, involving the airborne and Los Banos receiver sites, some additional short-term errors were introduced by the intermediate analog magnetic tape recording. These errors are discussed in the next section.

B. WIDE-SPACED MEASUREMENTS

Initial determinations of the strength and horizontal size of the observed weak irregularities were made using a transmitter in Bearden, Arkansas, a fixed receiving site at Los Banos, California, and a receiving system in an aircraft. The path length is about 2600 km. This configuration was used to allow a relatively rapid determination of the major characteristics of the received wavefronts. Flights were made in a generally north-south line, from 30 to 170 km north of the fixed receiving site (see Fig. 46). Each flight took between 20 and 40 min, and covered from 100 to 140 km. Ten flights were made, of which the eight most successful were used to determine the parameters of the irregularities. This section describes the equipment and methods used in making these measurements.

A DC-3 aircraft was used for the experiment. It was equipped with two monopole antennas, approximately 1/4 wavelength long. These were tuned so that a low VSWR was obtained over frequencies from 20 to 26 MHz. The same signal was received on both of the antennas and separately recorded. The results of processing data from both antennas were compared to eliminate any ambiguities resulting from fades due to ground reflections or incoming polarization changes. Generally, the data from the vertical antenna were used. Figure 47 is a photograph of the exterior of the aircraft. The antennas may be seen at the rear.

Figure 48 shows the interior of the aircraft with the equipment installed. All receivers were modified so that all conversion frequencies were synthesized from the cesium standard. The receiver audio outputs were recorded on analog magnetic tape. In addition, a 50 kHz signal derived from the cesium standard was recorded on the tape. This signal was used during data reduction to control the sampling of the data channels, thereby greatly reducing the effects of short-term tape speed fluctuations, and eliminating the effects of long-term fluctuations. A one pulse per second (pps) signal derived from the cesium standard was also recorded on the tape. This permitted precise synchronization of the tapes from the aircraft and from Los Banos, and prevented dropouts in the 50 kHz signal from degrading long term accuracy. Voice countdowns on the tape allowed exact matching of the time between Los Banos and the

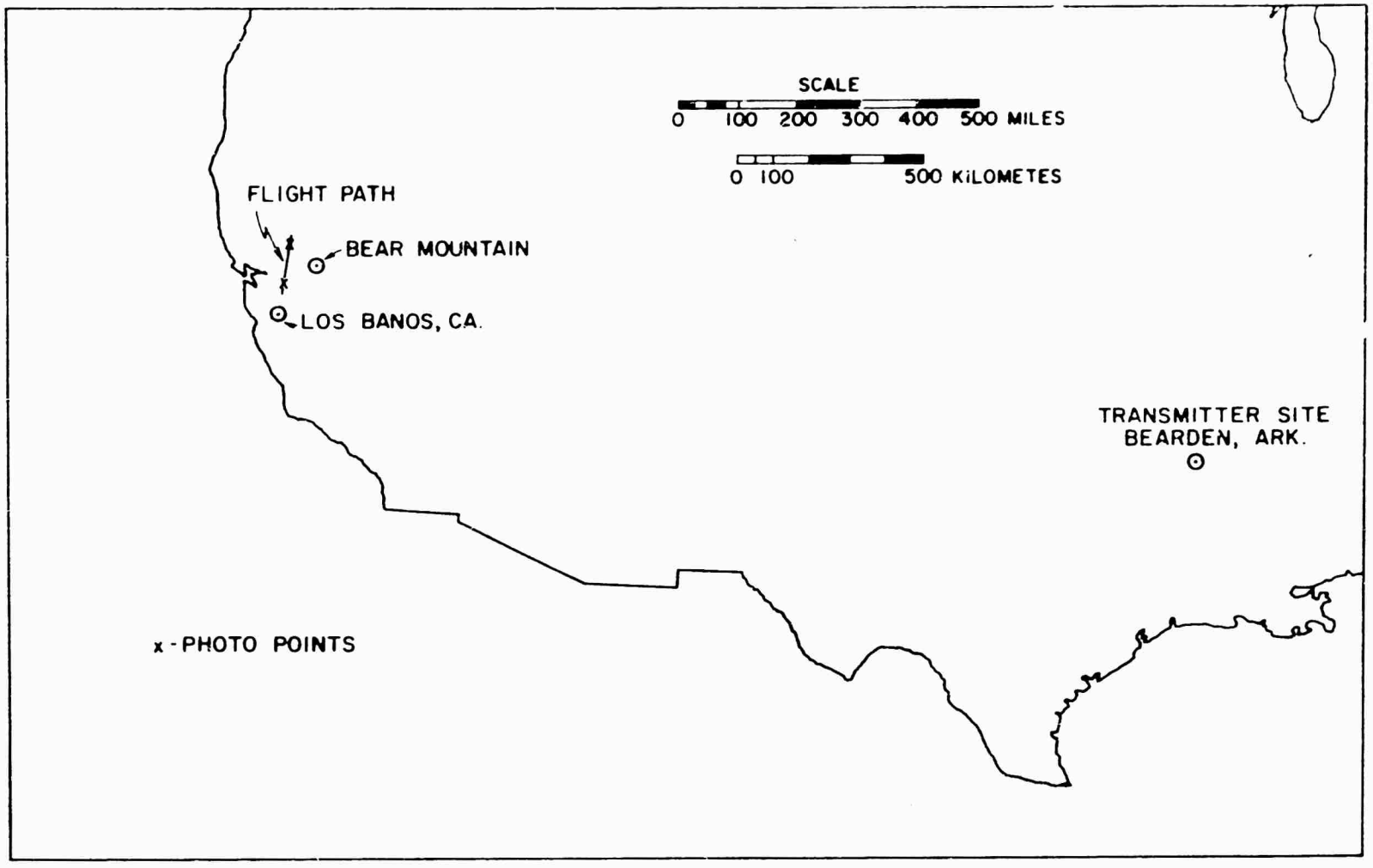

Figure 46. Map showing the area of the experiments.

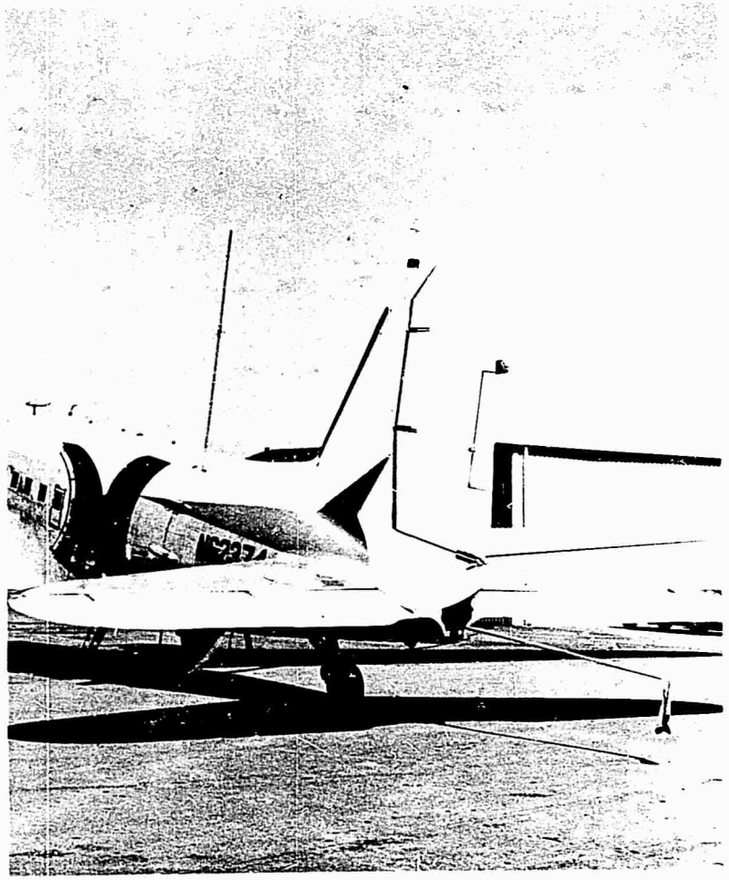

Figure 47 Exterior of aircraft.

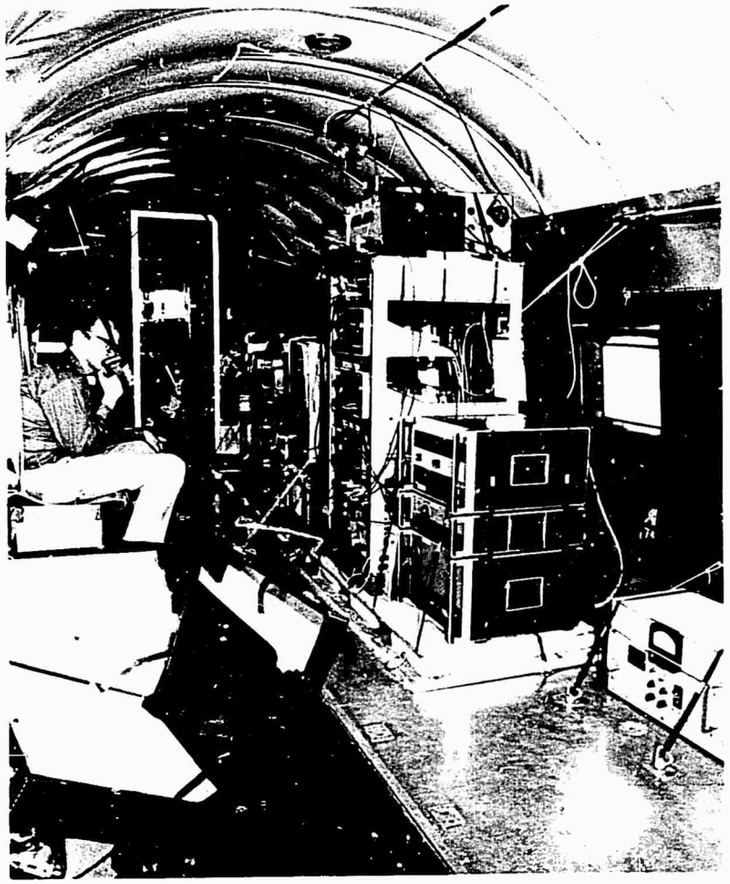

Figure 48 Interior of aircraft.

BLANK PAGE

aircraft. Tests of this method of recording and the associated data-reduction process showed that a phase accuracy of better than ±5 deg was maintained for the data channels (where only a single frequency component was present) and ±10 deg for the tracking channel (two frequencies, differing in strength by up to 30 dB, were used for the tracking system as described below). Figure 49 is a block diagram of the equipment on the aircraft.

The receiving equipment at Los Banos used basically the same technique. A single 1/4 wavelength vertical antenna was used. Again, all conversion frequencies were derived from a cesium beam frequency standard. The same data recording scheme was used.

CW transmissions from Bearden, Arkansas were provided by a crystal frequency standard, a frequency synthesizer and a 1000 watt linear amplifier. The antenna used was a vertical monopole. The frequency stability of the crystal frequency standard is specified as 10^{-10} for averaging times from 1 sec to 1 hr. This can introduce an uncorrected doppler frequency of up to 0.0025 Hz for a typical pass. The peak-measured doppler (dP/dt) for all flights ranged from 0.05 Hz to 0.2 Hz. Errors in relative doppler between Los Banos and the aircraft are determined by the stability of the cesium standards at Los Banos and on the aircraft. These errors were of the order of 0.00025 Hz.

C. AIRCRAFT TRACKING SYSTEM

An accurate determination of wave-front shape from a moving aircraft requires an accurate means of determining the location of the aircraft. The accuracy with which the position of the aircraft can be determined sets a limit on the accuracy of the measurements which can be made. A tracking system was used for these experiments which provided continuous measurements of the position of the aircraft. The estimated accuracies for this tracking system are discussed below and summarized in Table 1.

The tracking system consisted of a CW doppler system, an aneroid differential altimeter, and an aerial camera. The CW doppler system measured changes in distance to the aircraft from two ground points within a direct line-of-sight of the aircraft. Two doppler transmitting sites

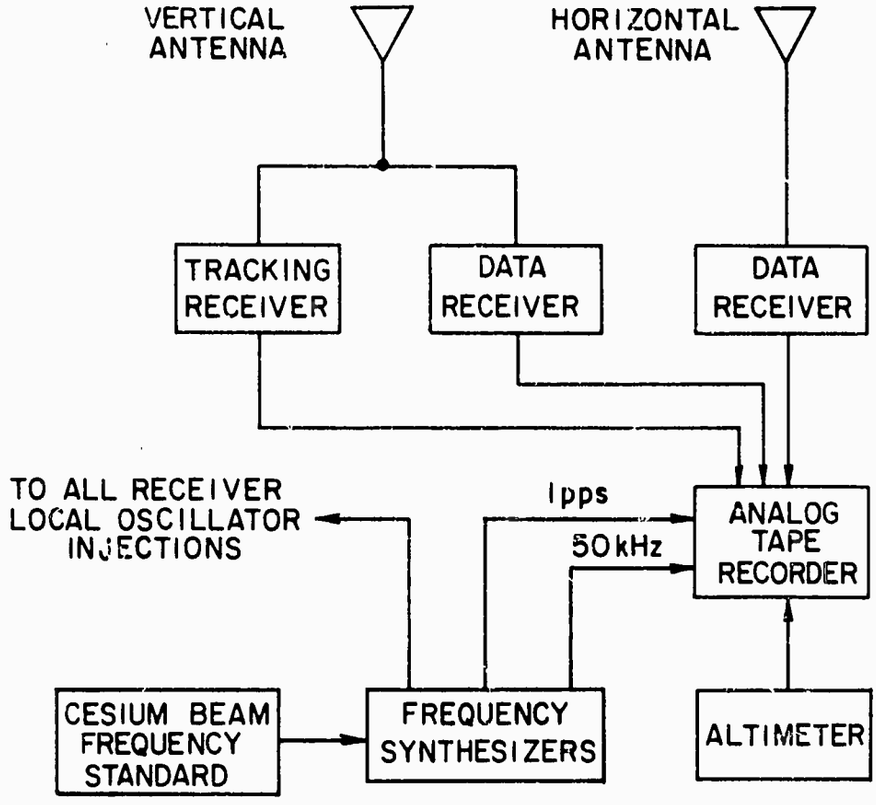

Figure 49. Block diagram of major equipment of the aircraft.

were used (see Fig. 46), one located near the southern end of the flight path (Los Banos), and one to the east of the flight path in the Sierra foothills (Bear Mountain). Both transmission paths to the aircraft were unobstructed along the entire flight path. Frequencies near 25 MHz were used for reasons of simplicity and economy in the transmitting and receiving equipment. The frequencies of the two transmitters were offset by 3.0 kHz. The signals were received in the aircraft using the same vertical antenna that was used for receiving the ionospherically-propagated signals. Both tracking signals were received by a single receiver having a 6 kHz bandwidth. The audio output of this receiver (at 3 and 6 kHz) was recorded on one track of the analog tape recorder. All transmitting and receiving mixing frequencies for the tracking system were synthesized from a single frequency standard at each location. The frequency standards in the aircraft and at Los Banos were cesium-beam standards. A crystal frequency standard was used at the Bear Mountain transmitting site. In order to remove the effect of frequency fluctuations in the crystal frequency standard, the signal transmitted from Bear Mountain was also received at Los Banos, using a receiver having all conversions synthesized from the Los Banos cesium standard, and recorded for use during the tracking data reduction.

The specified accuracy and long-term stability of the cesium-beam frequency standards is $\pm 1 \times 10^{-11}$. Short-term stability is such that the accumulated phase error never exceeds that due to the accuracy specification by more than 1 milliradian at 25 MHz. Measurements made on the two cesium standards that were used indicate a relative drift of less than 1 μsec/day between them. This is within the specification value. A typical pass over the flight path requires about 1/2 hr. During this period, the total phase change is approximately $25 \times 10^6 \times 2\pi \times 1800$ rad. The phase error expected would then be

$$25 \times 10^6 \times 2\pi \times 1800 \times 10^{-11} = 2.8 \text{ rad} \quad .$$

For a frequency of 25 MHz ($\lambda = 12$) this corresponds to a distance error of 5 m over a 30 min flight, and proportionally less over shorter portions of a flight.

Changes in the height of the aircraft were measured with a precision aneroid altimeter. It was used in a differential mode with a full-scale output of ±40 m. In this mode the primary source of instrument error is hysteresis, which is specified at ±3 m. Corrections for variations in air pressure with time and along the flight path were made when necessary, using temperature-corrected barometric readings from the Sacramento and Stockton, California, Weather Bureau stations. These readings were taken at half hour intervals during the period of the flights. For a majority of the flights no correction was made, as the indicated correction was less than 10 m. Because the elevation angle-of-arrival for the ionospherically propagated signals from Bearden is low (~ 10 deg), errors in altitude affect the phase-path measurements by less than 1/5 as much as do errors in horizontal position.

The three measurements made by the doppler system and the altimeter are sufficient to determine the location of the aircraft, continuously if an initial location can be determined from other means. For the measurements involved in these experiments, although it is important to know accurately only changes in the great circle distance to the transmitter and changes in altitude, the geometry of the doppler system requires that a fixed point be used as a starting reference. The error in change of distance will be about half the error in the location of the fixed point for the transmitter locations employed. (If only portions of the flight path near the center are used, where the angle between the flight path and the transmission from Bear Mountain is reasonably large, less error in change of distance will result.)

Photogrammetric reduction of the aerial photographs taken over two "photo points" (Fig. 46) on the flight path (a stereo pair at each point) was used to establish the fixed point required by doppler/altimeter system, and to check the closure error of the tracking system. The stated accuracy of the photographic position determination is ±50 m in the horizontal plane, and ±100 m in altitude.

The final accuracy of the tracking system is estimated in terms of the effects of various errors on relative position, rather than absolute position determination which is not important for the experiments. Table 1 summarizes the various sources of error in the tracking system, and their contribution to relative position error.

TABLE 1

AIRCRAFT TRACKING SYSTEM ERRORS
(30 Min. Flight Time)

Error Source	Estimated rms Error (m)
Frequency Standards	5.0
Altimeter (3.0/5)	0.6
Air Pressure Changes (10.0/5)	2.0
Photogrammetry--Horizontal (50/2)	25.0
Photogrammetry--Vertical (100/10)	10.0
Tracking Frequency Ground Reflections ($\lambda/6$)	2.0
Phase Measuring System (Insignificant)	--
TOTAL	27.4

As a check on long-term error, photographic position determinations were made at both ends of the flight path for four flights. These were compared with the positions determined by the tracking system. Closure errors were 20, 25, 35, and 60 m for these flights. No systematic errors were visible on the data. It is therefore believed that tracking-system errors contributed an rms error of about 10 per cent to the experimental data from the aircraft.

D. DATA PROCESSING

Each pass over the flight path resulted in one analog tape each from the aircraft and from Los Banos. Table 2 lists the channel assignments for these tapes. The first step in the data reduction was to play back the tapes, and, using a Scientific Data Systems Sigma V computer with analog-to-digital converter, convert the audio signals to a digital tape which represented the total number of cycles (including fractions) from the start of the tape. This was done for each of the six audio signals on the tapes. Sampling of the signals was clocked by the 50 kHz or 25 kHz tones on the tapes. The one pps signal was also sampled to indicate the start of each second, in the event that dropouts occurred in the 50 kHz signal. A test was made during sampling to assure that between 0.8 and 1.2 seconds of real time elapsed between occurrences of the 1 pps

TABLE 2

DATA RECORDED ON ANALOG TAPES

Aircraft Tapes -- 30 in./sec -- Direct record (except FM where marked with asterisk)

Track	
1.	Tracking Receiver Output - 3 & 6 kHz
2.*	Voice commentary & countdowns, & camera exposure tone
3.	1 pps from cesium standard
4.*	Differential altimeter - ± 40 m
5.	50 kHz sine wave from cesium standard and divider
6.	Horizontal antenna data-receiver output - 3 kHz
7.	Vertical antenna data-receiver output - 3 kHz

Los Banos Tapes -- 15 in./sec

Track	
1.	Beam Mountain tracking correction signal - 3 kHz
2.*	Voice commentary and countdowns
3.	1 pps from cesium standard
5.	25 kHz sine wave from cesium standard and divider
7.	Data receiver output - 3 kHz
4 & 6.	Not used.

signal from the tape. This insured that seconds would not be "lost" if there were dropouts in the 1 pps channel. Finally, the altimeter channel and its calibration were sampled each second.

The resulting digital tapes were listed, and a test was made to determine that the doppler frequency each second was within 1/2 Hz of the doppler frequency for the preceding second. If not, the data were flagged at that point to indicate a tape or signal dropout. Between 0 and 40 points for each tape (in a total of about 1500 points) were flagged. An editing program was then used to correct flagged points, align all tape playbacks to a common starting point, and convert from cycles to distance. The latter conversion required inversion of some of the

frequencies (where the receiver used an odd number of inverting conversions), and multiplication by the particular wavelength for the frequency involved. The resulting tape was then processed to obtain the required results in terms of changes in phase path length to the transmitter. Three of the six audio frequencies on the analog tapes result in two records, describing changes in distance between the aircraft and Los Banos and between the aircraft and Bear Mountain. The altimeter samples result in a record of changes in altitude of the aircraft. (Corrections for changes in barometric pressure are also included in the editing program.) These three records are used, together with an initial point determined from photography, to calculate the location of the aircraft each second, and to calculate the great circle distance to the transmitting site each second.

The remaining three audio frequencies produce records representing the change in phase path length of the ionospherically propagated signal received at Los Banos and on the aircraft horizontal and vertical antennas. The data from the aircraft are then corrected for the effect of changes in aircraft distance from the transmitter and changes in altitude. The resulting records for the aircraft represent measurements comparable to the Los Banos measurements. Finally a constant doppler (linear phase-path change) term is subtracted from all the data for a given flight. The quantity subtracted is the average doppler at Los Banos for a period of a half hour to an hour, including the time of the flight. The resulting records show changes in phase-path length between the transmitter and Los Banos, and between the transmitter and the aircraft, with a linear term removed from both. Typical records are included in Chapter II. The difference in doppler at varying separations of receiving sites is determined by measuring the slopes of the two curves at various times and corresponding separations.

E. LATER LOS BANOS MEASUREMENTS

The measurements made during the winter and spring of 1970 involved only the Los Banos receiving site and the Bearden transmitting site. The basic measurement was the same, but the equipment used was somewhat

different. The transmitting site transmitted two synthesized frequencies. The receiving site was equipped with a small computer with an analog-to-digital converter and a digital tape recorder. These were used to considerably simplify the data processing. Receiving antennas were available which were located on a line perpendicular to the direction of the transmitting site. These were eight vertical monopoles spaced 360 m between each element. A maximum of three elements was used at any one time.

APPENDIX B

THE EFFECT OF CHANGES IN RAY REFLECTION HEIGHT

This appendix discusses the possibility that the relation which was derived between the measured changes in phase-path length, and the changes in refractive index and electron density which are required to produce them, may not be accurate. Two distinct simple models of the ionosphere are commonly used in considering the source of doppler effects on ionospherically propagated waves (Davies '65). The first assumes that variations in refractive index occur along straight (non-deviating) portions of the ray paths (i.e., not near the reflection height). This is the assumption made in the two-dimensional model used in Chapter III. The second commonly-used model assumes that if there are ionospheric variations near the reflection height (where in fact it appears that the observed irregularities are located), these can be analyzed in terms of a change in height of a reflecting mirror. This latter idea implies that an irregularity may change the height at which a ray is reflected. The effect of such a change in reflection height is now to be considered.

It might be anticipated that when an irregularity disturbs the path of a ray in the ionosphere, causing a change in the reflection height of the ray, the measured change in path length may be greater than that which would occur for a ray passing directly through the irregularity when the latter is so located as not to affect the reflection height--i.e., when the irregularity is on the ray path but not near the region of significant ray bending. Figure 50 shows the effect of a change in reflection height caused by the presence of an irregularity near the region of significant ray bending. From Eqs. (5) and (4) we have

$$\frac{dP}{dt} = \int_{\text{RAY PATH}} \frac{\partial \mu}{\partial t}\, ds \quad . \tag{B.1}$$

It will now be shown that the change in reflection height does not affect the relations which were used in determining changes in refractive index and electron density.

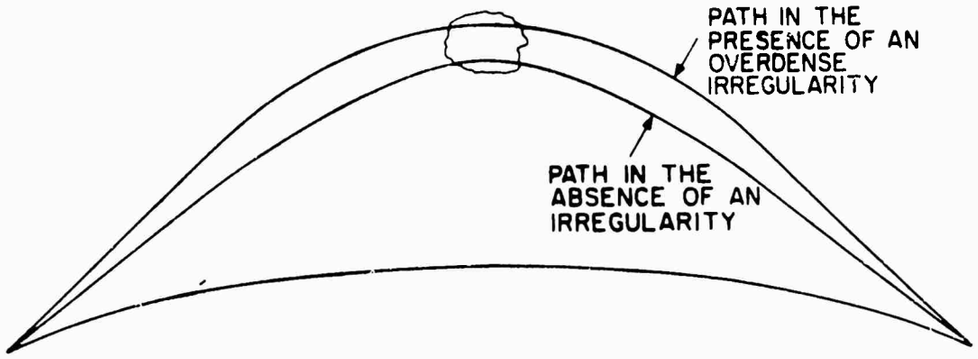

Figure 50. Ionospheric ray paths showing a change in reflection height caused by an irregularity near region of significant ray bending.

Consider first a non-moving irregularity described by

$$\frac{\Delta\mu}{\mu} = f(t) \cdot g(x,y,z) \quad .$$

In this expression $g(x,y,z)$ describes a fixed shape for the irregularity, and $f(t)$ describes some time function. Let the irregularity be isolated from the slowly varying ionospheric background, i.e., let it be immersed in a medium of constant refractive index. At any time t, define a geometrical ray path G_m within the irregularity as the path which exhibits the maximum doppler at the time. That is,

$$\int_{G_m} \frac{\partial\mu}{\partial t}\, ds = \max \quad . \tag{B.2}$$

Now at any instant t, the rate of change of phase path, dP/dt, along the geometrical path G_m will correspond to the maximum possible value of the integral in Eq. (B.1). If the irregularity is now immersed in the ionosphere, the only portion of any ionospheric ray path which can contribute to a change in the value of the integral is the portion (if any) which lies within the irregularity, since outside the irregularity, $\partial\mu/\partial t = 0$. Therefore, at any instant, the doppler over the ionospheric path must be less than or equal to the doppler along G_m within the isolated irregularity. For simple shapes of irregularities of arbitrary strength (excluding the possibility of total ray reflection) and for arbitrary shapes of weak irregularities, we can show that G_m is a fixed path. In the case of a spherically symmetric irregularity, G_m is any diameter of the irregularity. For an ellipsoidal irregularity, G_m is the major axis of the irregularity. In the case of weak irregularities, where in this case 'weak' implies that rays are not displaced within the irregularity, but only deflected in angle, all ray paths within the irregularity are straight lines, and every straight line is a ray path. G_m is then a fixed straight line defined by

$$\int_{\substack{\text{STRAIGHT}\\ \text{LINE}}} g(x,y,z) = \text{maximum} \quad . \tag{B.3}$$

The irregularities which were described based on the ionospheric measurements of this work satisfy the 'weak' approximation with little error. The result states that regardless of the smooth bending geometry of the ionosphere itself, irregularities produce a doppler which is at every instant less than or equal to the doppler that would be measured for a path G_m in the irregularity when the latter is isolated from the ionosphere. Therefore, the total measured change in phase-path length when the irregularity is in the ionosphere will be less than or equal to the change in phase-path length along a path G_m through the isolated irregularity. So, despite the fact that an irregularity may change the reflection height of a ray in the ionosphere, and therefore also change the phase-path length of the ray outside the region of the irregularity, the total measured change will be no greater than the change which would be predicted from propagation through an isolated irregularity, having the same profile, which is not close to the reflection height.

If the irregularity is assumed to move, little is changed in the argument. Since the total ionospheric ray path at a given time is not a function of its history, the integral of dP/dt will be the same whether the irregularity reached its present position by moving there or by developing there. This leads to the conclusion that the method used in relating ΔP to $\Delta\mu$ is valid.

REFERENCES

Al'pert, Ya. L., Radio Wave Propagation and the Ionosphere, (Authorized Translation from the Russian), Consultants Bureau Enterprises, Inc., New York, 1963.

Barry, G. H. and R. B. Fenwick, "Extraterrestrial and Ionospheric Sounding with Synthesized Frequency Sweeps," Hewlett-Packard Journal, Vol. 16, No. 11 8 (1965).

Bennett, J. A., "The Calculation of Doppler Shifts Due to a Changing Ionosphere," J. Atmos. Terrest. Phys., Vol. 29, 887 (1967).

Booker, H. G., J. A. Ratcliffe and D. H. Shinn, "Diffraction from an Irregular Screen," Phil. Trans. Roy. Soc. London, Vol. A-242, 579 (1950).

Born, M. and E. Wolf, Principles of Optics, Pergamon Press, New York, 1964.

Boys, J. T., "Statistical Variations in the Apparent Specular Component of Ionospherically-Reflected Radio Waves," Radio Sci., Vol. 3 (New Series), 984 (1968).

Bracewell, R. N., "Antenna Tolerance Theory," Statistical Methods of Radio Wave Propagation, Pergamon Press, London, 1960.

Bramley, E. N., "Direction-Finding Studies of Large-Scale Ionospheric Irregularities," Proc. Roy. Soc., Vol. A-220, 39 (1953).

Bramley, E. N., "Some Comparative Directional Measurements on Short Radio Waves over Different Transmission Paths," Proc. IEEE, Vol. 43, 544 (1955).

Budden, K. G., Radio Waves in the Ionosphere, The University Press, Cambridge, 1961.

Chan, K. L. and O. G. Villard, Jr., "Observation of Large-Scale Traveling Disturbances by Spaced-Path High-Frequency Instantaneous-Frequency Measurements," J. Geophys. Res., Vol. 67, 973 (1962).

Chernov, Lev A., Wave Propagation in a Random Medium, McGraw-Hill Book Company, New York, 1960.

Croft, T. A., "Methods and Applications of Computer Raytracing," Report SEL-69-007 (TR No. 112), Stanford Electronics Laboratories, Stanford, California, 1969.

Davies, K., Ionospheric Radio Propagation, U. S. Govt. Printing Office, Washington, D. C., 1965.

Dieminger, W., "The Scattering of Radio Waves," Proc. Phys. Soc., Vol. B-64, 142 (1951).

Georges, T. M., "Ionospheric Effects of Atmospheric Waves," IER 57-ITSA 54, Institute for Telecommunication Sciences and Aeronomy, Boulder, Colorado, 1967.

Hines, C. O., "Atmospheric Gravity Waves: A New Toy for the Wave Theorist," Radio Sci., Vol. 69D, 375 (1965).

Jones, R. M., "A Three-Dimensional Ray-Tracing Computer Program," Radio Sci., Vol. 3 (New Series), 93 (1968).

Kato, S., "A Contribution to the Theory of Irregularities in a Medium with a Mean Density Gradient," J. Atmos. Terrest. Phys., Vol. 27, 367 (1965).

Lee, R. W. and J. C. Harp, "Weak Scattering in Random Media, with Applications to Remote Probing," Proc. IEEE, Vol. 57, 375 (1969).

Little, C. G. and O. K. Garriott, "The Use of Geostationary Satellites for the Study of Ionospheric Electron Content and Ionospheric Radio Wave Propagation," J. Geophys. Res., Vol. 65, 2025 (1960).

Manning, L. A., "The Effects of Irregularity Scale on Usable Antenna Aperture," Report SEL-68-051 (TR No. 141), Stanford Electronics Laboratories, Stanford, California, 1968.

Munro, G. H., "Travelling Disturbances in the Ionosphere," Proc. Roy. Soc., Vol. 202, 208 (1950).

Munro, G. H., "Travelling Ionospheric Disturbances in the F Region," Aust. J. Phys., Vol. 11, 91 (1958).

Peterson, A. M., "The Mechanism of F-Layer Propagated Back-Scatter Echoes," J. Geophys. Res., Vol. 56, 221 (1951).

Rice, S. O., "Mathematical Analysis of Random Noise, Pt. III," Bell System Tech. J., Vol. 23, 282 (1945).

Sweeney, L. E., Jr., "Spatial Properties of Ionospheric Radio Propagation as Determined with Half-Degree Azimuthal Resolution," Dissertation Submitted in Partial Fulfillment of the Requirements for the Degree of Doctor of Philosophy, Stanford University, Stanford, California, 1970.

Tatarski, Wave Propagation in a Turbulent Medium, McGraw-Hill Book Company, New York, 1961.

Titheridge, J. E., "Large-Scale Irregularities in the Ionosphere," J. Geophys. Res., Vol. 68, 3399 (1963).

Titheridge, J. E., "Periodic Disturbances in the Ionosphere," J. Geophys. Res., Vol. 73, 243 (1968).

Whale, H. A. and J. T. Boys, "Measurements of the Coherence Ratio of Ionospherically Propagated Radio Waves," Radio Sci., Vol. 3 (New Series), 977 (1968).

Whale, H. A. and C. W. Gardiner, "The Effect of a Specular Component on the Correlation Between the Signals Received on Spaced Antennas," Radio Sci., Vol. 1 (New Series), 557 (1966).

UNCLASSIFIED

Security Classification

DOCUMENT CONTROL DATA - R&D

(Security classification of title, body of abstract and indexing annotation must be entered when the overall report is classified)

1 ORIGINATING ACTIVITY (Corporate author)	2a. REPORT SECURITY CLASSIFICATION
Stanford Electronics Laboratories Stanford University, Stanford, Calif 94305	Unclassified
	2b GROUP

3 REPORT TITLE

IRREGULARITIES IN THE QUIET IONOSPHERE AND THEIR EFFECT ON PROPAGATION

4. DESCRIPTIVE NOTES *(Type of report and inclusive dates)*

Technical Report No. 156, August 1970

5 AUTHOR(S) *(Last name, first name, initial)*

Philip A. Fialer

6. REPORT DATE	7a. TOTAL NO. OF PAGES	7b. NO. OF REFS
August 1970	137	32

8a CONTRACT OR GRANT NO.	9a. ORIGINATOR'S REPORT NUMBER(S)
Nonr-225(64)	TR No. 156 SEL-70-037
b. PROJECT NO. 3808	
c.	9b. OTHER REPORT NO(S) *(Any other numbers that may be assigned this report)*
d.	

10. AVAILABILITY/LIMITATION NOTICES

This document has been approved for public release and sale; its distribution is unlimited.

11. SUPPLEMENTARY NOTES	12. SPONSORING MILITARY ACTIVITY
	Office of Naval Research

13 ABSTRACT

The primary purpose of this investigation was to determine the nature and characteristics of a class of large, weak ionospheric irregularities which in certain circumstances significantly affect long-distance HF radio-wave propagation. A further purpose was to determine the relative practical importance of the diffraction produced by these inhomogeneities, in relation to the influence of other mechanisms such as Faraday rotation and scattering by small irregularities.

Measurements of quasi-periodic variations in phase-path length have been made on a 2600 km one-hop lower-ray F-region path. Variations of 8 to 75 wavelengths are regularly observed during winter daylight hours. They have a quasi period of about 20 minutes. Correlations of measurements made at spaced receiver locations indicate that these variations in phase-path length are produced by irregularities having a horizontal scale size of about 35 km. Multiple frequency measurements show a vertical scale size of about 15 km, with a maximum in the lower F region. A lower limit of 65 m/sec is determined for the horizontal velocity of the irregularities. A downward vertical velocity of 30 to 40 m/sec is observed. The irregularities limit achievable bandwidth and spatial resolution for one-hop HF ionospherically propagated waves under quiet ionospheric conditions.

A model of the irregularities has been devised and has been used to predict the signal-strength fluctuations which would result from propagation through a medium described by the model. Two classes of signal-strength behavior are predicted and observed experimentally, depending on the relative magnitude of the phase-path variations within the limits mentioned above. Signal-strength

DD FORM 1 JAN 64 1473

Security Classification

14 KEY WORDS	LINK A		LINK B		LINK C	
	ROLE	WT	ROLE	WT	ROLE	WT
FOCUSSING						
MULTIPATH						
SINGLE-MODE						
HIGH-FREQUENCY						
RADIO						
RAY-TRACING						
COHERENCE						
ANTENNAS						

ABSTRACT (Cont)

variations of a few dB, having a 20 min period, are observed when the changes in phase-path length are small, and are attributed to focusing caused by the irregularities. Larger, more rapid signal-strength fluctuations are also observed. These are attributed to multipath interference between several ray propagating through the same irregularity. Taken together, these rays make up what would be identified as the one-hop lower-ray F-layer mode, which is seen to be less homogeneous than had previously been supposed, for propagation over 2000-4000 km distances.